GEORGIA INSTITUTE OF TECHNOLOGY — OFFICE OF CONTRACT ADMINISTRATION

PROJECT ADMINISTRATION DATA SHEET

[X] ORIGINAL [ ] REVISION NO. ____

Project No. E-18-616 (R6089-0A0) GTRC/~~GIT~~ DATE 3 / 7 / 86

Project Director: A.T. Chapman, J.K. Cochran School/~~Lab~~ Materials Engr.

Sponsor: Martin Marietta Energy Systems, Inc.

Type Agreement: Subcontract No. 86X-22043C under DE-AC05-840R21400

Award Period: From 2/1/86 To 4/30/89 (Performance) 4/31/87 (Reports)

Sponsor Amount:	This Change	Total to Date
Estimated: $		$ 223,318
Funded: $		$ 75,000

Cost Sharing Amount: $ ____ Cost Sharing No: N/A

Title: Fabrication of Thin Wall Hollow Ceramic Spheres

ADMINISTRATIVE DATA OCA Contact John B. Schonk x-4820

1) Sponsor Technical Contact:

K J. A. Carpenter
Martin Marietta Energy Systems, Inc.
Manager, Materials Program
P. O. Box X
Building ~~45005~~ 4515, MS ~~261~~ 065
Oak Ridge, TN 37831

2) Sponsor Admin/Contractual Matters:

A. F. Johnson
Martin Marietta Energy Systems, Inc.
Purchasing Division
P. O. Box M
Oak Ridge, TN 37831
616/576-1406

Defense Priority Rating: N/A Military Security Classification: N/A

(or) Company/Industrial Proprietary: N/A

RESTRICTIONS

See Attached N/A Supplemental Information Sheet for Additional Requirements.

Travel: Foreign travel must have prior approval — Contact OCA in each case. Domestic travel requires sponsor approval where total will exceed greater of $500 or 125% of approved proposal budget category.

Equipment: Title vests with Sponsor; However, equipment < $5,000 shall vest in GIT if prior approval is received before acquisition.

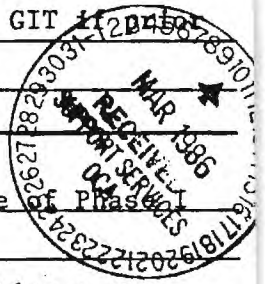

COMMENTS:

Only Phase I authorized. Phase II may be initiated after acceptance of Phase I draft final report.

The P.I. is requested to contact OCA/Subcontracting for initiating a consulting agreement.

COPIES TO: SPONSOR'S I. D. NO. 02.240.001.86.R01

Project Director
Research Administrative Network
Research Property Management
Procurement/GTRI Supply Services
Research Security Services
~~Reports Coordinator (OCA)~~
GTRC
Library

OFFICE OF CONTRACT ADMINISTRATION

NOTICE OF PROJECT CLOSEOUT

Closeout Notice Date 05/03/90

Project No. E-18-616 Center No. R6089-0A0

Project Director CHAPMAN A T School/Lab MAT ENG

Sponsor OAK RIDGE NAT'L LAB/MARTIN MARIETTA

Contract/Grant No. 86X-22043C Contract Entity GTRC

Prime Contract No. DE-A005-840R21400

Title FABRICATION OF THIN WALL HOLLOW CERAMIC SPHERES PHASEII

Effective Completion Date 891231 (Performance) 900331 (Reports)

Closeout Actions Required:	Y/N	Date Submitted
Final Invoice or Copy of Final Invoice	Y	
Final Report of Inventions and/or Subcontracts	Y	
Government Property Inventory & Related Certificate	Y	
Classified Material Certificate	N	
Release and Assignment	Y	
Other	N	

Comments

Subproject Under Main Project No.

Continues Project No.

Distribution Required:

Project Director	Y
Administrative Network Representative	Y
GTRI Accounting/Grants and Contracts	Y
Procurement/Supply Services	Y
Research Property Managment	Y
Research Security Services	N
Reports Coordinator (OCA)	Y
GTRC	Y
Project File	Y
Other	N
	N

NOTE: Final Patent Questionnaire sent to PDPI.

Georgia Tech

School of Materials Engineering

Georgia Institute of Technology
Atlanta, Georgia 30332-0245
(404) 894- 6075
FAX: (404) 853-9140

Fmil
E18-616

November 8, 1989

Dr. Stanley M. Wolf
ECUT Materials Program Manager
CE-12, Department of Energy
1000 Independence Avenue, SW
Washington, D.C. 20585

Dear Stan:

The Annual Progress Report for FY 89 on the Spheres is enclosed. Joe Cochran and I are working on a suitable view graph describing the recent success in using thermal pores to reduce the conductivity of the spheres.

We look forward to seeing you this weekend. Please call if additional information is required.

Very truly yours,

A.T. Chapman
Professor of Ceramic Engineering

/lmw
Enclosure

Annual Progress FY 89

Thin-Wall Hollow Ceramic Spheres from Slurries

J.K. Cochran and A.T. Chapman
School of Materials Engineering
Georgia Institute of Technology
Atlanta, GA 30332-0245
ORNL Subcontract 86X-22043C

Background -

The ongoing DOE supported program on "Thin-Wall Hollow Ceramic Spheres from Slurries" was initiated in January 1986. During Phase I the objective was to develop a process for fabricating the spheres. This was successfully done by dispersing ceramic powders in an organic liquid, blowing the individual spheres using a coaxial nozzle and drying the free-falling spheres in an updraft heated air column. Based on the success of Phase I the Phase II activity emphasized the assessment of the structural and insulation capability for the spheres, and modeling the sphere formation process. The Phase II program ended April 30, 1989 and was followed by a short four month effort, Phase III, to assess the potential of using an opacifier in the sphere walls to scatter radiation and decrease the high temperature thermal conductivity of sphere beds. This Annual Report briefly reviews the status of the Phase II milestones and the very encouraging Phase III results. Publications, presentations, personal participating in the project, and allied budgetary information are also included.

Milestone Status and Schedule (Phase II and III Effort)

1. Slurry Formation, Start 10/88 Finish 4/89

   a. Sphere Rheology: Measurement and Modeling

A model has been developed which describes the viscosity of non-aqueous stericly stabilized dispersions of ceramic powders as a function of solids concentration and viscosity of the liquid phase. Parameters controlling viscosity include particle size and surface area of the solid, the thickness of the polymer layer adsorbed on the ceramic particle, and the concentration of

particles and dissolved polymer in the organic liquid.

b. Sphere Formation: Process and Modeling

Mathematical expressions which describe various stages of the sphere formation process occurring as powders dispersed in fluids are forced through the concentric nozzle assembly have been developed. Work is underway to validate these models using ideal fluids as the sphere forming media. Noteworthy in this effort is the identification of the parameters which control the frequency of sphere formation and the agreement between predicted and measured frequency.

2. Sphere Development, Start 9/88 Finish 4/89

a. Forming Sphere Monoliths

A major effort has been made to bond both alumina and mullite spheres into a strong low-density monolith. The best results have occurred using beds of fired and unfired mullite spheres and bonding with a fluid mullite slip at the sphere contact points. Test shapes have displayed compressive strengths almost twice that available from commercial refractory brick of equivalent density. Examination of failed samples shows the fractures occurring in the sphere monoliths travel predominantly through the sphere walls rather than the bonding media between the spheres.

b. Development of New Compositions

During Phase II work, several new sphere compositions were developed, i.e. mullite. fused SiO_2, clay, ferrites, and PSZ. Based on the success with these new materials the capability of forming thin-wall spheres from virtually any powder chemistry is becoming a reality, although for some compositions significant effort may be required to develop the correct dispersion rheology compatible with the sphere forming process.

3. Properties of Spheres, Start 10/88 Finish 9/89

a. Mechanical Strength

In the past year, the understanding of uniaxial compressive strength

of thin-wall spherical shells has been advanced greatly. To develop an equation for compressive strength of two-point uniaxial loaded hollow spheres based on wall material flexure strength and sphere density, finite element modeling was used to calculate the failure load for sphere ranging in diameter, d, from 1 to 5 mm and wall thickness,t, from 25 to 125μm. Note that sphere density is a function of t/d. A parametric equation was developed from the data which indicated that, sphere strength was linearly dependent on $(t/d)^2$ rather than $(\text{relative density})^2$ as had previously been thought based on the modified Bratt equation. To move toward bonded sphere structures, finite element strengths were calculated for six point, uniaxial loading as if the sphere was in an HCP array and the load was applied by the upper and lower three spheres. This resulted in a parametric equation similar to two loading point loading but with strengths about 10% lower. Measurement of both two-point and six-point uniaxial crush strength for a variety of alumina and mullite spheres agreed well with the 10% strength reduction for six-point loading. FEM calculations are currently concentrated on uniaxial loading of a bonded bed of randomly packed spheres and bonded samples are being developed to test the FEM strength model. At that point, it should be possible to predict accurately the compressive strength of bonded monoliths based on two-point crush loads for specific sphere geometries and compositions.

b. Thermal Conductivity (Phase III)

Starting May 89 an interim four month program, Phase III, was initiated to demonstrate the feasibility of reducing the high temperature thermal conductivity (T/C) of the spheres. This was accomplished by the addition of a second-phase (opacifying phase) into the sphere wall to scatter thermal radiation. To date Al_2O_3 and mullite spheres have been opacified by the addition of voids, termed Thermal Pores (TP). The pores are generated by the addition of graphite to the slurry. Spheres are then produced normally and the graphite

burns out during the sintering process leaving TP of a known size range.

Mie Scattering Theory shows that there is an optimum opacifier particle size for scattering, depending on wavelength. For the air-filled pore/alumina system, the optimum opacifier particle size is 0.5μm - 3μm. For effective scattering, theory indicates only 1-3 v/o of opacifier need be added.

The T/C of the Al_2O_3 and mullite spheres with and without TP measured at Georgia Tech is shown in Figures 1 and 2. Both figures show that the addition of thermal pores to the sphere wall reduces thermal conductivity by approximately 30% in the 400°C - 1200°C temperature range. Optimization of the size and morphology of the TP may result in further reduction of the T/C by opacification.

In addition Figures 1 and 2 include lower temperature T/C measurements performed previously at ORNL on equivalent Al_2O_3 and mullite spheres (without TP). Measurements both at Georgia Tech and ORNL employed the radial heat flow technique and the agreement in T/C values is very good. The T/C of the spheres measured at Georgia Tech employed a recently purchased Unitherm Model 4141 Radial Thermal Conductivity Apparatus (RTCA) manufactured by Anter Laboratories, Inc. The RTCA is a computer driven system that measures absolute T/C values, utilizing no reference sample. The spheres are loaded into a high aspect ratio cylinder. A line-source heater is located in the center of the cylinder and produces a thermal gradient across the bed of spheres. The gradient is measured by radially located thermocouples. The heat flow in the sampling area is predominately radial, while axial heat flow is minimized by guard heaters. By determining power input, location of the thermocouples, and the thermal gradient across the sample, the T/C of the spheres can be calculated.

Publications:

A. Completed

1. S.A. Rickles, J.K. Cochran, T.H. Sanders, "The Production and Compressive Characteristics of a Low Density Syntatic Metal/Ceramic Foam," Proceedings of 13th Annual Conference on Composites and Advanced Materials, ed., R.E. Banks, Cocoa Beach, Florida, American Ceramic Society, Columbus, Ohio, January 1989.

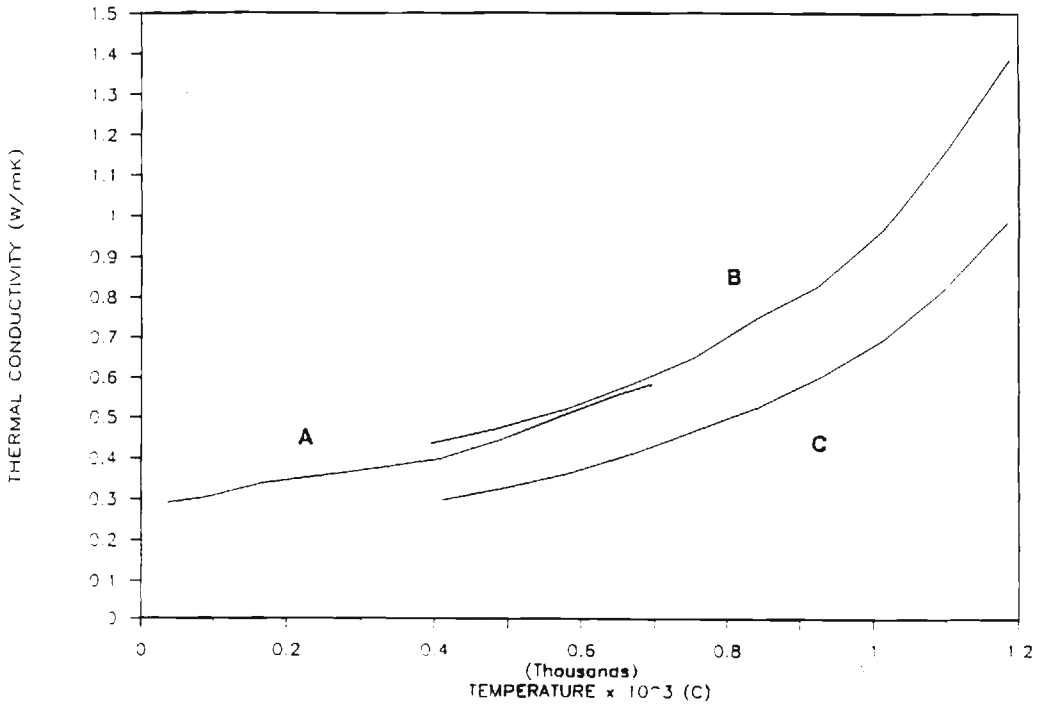

Figure 1. Thermal Conductivity of Random Packed Al_2O_3 Spheres; A. Previous ORNL Data B. GA Tech Data and C. Spheres with Thermal Pores.

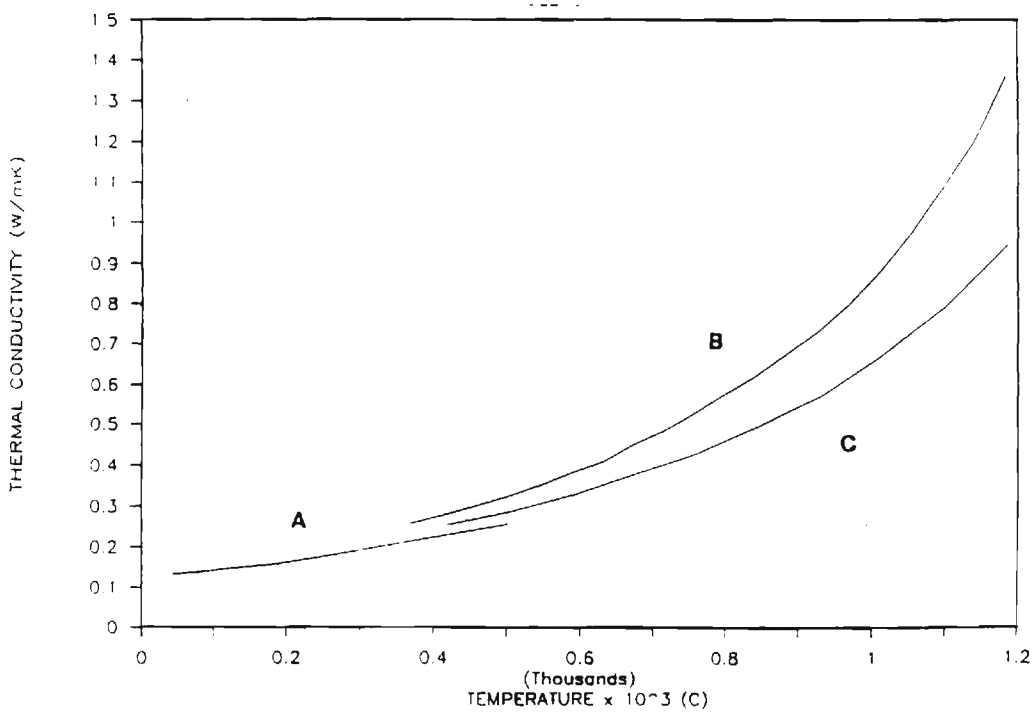

Figure 2. Thermal Conductivity of Random Packed Mullite Spheres; A. Previous ORNL Data, B. GA Tech Data and C. Spheres with Thermal Pores.

2. W.J. Drury, S.A. Rickles, T.H. Sanders, J.K. Cochran, "Deformation Energy Absorption Characteristics of a Metal/Ceramic Cellular Solid," Proceedings of TMS Conference on Light Weight Alloys, TMS Annual Meeting, Las Vegas, Nevada, February 1989.

B. In Progress

1. Thermal Conductivity of Thin-Wall Spheres
2. Mechanical Strength of Thin-Wall Spheres
3. Rheology of Ceramic Powders Dispersed in Liquids

C. Thesis Completed

M.K. Adicks, "Strength Characterization of Thin-Wall Hollow Ceramic Spheres From Slurries", M.S. Thesis, Georgia Institute of Technology, Atlanta, GA, May, 1989.

T.J. Hwang, "A Model for Viscosity of Organic Based Oxide Dispersions", Ph.D. Dissertation, Georgia Institute of Technology, June 1989.

D. Presentations

1. J.K. Cochran, S.F. Furlong*, M.J. Shapiro, A.T. Chapman and D.L. McElroy, "High Temperatures Insulation Capability of Thin-Wall Ceramic Spheres," XXI International Conference on Thermal Conductivity, Lexington, KY, Oct. 15-18, 1989.

2. S.A. Rickles, S.K. Cochran* and T.H. Sanders, "Compressive Strength of Metal-Aerosphere Composites," Annual Meeting Am. Cer. Soc., Indianapolis, IN April 23-27, 1989, paper 117-SI-89.

3. T.S. Hwang* and J.K. Cochran," BET Analysis of Absorption of PMMA on Oxides in Acetone," Annual Meeting Am. Cer. Soc., Indianapolis, IN April 23-27, 1989, paper 13-SIV-89.

4. T.S. Hwang* and J.K. Cochran, "Viscosity Model for Sterically Stabilized Organic Liquid Dispersions," Annual Meeting Am. Cer. Soc., Indianapolis, IN April 23-27, 1989, paper 39-SIVP-89.

5. J.K. Cochran*, A.T. Chapman and J.H. Chung, "Uniaxial Strength of Thin-Wall Ceramic Spheres," Annual Meeting Am. Cer. Soc., Indianapolis, IN April 23-29, 1989, paper 24-BP-89.

6. S.F. Furlong, "Thermal Conductivity of Aerospheres," Summer Meeting S.E. Section of Am. Cer. Soc., Boone, NC July 20-22, 1989.

7. T.J. Hwang, "Rheology of Organic Slurries", Summer Meeting S.E. Section of Am. Cer. Soc., Boone, NC July 20-22, 1989.

8. J.K. Cochran, "Hollow Insulating Ceramic Spheres - Aerospheres", USDOE, Building Retrofit Innovative Concepts Fair, Washington, D.C., Oct. 24, 1989.

COST INFORMATION

Project: Thin-Wall Hollow Spheres -
J.K. Cochran and A.T. Chapman

Reporting Period: Phase IIb and III (including FY 89)

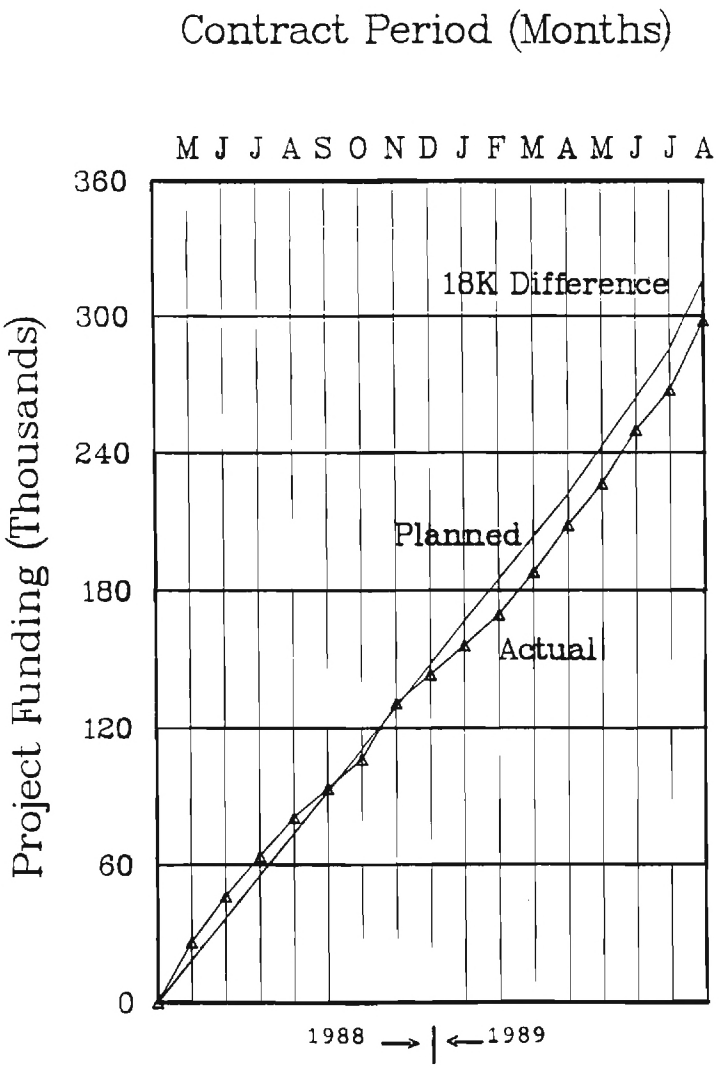

List of Investigators Participating in Project

Participation in days/week

Project: Thin-Wall Hollow Spheres from Slurries
J.K. Cochran and A.T. Chapman

Reporting Period: FY 89

	Name	Type of Position	Planned Project Time	Approximate Time FY 89	
A.	J.K. Cochran	Project Dir.	2	2	(40%)
B.	A.T. Chapman	Project Dir.	2	2	(40%)
C.	T.J. Hwang	Post Doctoral	5	5	
D.	J.H. Chung	Student	2-3	2.5	
E.	P.R. Chu	Student	2-3	2.5	
F.	S. Furlong	Student	2-3	2.5	
G.	C. Moore	Student	2-3[a]	2.5	

a. New student started work June 1989 on water-based dispersions.

GEORGIA TECH 1885-1985

DESIGNING TOMORROW TODAY

Georgia Institute of Technology
School of Materials Engineering
Atlanta, Georgia 30332-0245
(404) 894-

August 4, 1986

Ms. Patricia Wilson
Bldg. 4503, Room 204
Oak Ridge National Laboratory
P. O. Box X
Oak Ridge, TN 37831

Dear Patricia:

Enclosed is the Quarterly Report for ORNL Subcontract 86X-22043C covering the time period April 1 to June 30, 1986.

If there are questions, please give me a call. (404) 894-2851.

Sincerely,

A. T. Chapman
Professor

ATC/db

Enclosure

P.S. Would appreciate a supply of the typing photomaster sheets.

THIN-WALL HOLLOW CERAMIC SPHERES FROM SLURRIES

A. T. Chapman, J. K. Cochran, J. M. Britt, T. J. Hwang

School of Materials Engineering
Georgia Institute of Technology
Atlanta, GA 30332

(ORNL Subcontract 86X-22043C)

ABSTRACT

Work continued on the formation of hollow microspheres from slurries containing Al_2O_3 powders and binders dispersed in acetone. A facility to handle acetone-base systems was designed, constructed and tested. Preliminary evaluation of a variety of methods to recover free-falling spheres was performed. A systematic study of the parameters controlling sphere formation in acetone-based slips was initiated.

INTRODUCTION

The overall objective of this effort is to develop a process for economically fabricating thin-wall hollow ceramic spheres from conventional ceramic powders using dispersions. Thin-wall hollow ceramic spheres of small (.1-5mm) diameter might have numerous novel applications as high-temperature insulation or even lightweight structural materials.

Small solid spheres and, in a few cases, even thin-wall hollow spheres of ceramics have been made either from the melt or through solgel processes. This limits the production to either the lower temperature melting ceramics, such as glass, or those that can be made from solutions,

such as alumina. Small diameter spheres of SiC or Si_3N_4 have not been made. The basic approach in the present work is to use a recently developed and patented process whereby the sphere can be made from powder dispersions or slurries, thereby permitting the use of any ceramic. Work was initiated 1 February 1986.

In the last quarterly report the initial evaluation of the sphere forming characteristics and drying behavior of acetone-based slurries was described. Dispersion of ceramic powders in organic liquids is attractive because these fluids possess a higher vapor pressure, smaller heat of evaporation, less tendency to foam and reduced weight compared to aqueous systems. This reporting period a facility was designed and constructed to handle acetone-base slips for the blowing of microspheres using the coaxial nozzle configuration. The prospects of immediately capitalizing on the favorable evaporation properties of acetone was evaluated in a series of drying and collection experiments. A systematic study of the parameters controlling sphere formaton was initiated. The following sections describe the significant findings during this reporting period. Some of the conclusions and observations reported must be tentative because of the complex nature of the microsphere forming and drying process. Much of the present effort is intended to establish limits of process variables where identical microspheres can be reproducibly made. Some very uniform samples were produced during these trials and representative pictures of the resulting microspheres are included.

DISCUSSION OF CURRENT ACTIVITIES

Facility for Handling Acetone-Based Slurries

One of the major problems using acetone-base slips results from the high fluid evaporation rate. It is

difficult to prevent clogging in slip delivery lines, as well as the coaxial sphere forming nozzle. The system shown in Figures 1 and 2 was constructed to control slip delivery, cell pressurization and inner jet flow to the coaxial nozzle assembly. Several reservoirs and associated plumbing were added to independently flush various sections of the system with acetone. In addition, a small refrigeration unit was also incorporated in the facility to provide cooling for the blowing nozzle to retard the rate of acetone evaporation from the slip.

Slurries containing Al_2O_3 powder*, methyl methacrylate** and acetone were blown in the facility shown in Figures 1 and 2 and most of the sphere collection trials, described in the next section, were also conducted using this equipment. Three major problems were encountered using this facility:

1. The horizontal slip transfer lines eventually clogged despite repeated acetone flushes after each run.
2. The pure acetone flushes occasionally needed to remove clogging or restrictions in the concentric nozzle during an experiment, changed the rheology of the slip and concurrently the sphere forming characteristics.
3. A build-up and growth of dried slip would slowly form as the slurry exited the nozzle. Subsequent experiments demonstrated that reducing slip temperature was somewhat effective in minimizing this build-up. Increasing the flow velocity of the slip through the nozzle and/or providing a saturated acetone atmosphere surrounding the nozzle are also alternatives to impede the build-up of solid material at the exit of the nozzle.

As a consequence of the equipment construction and evaluation performed this work period , a "disposable"

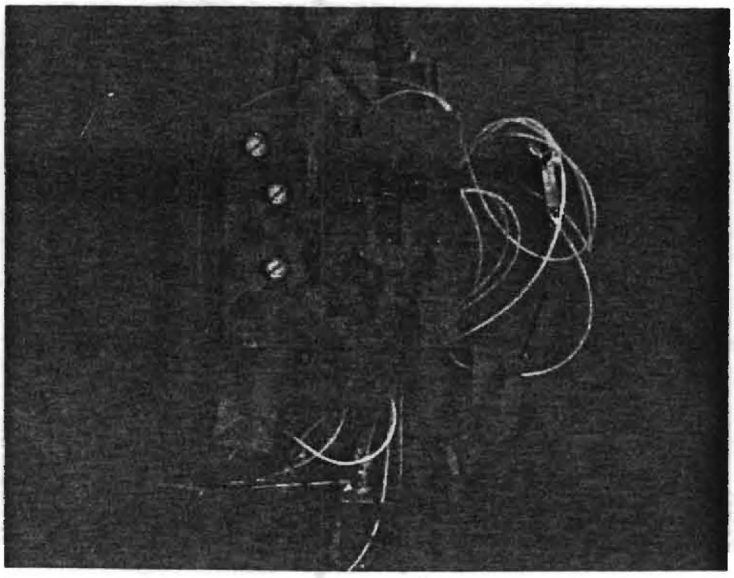

Figure 1 Slurry Delivery Facility for Acetone-base Systems showing controls for coaxial nozzle, and acetone flushing system.

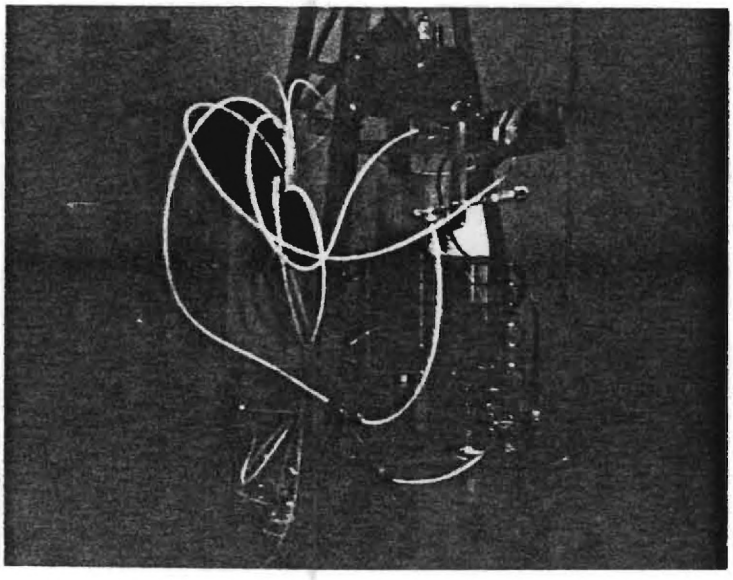

Figure 2 Front view of Facility to handle acetone base slurries showing refiguration unit and copper heat sink for cooling slip in the nozzle assembly.

system containing inexpensive "throw-away" plastic tubing and reservoir jars is being evaluated as the appropriate system for this research work, where frequent changes of processing variables are necessary.

Preliminary Drying and Collection Trials

Using the sphere forming equipment described in the preceeding section a series of very preliminary drying and collection experiments were performed on streams of free-falling microspheres containing alumina powder and methyl methacrylate binder dispersed in acetone. The merits of organic fluids, such as acetone, was readily apparent. Water-base spheres splattered on impact on a soft landing surface after 30 to 40 feet of free-fall; whereas, similar acetone-base bubbles bounced. This behavior immediately suggested the recovery of the partially dried bubble streams using a variety of methods. The bubble streams were first deflected off inclined planes and curved surfaces to lessen impact after free-fall. Air blowers and fans were employed to direct the spheres nearly horizontal for roll-out on flat surfaces. Various forms of fluidized beds and a transvector device (using compressed air to provide air cushion to transport light weight items) were tested to increase the bubble residency time before impact and recovery. All of the spheres collected using these approaches experienced damage on collision with adjacent spheres and/or impact with a solid surface. Most of the samples also possessed stringers or tails of various length. In an effort to completely dry the spheres the sphere streams were dropped through the 2 ft. tall focused infrared furnace operating above 1000°C. The spheres were heated ~10°C above room temperature during travel through the furnace. Dimpling and damage to the

sphere surface was still present after employing various collection modes below the furnace, although the degree of sphere damage was somewhat less than observed using collection without the furnace heating.

Significant observations noted during these collection trials include:

1. The high evaporation rate of acetone enhanced drying of spheres and also gave more stability to the stringers initially formed between the spheres.
2. The sphere forming process inherently produces thicker walls at the poles of the spheres and rapid drying tends to preserve this wall variation.

The formation and recovery of spheres constitutes two distinct processes. During sphere formation (SF) the slip viscosity must remain low to facilitate sphere-tail separation and achieve wall uniformity. During sphere recovery (SR) the loss of fluid and concurrent strength development must occur such that the sphere can survive some type of landing and recovery process. Obviously slurry composition and blowing conditions impact both formation and recovery. In spite of these problems, the acetone-based slips have run continuously forming identically shaped and spaced spheres for periods greater than 80 minutes (terminating only when the slip reservoir emptied) showing the process can run almost indifinitely if slip is continuously provided to the nozzle.

The experience gained during these preliminary drying and collection experiments suggested a more systematic study is needed of the major parameters controlling sphere formation and recovery. The following section describes our initial efforts to evaluate the parameters controlling sphere formation using acetone-base slurries.

Systematic Analysis of the Microsphere Forming Process

A systematic study was initiated to establish the critical parameters controlling the sphere formation process in acetone-based dispersions. First and foremost acetone evaporation must be retarded initially to prevent dried slip build-up as the slurry exits the nozzle, to maintain the necessary elasticity of the fluid for sphere formation without "blow-out" through the wall and to minimize the size and extent of tail formation. The variables though most important, at present, include:

1. Slip viscosity
2. Concentration of acetone vapor surrounding the forming spheres
3. Slip temperature
4. Slip flow rate through the nozzle

The influence of these variables is being studied using a video camera and tape recorder for continuous filming of the runs along with conventional analysis of dried and fired product. To date forming spheres using comparatively low viscosity slip in a chamber saturated with acetone vapor has produced the most uniformly spherical product. Under some conditions the stringer connecting the spheres initially have detached, and sphereodized within the acetone chamber, appearing as small satellites exiting the chamber with the larger hollow spheres. An example of the stream geometry achieved in the acetone chamber is shown in Figure 3. The "as recovered" spheres from a run incorporating the saturated acetone chamber to minimize the extent of remnant tails are shown in Figure 4. The major damage and indentations of these bubbles resulted on impact(s) during collection of partially dried material. Samples of the "best" product from similar experiments are shown in Figure 5. A well formed broken sphere representative of typical wall thickness and uniformity is displayed in Figure 6.

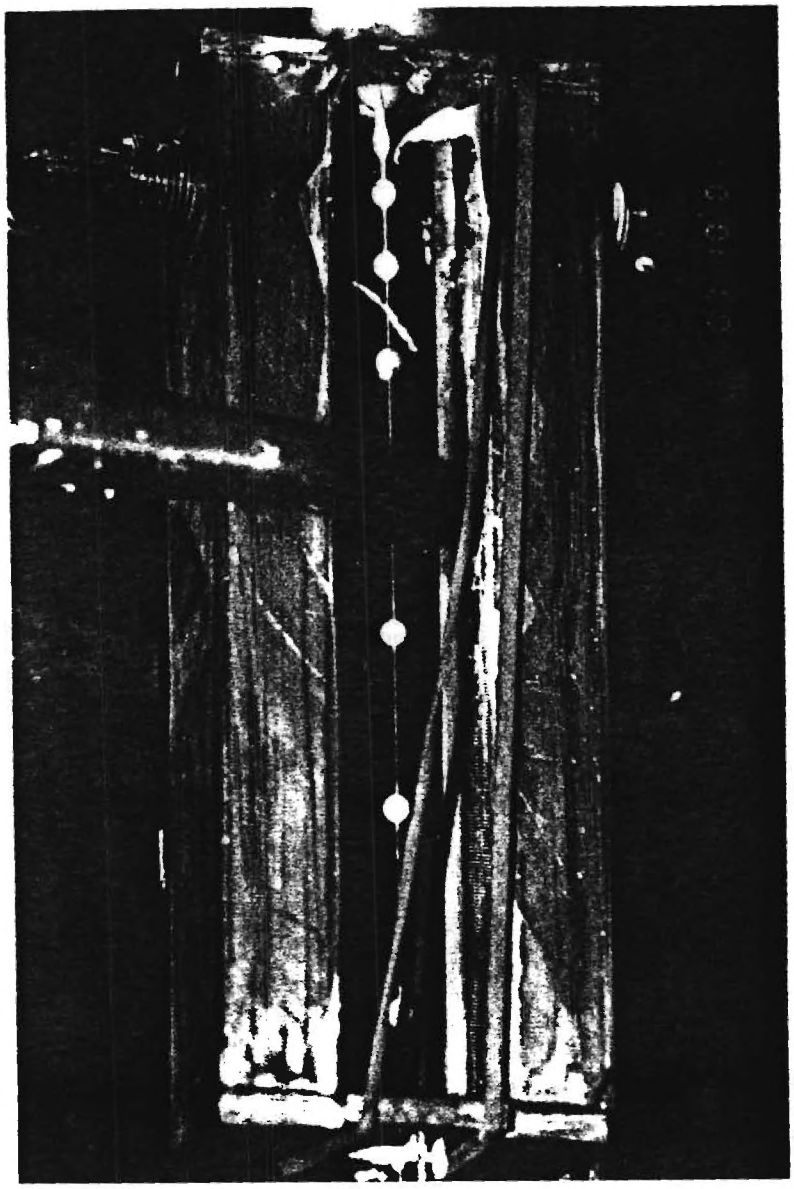

Figure 3 Stream of Al_2O_3 microspheres exiting nozzle into saturated acetone atmosphere containment chamber. Note the high degree of spheroidicity achieved in the chamber and the very thin connecting tail between spheres at the exit of chamber.

Next reporting period the analysis of the sphere forming process will continue and several of the more promising recovery methods will be refined to assess their potential for recovery of a dimple-free product.

* Alcoa - Grade XA3000

** Dupont - "ELVACITE" Acrylic Resins - Grade Numbers; 2041 and 2008

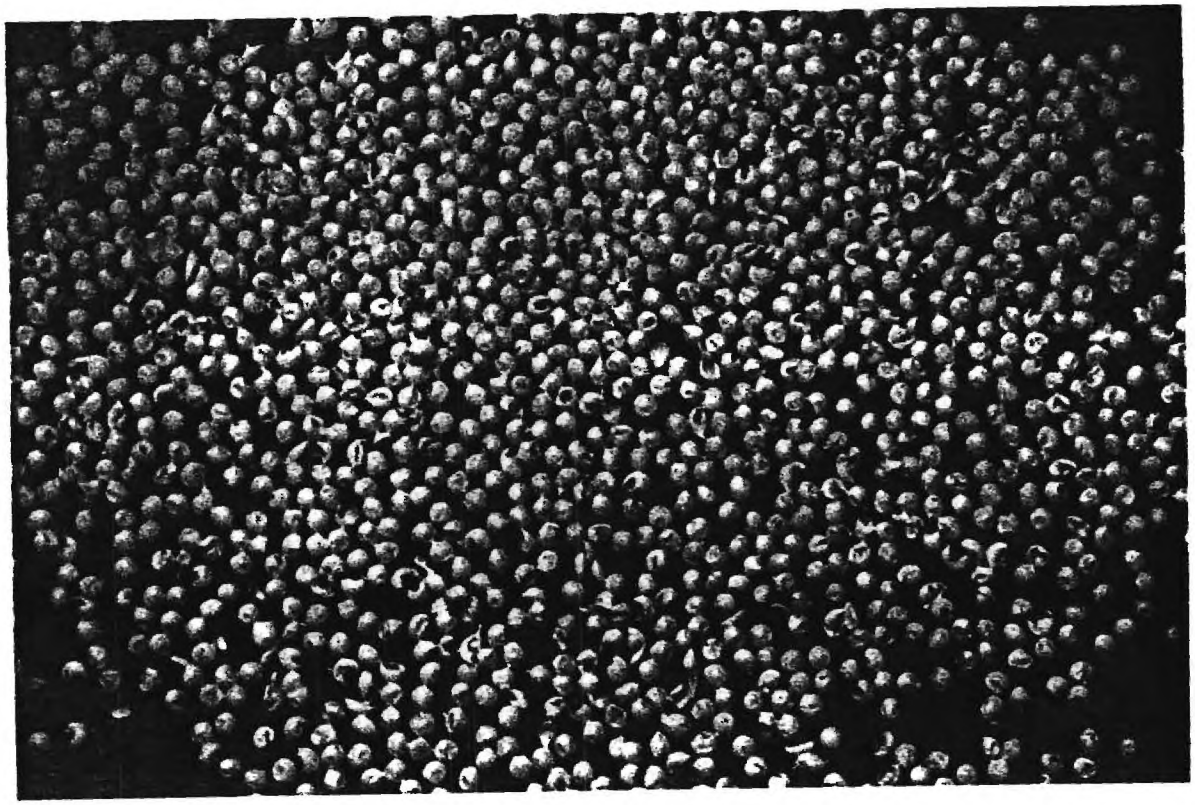

Figure 4 Unsorted fired 3 mm diameter Al_2O_3 spheres blown into acetone chamber and recovered using hot air gun. Note the almost total absence of tails; Most of the damage, bruising and breakage occurred during collection.

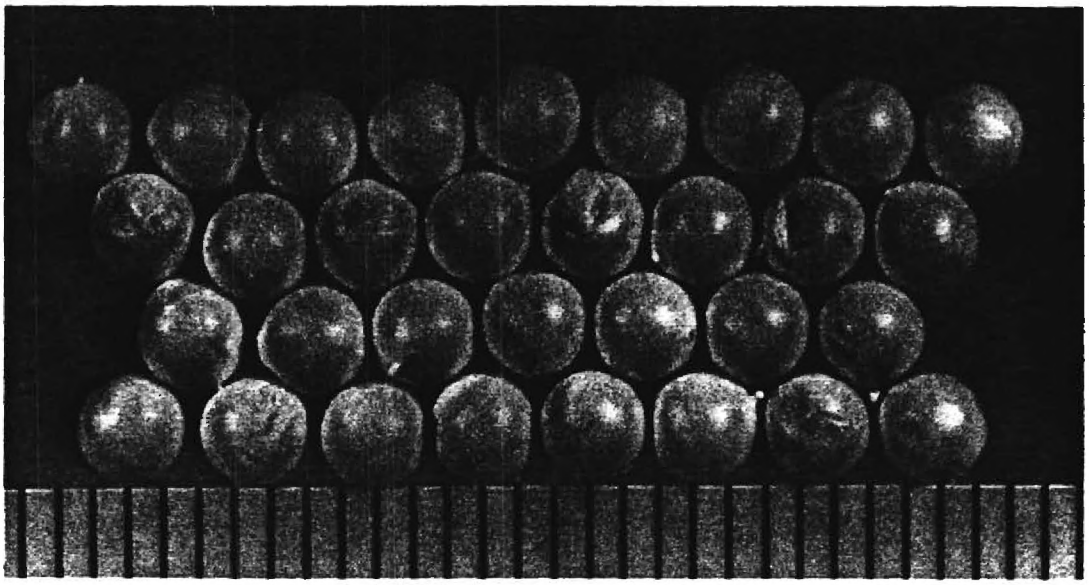

Figure 5 Hand selected 3 mm diameter fired Al_2O_3 spheres showing size uniformity, small remnants of the tails and limited damage.

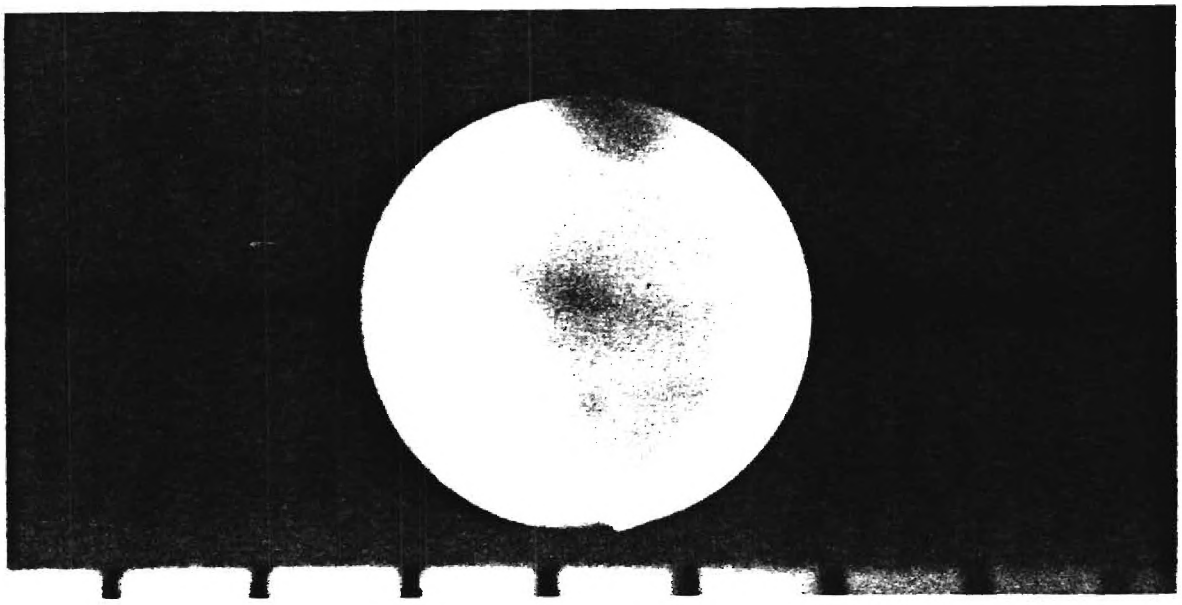

Figure 6 Fractured 3 mm diameter sphere displaying wall thickness and uniformity.

E-18-616

12/10/85

Revised
4/6/87

Revised
4/26/89

STATEMENT OF WORK

Fabrication of Thin Wall Hollow Ceramic Spheres

Introduction

The overall objective of this effort is to develop a process for economically fabricating thin wall hollow ceramic spheres from conventional ceramic powders using dispersions. Thin wall hollow ceramic spheres of small (.1—5mm) diameter might have numerous novel applications as high temperature insulations or even lightweight structural materials.

Small solid spheres and, in a few cases, even thin wall hollow spheres of ceramics are and have been made either from the melt or through sol-gel processes. This limits the production to either the lower temperature melting ceramics such as glass or those which can be made from solutions, such as alumina, respectively; thus, for example, small diamter spheres of SiC or Si_3N_4 have not been made. The basic approach in the present work is to use a recently developed and patented process whereby the sphere can be made from powder dispersions or slurries, thereby permitting the use of any ceramic.

R-Revised
N-New
D-Deleted

Current technology is based on the Torobin coaxial nozzle process in which a rheologically controlled disperison is fed through an outer, downward-pointing nozzle while gas is forced through an inner nozzle. A tear-shaped droplet first forms which, as it descends in free space, tends to dry and harden and become more and more spherical. Currently, the drying is so slow however that by the time the droplet reaches the bottom of the free fall space and hits the collector, it is not fully hardened nor perfectly spherical; this results in a hollow particle with one flattened side and one pointed side. The nearest term objective, then, is to develop a process for fabricating nearly spherical thin wall hollow spheres of small diameter; this is the point of Phase I below. In Phase II the objective is to characterize process variables and in Phase III the objective is to measure the properties of the spheres.

Technical Tasks

Phase I. Process Development

A process for producing thin wall hollow ceramic spheres from alumina (Al_2O_3) based slurries shall be developed. The process shall be capable of handling slurries, with viscosities ranging from at least 20 poise to 200 poise at room temperature. The process shall be capable of producing spheres at least 2 to 6 mm in diameter with wall thicknesses 12 to 100μm at rates no less than 30 spheres per second. All spheres shall be spherical such that both the inside and outside diameters of all spheres are

within 2% of the means of 100 randomly selected spheres as measured by optical microscopy. All spheres shall have a size distribution such that 99% have an outside diameter ± 10% of the mean of 100 spheres from each batch, also as measured by optical microscopy.

Phase II. Investigation of Process Parameters

R
4/6/87

The main objective of this phase is to assess the potential of thin wall hollow ceramic spheres as structural and insulating materials.

Phase II.a Assessment of Applications Potential

Task 1. Assessment of Structural Potential

Models shall be used to calculate the ranges of stiffness and strength possible for the thin wall hollow ceramic spheres as individuals and as loose and bonded packed beds. If possible, models shall also be developed to predict the energy absorption properties.

For individual spheres, the three properties shall be calculated for the cases of isostatic tensile and compressive loadings and uniaxial compressive loadings. The sphere parameters to be varied shall include outside diameter, wall thickness, spheroidicity (degree of roundness) and surface roughness of the sphere; stiffness, strength, Poisson's ratio and, if possible, toughness of the wall materials; and ambient (room temperature) pressure differential between the inside and outside of the sphere. These parameters shall be varied in ranges to be specified in consultation with the ORNL technical monitor.

For packed beds of the spheres, the three properties shall be calculated for the case of uniaxial compressive loading with and without side support of the bed. In addition to the sphere parameters above, the packing density of the bed, assuming uniformly sized spheres, shall be varied between the extremes of random loose fill and close packing. For the case of close packing, the direction of application of force on the bed shall also be considered. The two cases of perfect non-bonding (i.e. frictionless) and perfect bonding (infinite friction) between the spheres shall be considered. If possible, effects of filling the interstitial spaces between the spheres with smaller solid or hollow spheres or continuous matrix materials shall also be modeled. The properties of the interstitial spheres and matrix materials will be specified in consultation with the ORNL technical monitor.

Selective experimental measurements shall be made in order to verify or calibrate the models. The exact number and nature of the measurements shall be decided in consultation with the ORNL technical monitor based upon the predictions of the models.

Task 2. Assessment of Insulation Potential

The Seller shall prepare and supply to ORNL thin wall hollow ceramic spheres of various compositions, sizes and wall thicknesses, to be specified in consultation with the ORNL technical monitor based on modeling performed by ORNL, for measurements at ORNL of the thermal conductivities of packed beds of the spheres. Seller shall also provide personnel to ORNL to assist with the modeling and thermal conductivity measurements.

Task 3. Identification of Possible Specific Applications

Seller shall contact industrial firms and other government sponsors in order to identify possible specific applications of the spheres and, upon approval of the ORNL technical monitor, prepare and provide limited quantities of spheres for testing by the industrial firms or government sponsors.

Phase II.b. Sphere Production Studies

Task 1. Modeling of Process

In support of Tasks 1 and 2 of Phase II.a, the Seller shall attempt to model the process and parameters controlling the sphere formation from powder slurries blown with the concentric nozzle assembly. Emphasis shall be placed on establishing the parameters that dictate the probable upper and lower limits of diameters and wall thickness that can be expected from this technology.

Task 2. Geometry Studies

The Seller shall conduct a systematic study of process parameters according to a test matrix to provide data on sphere diameter, wall thickness, wall thickness variability, and production rate using alumina-based dispersions as functions of slip rheology, and nozzle geometry and sphere forming conditions. The slip rheology variables will be viscosity, solids content and organic additives. Nozzle geometry variables will be dimensions of the inner jet and liquid delivery cylinder. Sphere forming conditions to be varied shall include slip flow rate and blowing gas flow rate.

Task 3. Properties Studies

Based on knowledge gained in Task 1 and 2 above, attempts shall be made to produce spheres with properties indicated by the tasks in Phase II.a.

Phase III-A. Investigation of Thermal Conductivity of Thin-Hollow Ceramic Spheres

N

Introduction 4/26/89

The object of this phase is to demonstrate that by properly opacifying sphere walls with efficient infrared wavelength scattering centers, high temperature thermal conductivity for the hollow spheres will be significantly reduced compared to the same spheres without opacified walls.

This work shall determine the effects of opacifying structures or phases on slurry rheology, sphere forming capability and mechanical strength of the spheres. In addition the effect of the opacifying structures or phases on thermal conductivity of the thin walled spheres shall be determined.

The seller shall optimally design a radiation scattering system considering the following:

1. Optimum Ratio of Opacifier Size to Radiation Wavelength,
2. Relative Index of Refraction of the Opacifier and Sphere Wall,
3. Wavelength Range of Radiation to be Scattered vs Temperature,
4. Refractive index of Scatterers and Wall Over the Wavelength Range,
5. Absorption of Scatterers and Wall Over the Wavelength Range,
6. Quantity of Scatterers Needed for Optimum Effect, and
7. Thermal Stability of the system. 1

Task 1. Development of Slurry Rheology

The seller shall modify the presently used acetone based slurries. Both Zr_2O and carbon additions to alumina and mullite slurries shall be performed: (a) Zr_2O possesses a large density difference from each of the base compositions thus, the affects of settling rates shall be determined; (b) a dispersant for carbon in acetone shall be found. Slurries of the base compositions without opacifiers shall also be prepared.

Task 2. Formation of Spheres

The seller shall produce thin wall spheres of the same diameters and densities from the different slurries to allow for the comparison of the thermal conductivity of spheres of different composition.

Task 3. Thermal Conductivity Analysis

The seller shall measure the thermal conductivity of the spheres with and without scattering centers from room temperature to 1300°C in a radial heat flow apparatus. Analysis of the data with respect to the size distribution of the scattering medium shall be performed. The development of analytical models for thermal conductivity of beds of spherical shells and comparisons of theory with experimental results shall be completed.

Task 4. Effect of Scattering Centers on Sphere Strength

The seller shall measure the uniaxial crush strength for spheres with and without scattering structures or phases. The suitability of crystalline phases versus pores shall be delineated.

Phase III-B

The development of opacified spheres of different matrix compositions shall continue. In addition slurry rheology shall focus on a water based system rather than an acetone based system. This will require much further development for the base matrix materials of Al_2O_3, Mullite, glass, clay based ceramics, amorphous SiO_2 and Zirconia. In addition development of nonoxide thin wall spheres shall commence considering both the water and acetone based routes. Carbides and nitrides shall be the first materials to be developed.

REPORTING REQUIREMENTS

Bimonthly progress reports, a summary report on each phase and any reports submitted as specified to R 4/26/89

Dr. Peter Angelini
Manager
ECUT Materials Program
Oak Ridge National Laboratory
P. O. Box 2008
Building 4515, MS 6065
Oak Ridge, Tennessee 37831

or as otherwise designated by the ORNL technical monitor.

1. Bimonthly Progress Report

Bimonthly reports on the status of the work and any significant results shall be submitted by close of business on the fifteenth day, or the first working day thereafter, of the month following the close of the two month reporting period in which the subcontract is active. In addition, an annual progress report and an annual technical report shall be supplied at least one week prior to the end of this subcontract.

E-78-610
1st Quarterly -
Jan-86 thru Mar 31-86

Bull Proof -

THIN-WALL HOLLOW CERAMIC SPHERES FROM SLURRIES

A. T. Chapman, J. K. Cochran, J. M. Britt, T. J. Hwang

School of Materials Engineering
Georgia Institute of Technology
Atlanta, GA 30332

(ORNL Subcontract 86X-22043C)

INTRODUCTION

The overall objective of this effort is to develop a process for economically fabricating thin-wall hollow ceramic spheres from conventional ceramic powders using dispersions. Thin-wall hollow ceramic spheres of small (.1-5mm) diameter might have numerous novel appliations as high-temperature insulation or even lightweight structural materials.

Small solid spheres and, in a few cases, even thin-wall hollow spheres of ceramics have been made either from the melt or through solgel processes. This limits the production to either the lower temperature melting ceramics, such as glass, or those that can be made from solutions, such as alumina, respectively; thus, for example, small diameter spheres of SiC or Si_3N_4 have not been made. The basic approach in the present work is to use a recently developed and patented process whereby the sphere can be made from powder dispersions or slurries, thereby permitting the use of any ceramic. Work was initiated 1 February 1986.

DISCUSSION OF CURRENT ACTIVITIES

Microwave Heating

At the out set of this program methods to form thin-wall Hollow spheres from a variety of conventional ceramic powders dispersed in fluids had been demonstrated. The immediate objective was to evaluate means to dry, recover and collect moisture laden free-falling spheres. The initial approach considered most attractive for water-based

systems was the direct internal heating of the water containing spheres using microwave energy. Accordingly several suppliers of industrial microwave equipment were contacted to review the prospects of effectively heating and drying a stream of widely seperated hollow spheres. The Microdry Corporation of San Ramone, CA reviewed this geometry for microwave drying and expressed some concern over the very low material density in the microwave chamber. In an effort to evaluate the efficiency of microwave heating as a function of size, Microdry personnel ran a short series of experiments using their 6,000 watt generator radiating into a wave guide about 2" x 4" in cross section. They inserted a water soaked cardboard sample, 6" long and 4" wide, aligned with the axis of the wave guide and operating at full power. The water "boiled" in 3 seconds. However, when the same size cardboard, containing only several drops of water several centimeters apart was inserted in the wave guide no detectable heating was observed even after exposure to the microwave energy for three minutes. Obviously widely dispersed millimeter size samples are essentially transparent to the centimeter long microwaves and almost no absorbtion of energy occurred. Similar experiments comparing heating rates of thimbles vs. cups of water in a conventional home microwave oven yielded similar results, although not nearly as dramatic as observed in a high power wave guide.

Methods for increasing the microwave heating efficiency of widely dispersed small volumes of water are currently being considered. Increasing the frequency would decrease the wavelength of the microwave energy to the millimeter range and increase coupling efficiency. However, this

change results in a great reduction of the continuous power available because of dimensional constraints in the oscillator tube. Alternatively, the use of a resonant or tuned chamber operating at the conventional microwave frequency of 455 Mhz to greatly increase the power density within the enclosure, is also being explored.

Resistive Heating

Several methods designed to increase the temperature of water-based dispersions prior to blowing spheres and during free-fall were also examined. The most expedient method to increase the slip temperature would be to heat the nozzle and supply vessel using conventional heating tapes. This approach was tested and the water-based dispersions could be readily formed into spherical geometries at temperatures up to ~90°C; however, in the higher temperature range, above 80°C, the increased evaporation rate led to skinning and some clogging of the blowing nozzles.

Radiant Heating

In an effort to assess the potential of conventional radiant heating to increase the temperature of a stream of free-falling spheres, a Model 4-25 Infrared Heater was obtained from Energy Systems Division of Research Inc. This furnace focuses 10,000 watts of radiant energy into a column about 1/2" in diameter by 25 inches in length. A stream of water-based spheres was dropped thorugh this furnace operating at full power and a 20°C raise in slip temperature was recorded. This test was performed with the furnace about one foot below the nozzle and the residence

time in the furnace was much greater than that available when the spheres reach terminal velocity (~4 cm/sec) several feet below the nozzle. A combination employing heated slips falling through conventional radiant and convection energy furnaces remain a potential method for drying spheres formed from water-based slips.

Free-Fall Behavior

The first extensive examination of the free-fall characteristics of the spheres was performed by blowing Al_2O_3 spheres and allowing them to free-fall ~40 feet. The spheres were examined at various levels during their free-fall using strobe light. Somewhat suprisingly the very "in-line" nature of the stream rapidly diverged after falling about 10 feet and, at impact 30 feet later, the spheres had dispersed to land in a circle ~3 feet in diameter. Apparently normal aerodynamic forces and the wake trailing the individual bubbles generate enough turbulence, even in a relatively closed area, to scatter the bubbles and result in a wide landing area. Consequently the prospects of keeping the spheres "in-line" and off the walls of a coventional wave guide, approximately 2 by 4 inches in cross section, or on the center line of a infrared focussed furnace for any extensive distance may be impossible. This problem would be further compounded during heating by the resulting convective air currents. More encouraging was the visual observation that the degree of spheridicity of the bubbles was almost identical at all levels of observation prior to impact.

Acetone-based Dispersions

Many additional drying schemes and slip compositions are potentially useable to provide more residence time, decrease drying time and provide softer landing of the spheres. The dispersion of powders in high volitility organic fluids is very attractive for serveral reasons. For example, acetone has a significantly greater vapor pressure and a much smaller heat of vaporization than water, the major factors controlling rate of fluid removal from the spheres. In addition, organic liquids typically have lower surface tension than water and, hence, should readily form the films required to produce the thin-walled structures.

Lastly the density of acetone is less than water and the weight of the sphere in free fall is somewhat reduced. Very preliminary testing of Al_2O_3 powders dispersed in acetone demonstrated that a very uniform stream of spheres could be produced for short periods at room temperature, although the high fluid evaporation rate lead to clogging of the blowing nozzle (analogous to the behavior of the water-based systems at 80°C and above). Additional work with the acetone slip is planned because of this very encouraging performance. A system to handle the acetone slips and provide temperature control of the nozzle (to remedy the nozzle clogging problem) are being designed and will be described next reporting period.

THIN-WALL HOLLOW CERAMIC SPHERES FROM SLURRIES

A. T. Chapman, J. K. Cochran, J. M. Britt, T. J. Hwang

School of Materials Engineering

Georgia Institute of Technology

Atlanta, GA 30332

(ORNL Subcontract 86X-22043C)

INTRODUCTION

The overall objective of this effort is to develop a process for economically fabricating thin-wall hollow ceramic spheres from conventional ceramic powders using dispersions. Thin-wall hollow ceramic spheres of small (.1-5mm) diameter might have numerous novel applications as high-temperature insulation or even lightweight structural materials.

Small solid spheres and, in a few cases, even thin-wall hollow spheres of ceramics have been made either from the melt or through sol-gel processes. This limits the production to either the lower temperature melting ceramics, such as glass, or those that can be made from solutions, such as alumina. Small diameter spheres of SiC

or Si_3N_4 have not been made. The basic approach in the present work is to use a recently developed and patented process whereby the sphere can be made from powder dispersions or slurries, thereby permitting the use of any ceramic. Work was initiated 1 January 1986.

At the outset of this program a method to form thin-wall hollow spheres from a variety of conventional ceramic powders dispersed in water had been demonstrated. The immediate project objective was to evaluate means to dry and recover the moisture-laden free-falling spheres. A variety of methods were considered including; microwave drying, hot air furnaces and direct infrared radiant heating. The microwave drying approach was considered most attractive because the energy would be absorbed directly in the walls of the spheres. Several suppliers of microwave drying equipment were contacted and a series of experiments were performed to assess the feasibility of drying the free-falling thin-wall spheres with microwave energy. Unfortunately the small volume occupied by the widely spaced spheres resulted in ineffective heating using conventional microwave frequencies and waveguides.

Alternative drying schemes were reconsidered along with process and compositional changes that would provide faster drying for the free-falling spheres. The dispersion of powders in a high volatility organic fluid is attractive

for several reasons. For example, acetone has a much larger vapor pressure, smaller heat of vaporization, and a lower surface tension and density than water. Initial testing of Al_2O_3 powders dispersed in acetone demonstrated that a very uniform stream of spheres could be produced for short periods at room temperature, although the high fluid evaporation rate lead to clogging of the sphere blowing nozzle. An acetone slip handing system was designed and constructed containing a small refrigeration unit to provide cooling for the blowing nozzle (to retard the rate of acetone evaporation from the slip) and prevent clogging. In addition this facility controlled slip delivery, cell pressurization and inner jet flow to the coaxial nozzle assembly. Several acetone reservoirs and associated plumbing were added to independently flush various sections of the system. Extended use of this facility demonstrated that acetone flushes were inadequate to keep delivery lines open and served to unintentionally vary the rheology of the slip. This "fixed piping" facility has been replaced with inexpensive throw-away plastic tubing and reservoir jars.

The merits of dispersions made with acetone was readily apparent when water-based spheres splattered on impact on a soft landing surface after 30 to 40 feet of free-fall; whereas, similar acetone-based bubbles bounced. This behavior immediately suggested the recovery of the

partially dried bubble streams using a variety of methods including: slight deflection off inclined surfaces, horizontally blown spheres for roll-out on flat surfaces and heating using an infrared furnace. All of the spheres collected using these approaches experienced damage on collision with adjacent spheres and/or impact with a solid surface.

A newly designed updraft drying and recovery system consisting of a vertical tower, approximately 14 feet tall and 1 foot in diameter, combined with an air blower and sphere forming nozzle assembly has been constructed and tested. When the updraft air velocity and sphere diameter and weight are properly balanced, the residency time for adequate drying (4 to 5 sec) can be maintained in this tower and a "soft loading" achieved without mechanical damage. Recent runs using this facility have produced the best defect-free high strength thin-walled Al_2O_3 spheres achieved to date.

CURRENT ACTIVITIES

The major effort this reporting period (July thru September 1986) has been: 1) the analysis of the rheology of the alumina/acetone dispensions containing varying amounts of methylmethacrylate acting as disperants and binders, and 2) the continuing evaluation of a variety of sphere recovery methods. The following sections describe

the procedures and terminology used to characterize the pseudoplasticy and Neutonian behavior of the acetone-based slip, the influence of the organic binder on slip rehology and, lastly, the latest recovery system that has yielded virtually "flaw-free" high strength thin-walled Al_2O_3 spheres.

Characterization of Acetone-based Dispersions

The rheology of alumina/acetone slips has been investigated to provide suitable dispersions for production of hollow polycrystalline spheres. It is necessary that the alumina powder be well dispersed to yield a reproducible process and to permit a high solids volume content which minimizes the quantity of solvent to be removed. In addition, the slips must possess a viscoelastic character sufficient for blowing and the hollow spheres formed must be strong enough for recovery. For these purposes, methylmethacrylate DUPONT Elvacite, resins are added to the dispersions. Elvacite #2008 was added as a dispersant and a binder, while #2041 served as a binder and a rheology modifier. To characterize the rheology of these dispersions, the viscosity was measured with Brookfield LV Viscometer at a shear rate between 0.1-50 sec^{-1}.

Due to the use of organic polymers, the dispersions exhibit pseudoplasticity. This property can be described

by the power law (also known as Ostwald-deWaele equation).

$$\tau = K\gamma^n \qquad (1)$$

where τ is shear stress, γ is shear rate, K is the consistency index and n is the flow behavior index. The value of n is less than 1 for pseudoplastic flow, and decreases as the degree of pseudoplasticity increases. If n is close to 1, the liquid is Newtonian. The power law equation can be related to viscosity, η, by:

$$\eta = K\gamma^{(n-1)} \qquad (2)$$

Transformed for linear plotting, this equation is rewritten as

$$\log \eta = \log K + (n-1) \log \gamma \qquad (3)$$

The value of γ is not accurately known since γ varies with distance from the rotating spindle thus causing a variation of γ, for non-Newtonian liquids. However, to a first approximation, γ can be treated as in a Newtonian liquid so that

$$\gamma = \frac{2\pi rR}{dr} = 2\pi R, \qquad (4)$$

where r is the radius at which γ is desired to be known, and R is the rotational speed of the spindle. Therefore equation (3) can be transferred to

$$\log \eta = \log K + (n-1) \log 2\pi + (n-1) \log R \qquad (5)$$

The rheology of additional alumina/acetone slips as well as additional ceramic materials will be studied by characterizing η and n for various compositions in order to improve the quality of the thin walled spheres.

Slip Viscosity Measurement Procedures

As stated above, the materials used for slip preparation were ALCOA XA-3000 Al_2O_3, acetone, plus Elvacite 2008 and Elvacite 2041. Used as a slip casting alumina, XA-3000 Al_2O_3 powder has a mean particle size of 3 μm, and a broad particle size distribution designed for slips. Elvacite 2008 is a low molecular weight binder and dispersant, which provides low viscosity at high solids content. Elvacite, 2041 is a very high molecular weight binder which increases viscosity with small additions.

The dispersions investigated had a fixed Al_2O_3 content of 51v/o based on the acetone plus alumina volumes. The slips were designated according to type of powder, solvent, and weight concentration of polymers based on powder content, i.e. A-A-0.6 indicates Al_2O_3 as the powder, acetone as the solvent, and 0.6 w/o of 2008, or A-A-1.2-0.67 indicates the same powder and solvent, but 1.2 w/o of 2008 and 0.67 w/o of 2041.

After weighing, Al_2O_3, acetone and 2008 were mixed by rolling in a polyethylene jar on a ball mill rack at 70-90 RPM for 24 hours. Then 2041 was added to the slip if

needed and milled for an additional 24 hours. Viscosity was measured with a Brookfield LV viscometer using proper spindles at rotational speeds of 1.5 to 60 RPM.

Rheology Measurements of Alumina/Acetone Slips

The viscosities of dispersions were plotted as log η vs. log R as shown in Figures 1,2,3, and 4 in accordance with equation 5. All slips were pseudoplastic as shown by the negative slope, (n-1), in Figures 1-4. The flow behavior as indicated by n values, were calculated and are listed in Table 1 along with viscosities at 30 RPM. The effect of 2008 concentration on viscosity is shown in Figure 5. It can be seen that n values increase with 2008 concentration indicating that the slips approach a Newtonian fluid as the powder becomes well dispersed.

The curves in Figure 5 all show minimum viscosity around 1.7-2.0w/o 2008. This minimum point is indicative of monolayer adsorption of the polymer on the alumina particles. For slips without 2041 the increase of viscosity as the 2008 content was increased beyond the minimum may be due to excess 2008 going to solution. The rate of viscosity increase in this range should be equal to the rate of viscosity increase for a powder free 2008/acetone solution. Therefore, viscosities of 2008/acetone solutions were measured for comparison to slip viscosities, Table 2. A comparison between slips and

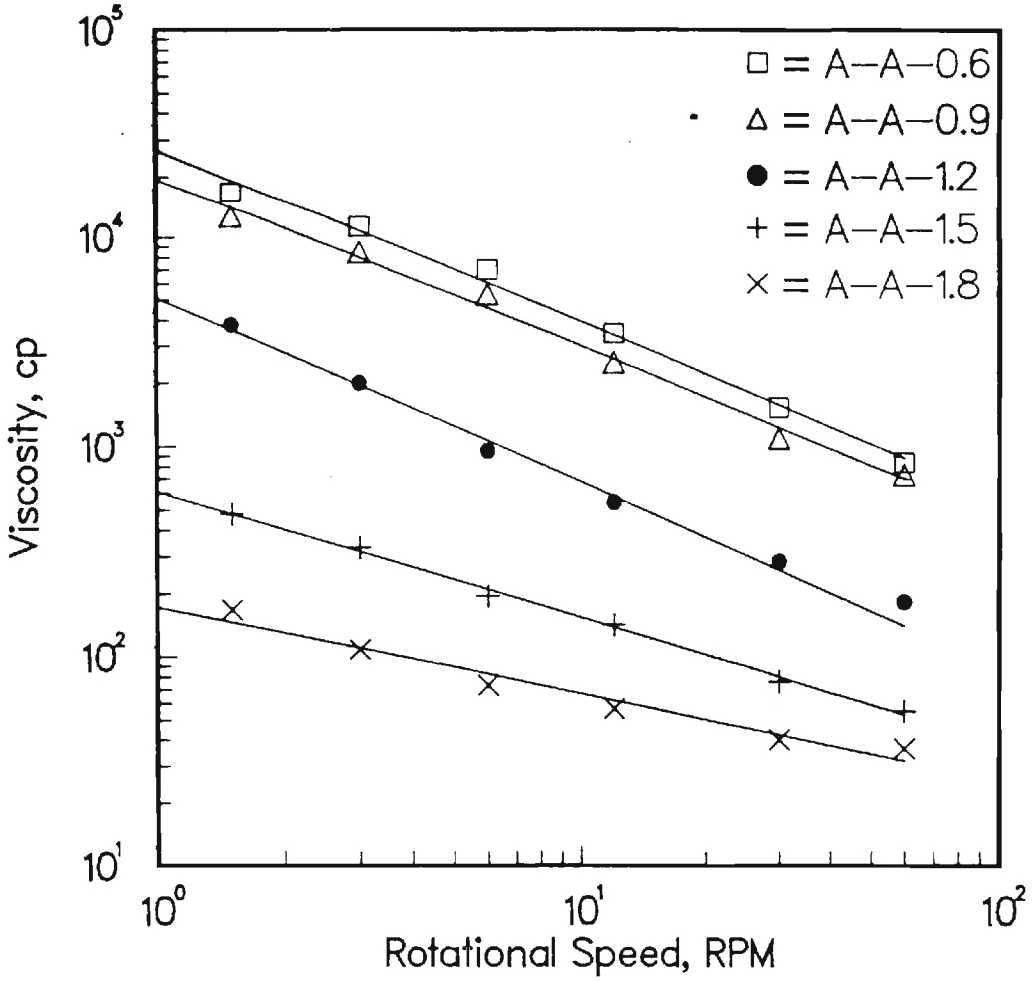

Fig.1. Viscosity of Alumina/Acetone Slips vs Rotational Speed for Various PMMA Concentrations of 2008

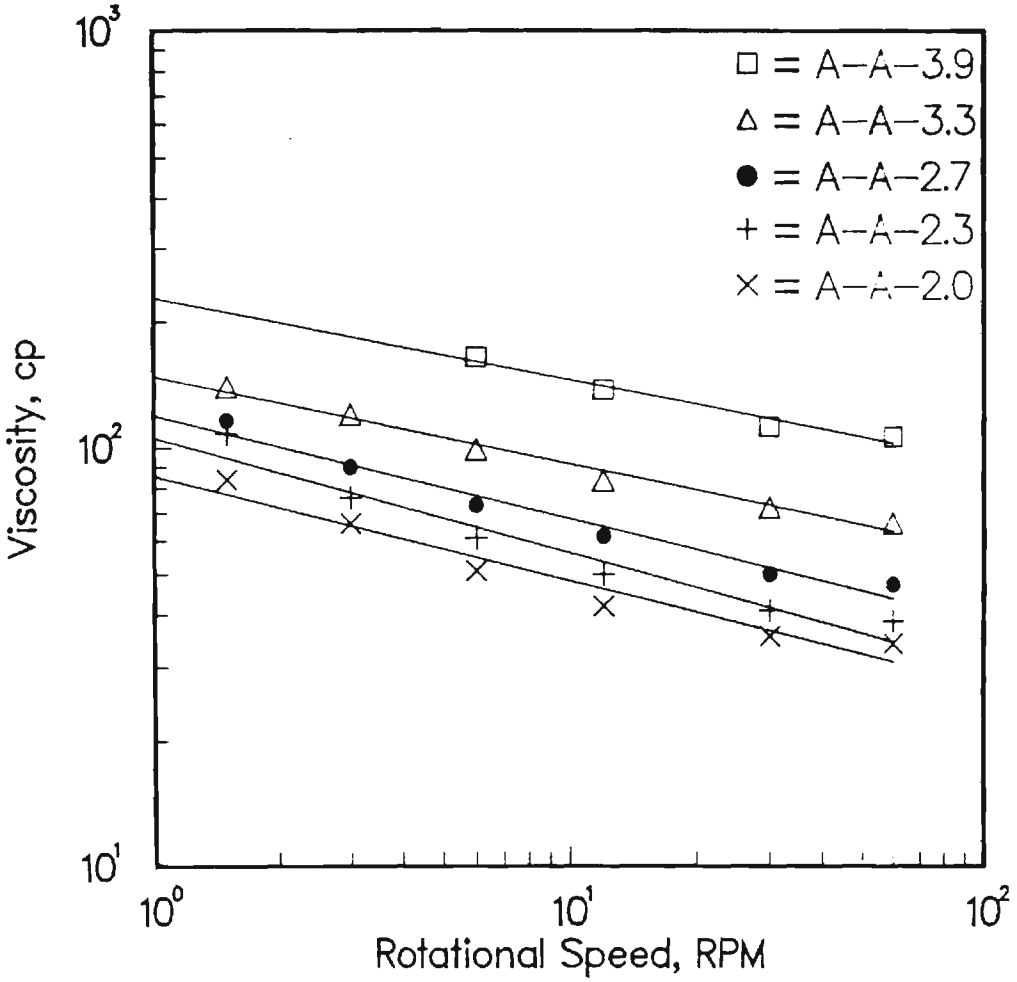

Fig.2. Viscosity of Alumina/Acetone Slips vs Rotational Speed for Various PMMA Concentrations of 2008

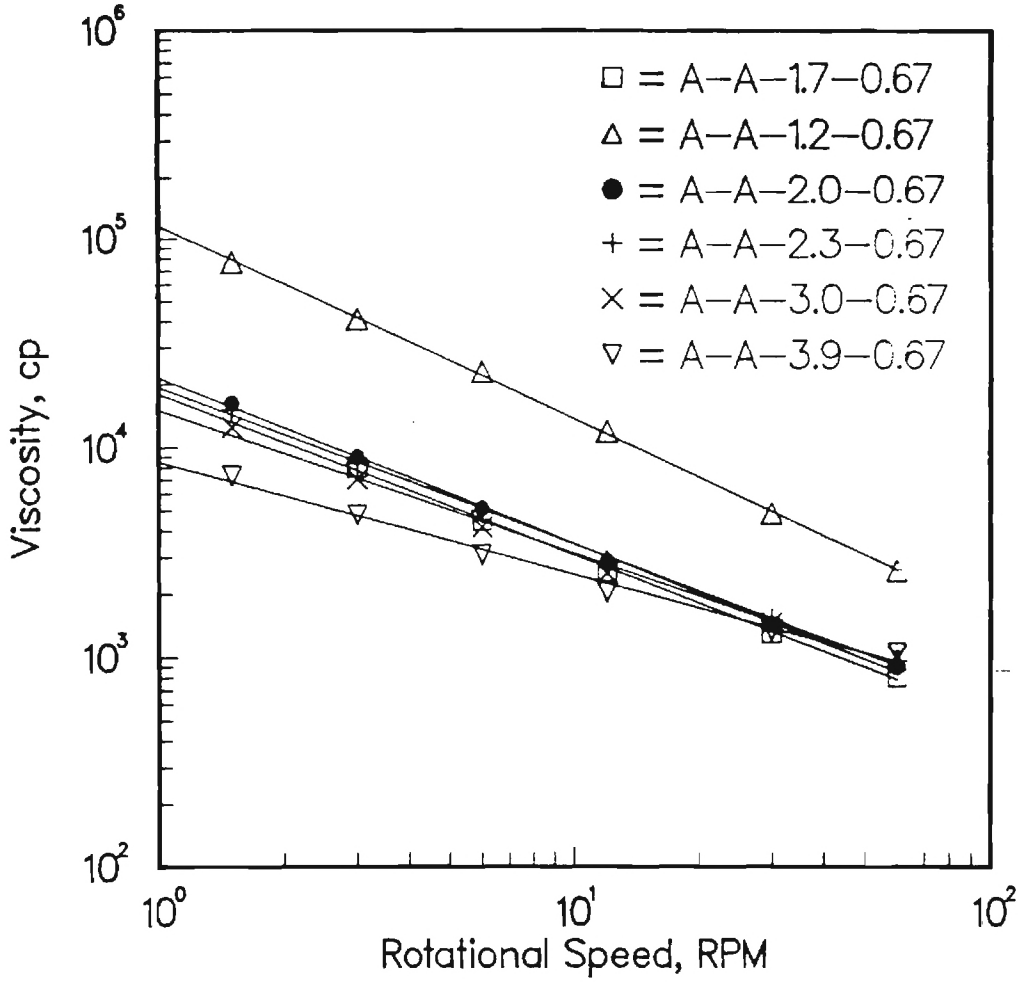

Fig.3. Viscosity of Alumina/Acetone Slips vs Rotational Speed for Various PMMA Concentrations of 2008 at a 2041 Concentration of 0.67 w/o.

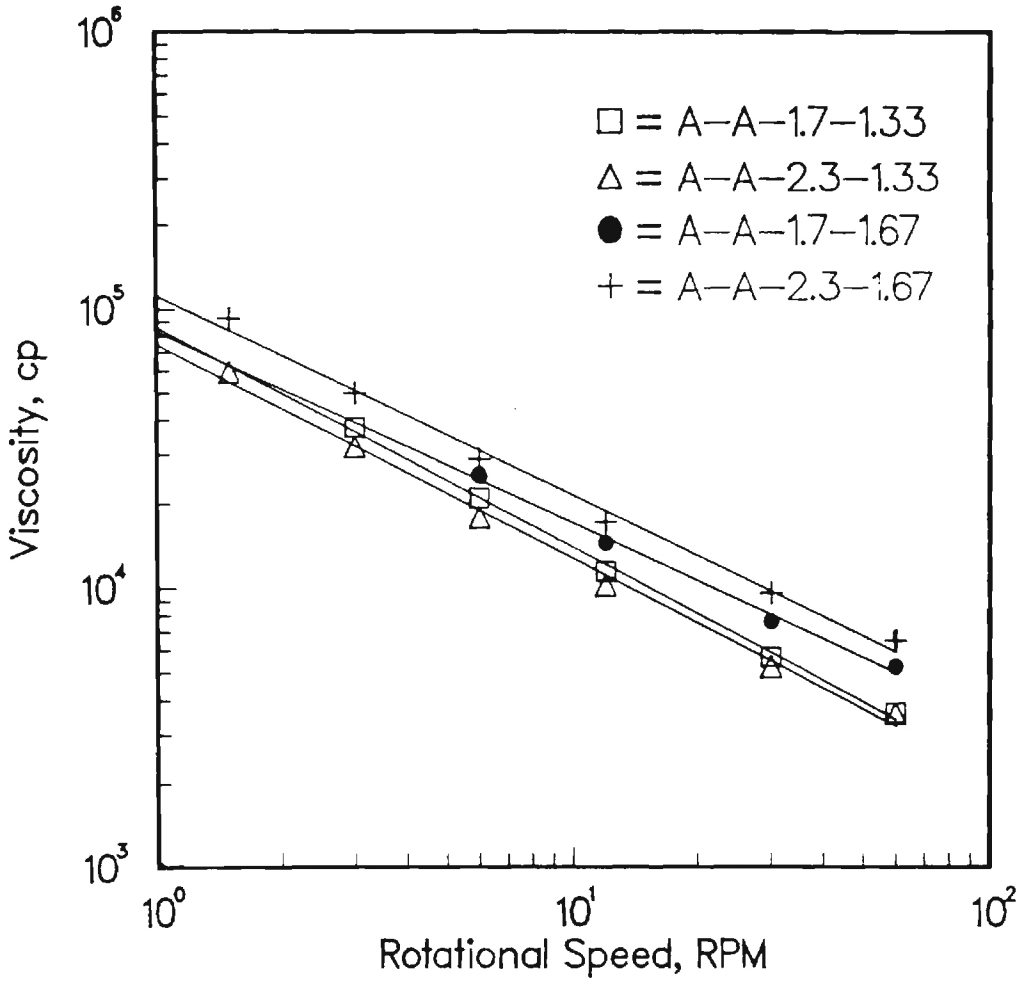

Fig.4. Viscosity of Alumina/Acetone Slips vs Rotational Speed for Various PMMA Concentrations of 2008 at 2041 Concentrations of 1.33 & 1.67 w/o.

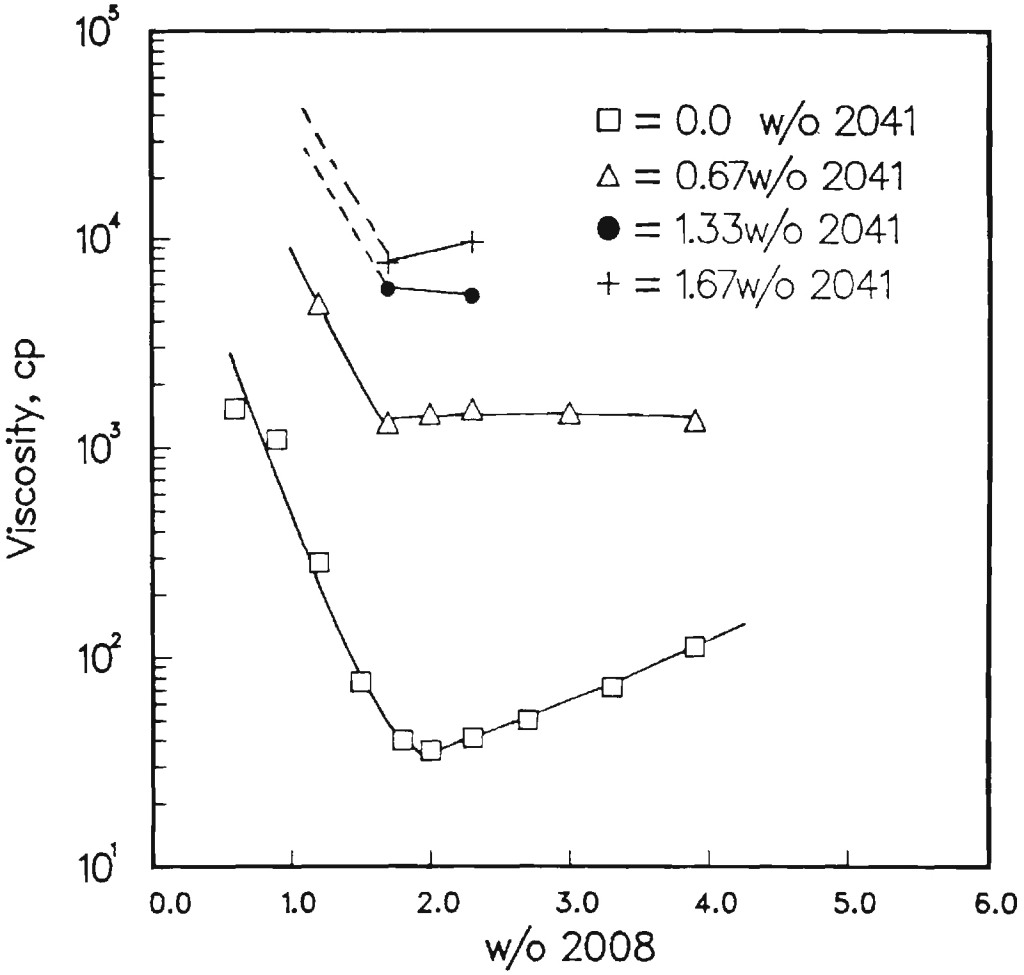

Fig.5. Plot of Viscosity at 30 RPM, vs Elvacite 2008 Concentration, with w/o Based on Solids Content.

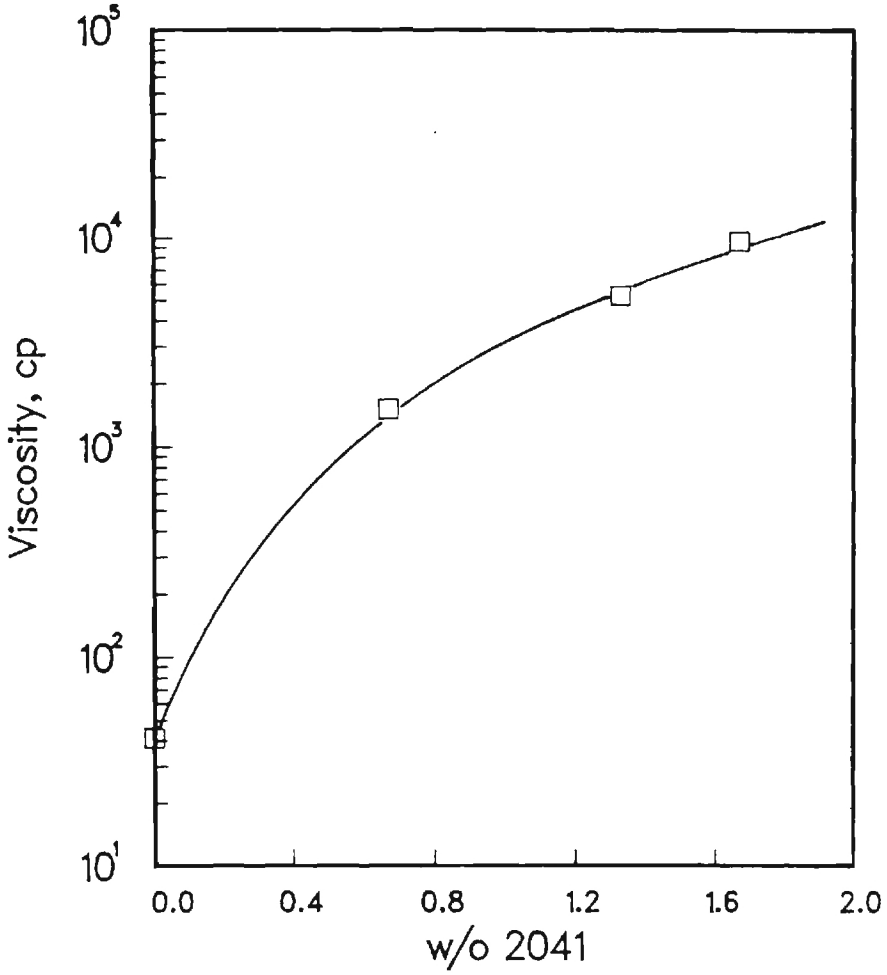

Fig.6. Effect of 2041 Content on Viscosity (30RPM) of Alumina/Acetone Dispersions with 2008 Concentration Fixed at 2.3 w/o.

Table 1. Rheology of Alumina/Acetone Slips. (Viscosities were measured at 30 RPM with Brookfield LV Viscometer, while n is the flow behavior index from the power-law equation.)

Sample	Viscosity cp	n
A-A-0.6	1528 (#3)*	0.05
A-A-0.9	1092 (#3)	0.02
A-A-1.2	284 (#2)	0.25
A-A-1.5	76 (#2)	0.41
A-A-1.8	40 (#1)	0.63
A-A-2.0	36 (#1)	0.78
A-A-2.3	41 (#1)	0.75
A-A-2.7	50 (#1)	0.76
A-A-3.3	72 (#1)	0.80
A-A-3.9	112 (#2)	0.76
A-A-1.2-0.67	4860 (#4)	0.03
A-A-1.7-0.67	1310 (#4)	0.23
A-A-2.0-0.67	1440 (#3)	0.21
A-A-2.3-0.67	1512 (#3)	0.26
A-A-3.0-0.67	1456 (#3)	0.35
A-A-3.9-0.67	1340 (#3)	0.45
A-A-1.7-1.33	5680 (#3)	0.19
A-A-2.3-1.33	5260 (#4)	0.24
A-A-1.7-1.67	7620 (#4)	0.25
A-A-2.3-1.67	9600 (#4)	0.32

* numbers in parentheses indicating spindles used

Table 2. Comparison of Viscosities of 2008/Acetone Solution and Alumina/Acetone Slips (without 2041)

2008 w/o in Slips Based on Acetone	Viscosity, cp	
	2008/Acetone Solutions	Alumina/acetone Slips
9.56	---	40
10.62	---	36
12.21	---	41
14.34	---	50
17.52	---	72
20.00	12	---
20.71	---	112
30.00	56	---
40.00	588	---
50.00	8320	---

solutions was made by converting the 2008 concentration in the slips to a w/o concentration based on solvent content. The viscosity increase rate, $[(\log \eta_1 - \log \eta_2)/(C_1 - C_2)]$, for the alumina/acetone slip in the range of 12.21w/o-20.71/w/o 2008 was 0.051 and for the 2008/acetone solutions in the range of 20-30 w/o 2008, the rate was 0.067. There is reasonable agreement between the two rates which indicates that after monolayer adsorption on the powder has been achieved, additional 2008 in solution increases the viscosity of slip to an extent similar to the system without powder.

For fixed 2008 concentrations, the effect of 2041 produces large viscosity increases as would be expected for a high molecular weight polymer, Figure 6. Addition of 0.67 w/o 2041 to the slips raised viscosity about 1 order of magnitude, but this effect was not linear as more 2041 polymer was added. If comparison of slips at the same 2008 content are made, it is evident that the 2041 also increases the pseudoplasticity along with the viscosity.

Sphere Recovery Activities

This section describes the continuing evaluation of a variety of sphere recovery (SR) methods. The SR techniques evaluated this reporting period have all utilized upward flowing air in an effort to increase the residency time for drying the free-falling Al_2O_3 spheres, and to decrease the

rate of descent to enable a "soft damage-free landing" for the thin-walled product. The most successful design tested to date consists of a 14' tall stack of plexiglass tubes (12" in diameter) joined on the upper end with a chamber containing the coaxial sphere forming nozzle, the smaller diameter tube containing the saturated acetone atmosphere to facilitate sphere formation and ducting to the air blower. A photograph of the components at the top of the recovery tower is shown in Figure 7. Air is drawn in at the base of the tower to develop the updraft necessary to retard the decent rate of the free-falling spheres. At the base of the tower the sufficiently dried spheres land on an inclined screen (Figure 8) and roll into a simple collection box (Figure 9). A process diagram describing the major steps for the manufacture of fired hollow ceramic sphere is shown schematically in Figure 10.

The updraft drying and recovery system described above has produced the most symmetrical damage-free thin-walled microspheres produced to date (Figure 11). Future modifications planned for this system include:

i. A larger capacity blower to increase the updraft air velocity to handle wide ranges of sphere diameters and densities,

ii. An improved air intake geometry to provide better laminar flow inside the tube,

iii. A larger diameter (low air velocity) chamber between the drying tower and blower to "drop-out" the fine light weight Al_2O_3 particles carried to the blower and

iv. The evaluation of intake deflectors (wings) that will generate a mild vortex motion in the raising air to help maintain the spheres in the center of the tower.

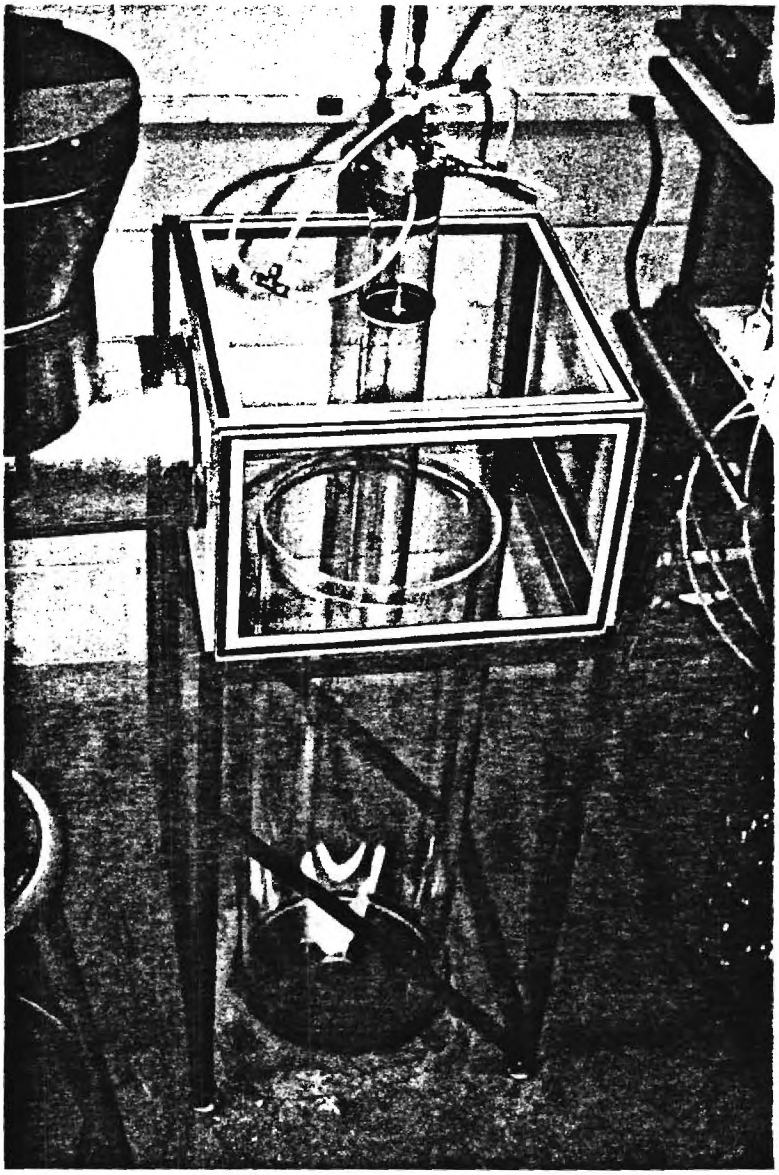

Figure 7. Photograph of Components at the Top of the 14 Foot Tall Sphere Recovery Tower.

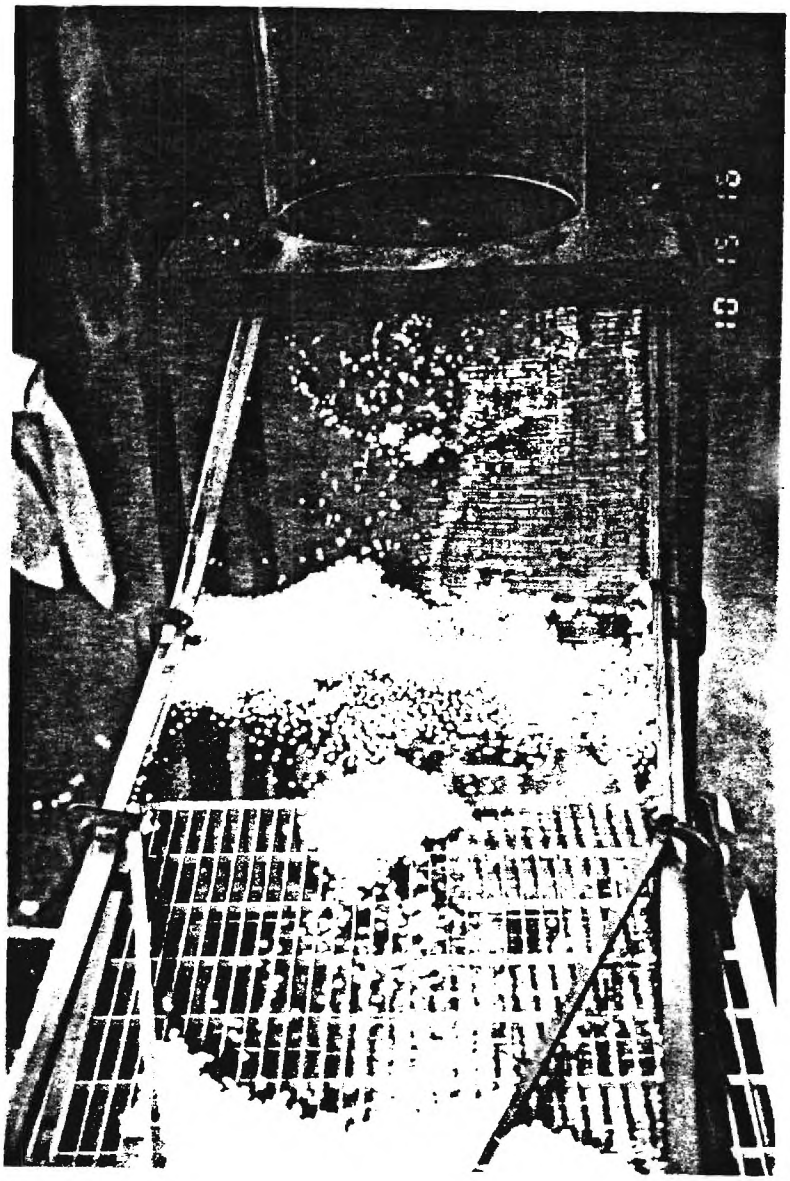

Figure 8. Photograph of Decending Dried Spheres Landing on Inclined Screen and Rolling-Out for Collection.

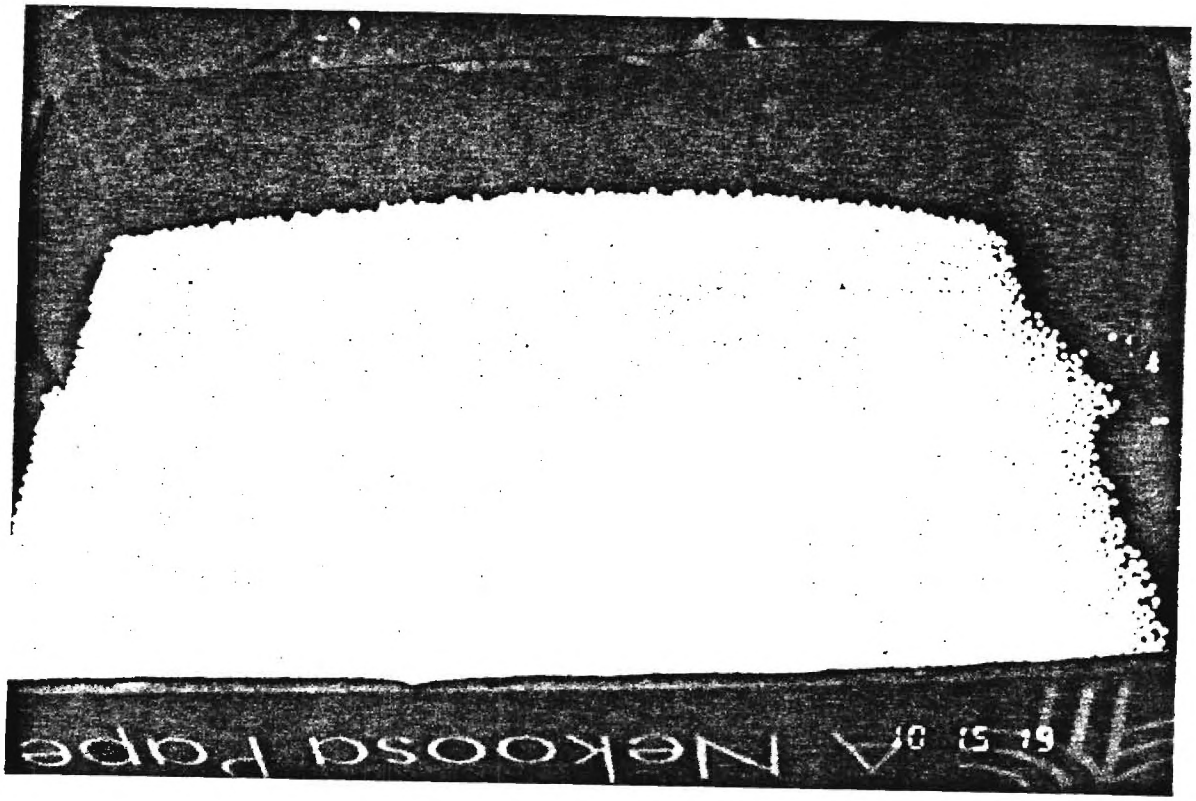

Figure 9. Photograph of Dried Hollow Spheres Collected from Recovery Tower during ~15 min. of Operation.

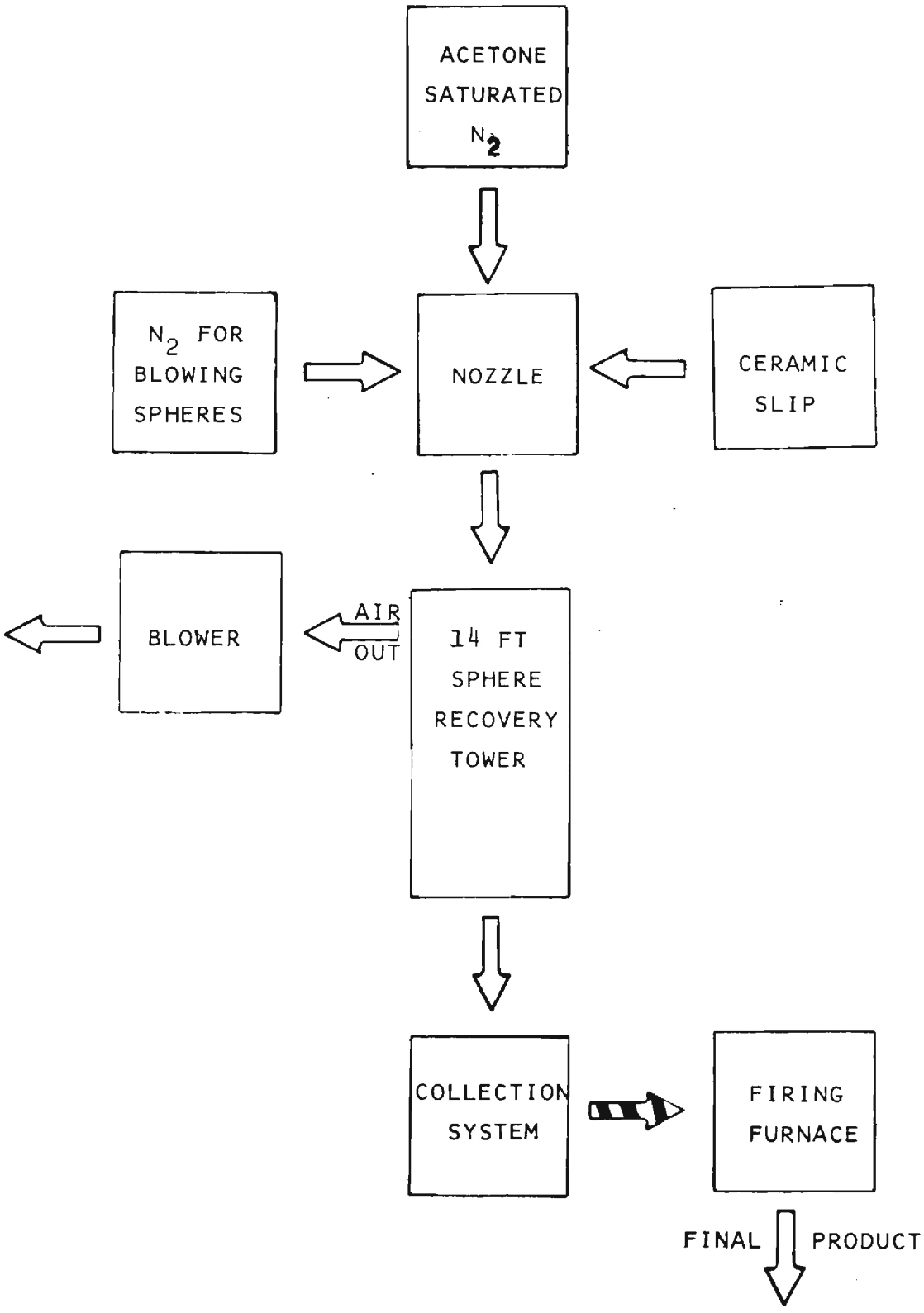

Figure 10. Schematic Process Diagram, Incorporating the 14' Tall Sphere Recovery Tower, for the Manufacture of Low Density Ceramic Spheres.

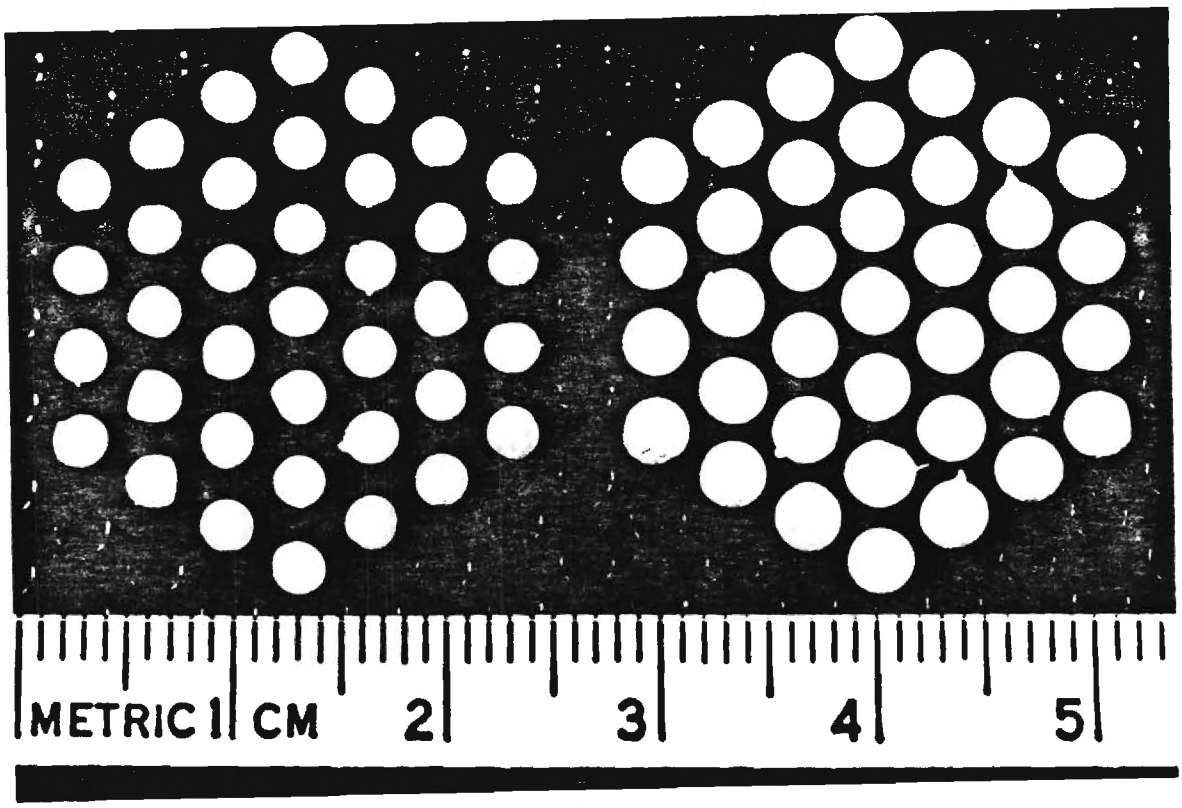

Figure 11. Typical Arrays of Fired Al_2O_3 Spheres Produced from Updraft Sphere Recovery Tower.

THIN-WALL HOLLOW CERAMIC SPHERES FROM SLURRIES

A.T. Chapman, J.K. Cochran, J.M. Britt, T.J. Hwang

School of Materials Engineering
Georgia Institute of Technology
Atlanta, GA 30332

(ORNL Subcontract 86X-2204 3C)

ABSTRACT

The object of this program was to develop a process for economically fabricating thin-wall hollow spheres from powder slurries using the Torobin coaxial nozzle process. This object was successfully met by developing acetone based alumina slips which were blown into individual spheres at rates of 50 to 60 per sec. The spheres were dropped into a forced air updraft column for recovering which provided free-fall residence times of 4-8 seconds. Such a residence time was sufficient for drying the spheres prior to landing at the column base. Approximately eight liters per hour of green spheres were producable by this system. The green spheres were conventionally fired to provide impervious walls. Process uniformity was demonstrated by characterizing two groups of spheres blown under different conditions. Sphere diameters were 2.5 and 3.2 mm with distributions having a 3σ limit of ~8%. Aspect ratios averaged 6% and 4% deviations from spherodicity for the small and large spheres respectively. Bulk densities of the fired spheres were 0.51 and 0.20 g/cc for the small and large spheres which corresponded to average wall thicknesses of 112 and 56 μm, respectively. As process controls are varied and improved, not only will the range of diameters and densities increase but distributions and deviations from spherodicity will approach a true monodispersed state.

INTRODUCTION

The overall objective of this effort is to develop and characterize a process for economically fabricating thin-wall hollow ceramic spheres from conventional ceramic powders using dispersions. These low density spherical shells of small (.1-5mm) diameter would have numerous novel

applications such as high-temperature insulation or even lightweight structural materials. Development of the spheres has been divided into three phases; I. Process Development, II. Investigation of Process Parameters, and III. Investigation of Sphere Properties. Each of these three phases was proposed as a one year task and the first year has been devoted to Process Development. This report constitutes the Final Report for Phase I covering the time period January 1, 1986 to December 31, 1986 and also provides a description of the accomplishments for the Fourth Quarter, October 1, 1986 to December 31, 1986.

For the first year, the technical objective was to develop a process for producing thin wall hollow ceramic spheres from alumina (Al_2O_3) based slurries based on the Torobin coaxial nozzle technique. The process should be capable of handling slurries, with viscosities ranging from at least 20 poise to 200 poise at room temperature. The process should be capable of producing spheres at least 2 to 6 mm in diameter with wall thickness 12 to 100μm at rates no less than 30 spheres per second. All spheres should be spherical such that both the inside and outside diameters of all spheres are within 2% of the means of 100 randomly selected spheres. Finally, all spheres shall have a size distribution such that 99% have an outside diameter $\pm$ 10% of the mean of 100 spheres from each batch.

Prior to the start of this program, a method to form thin-wall hollow spheres from a variety of conventional

ceramic powders dispersed in water had been demonstrated. The initial project objective therefore was to evaluate means to dry and recover the moisture-laden free-falling spheres. A variety of methods were considered including; microwave drying, hot air furnaces, and direct infrared radiant heating. The microwave drying approach was considered most attractive because the energy would be absorbed directly in the walls of the spheres. Several suppliers of microwave drying equipment were contacted and a series of experiments were performed to assess the feasibility of drying the free-falling thin-wall spheres with microwave energy. Unfortunately the small volume occupied by the relatively widely spaced falling spheres resulted in inefficient heating using conventional microwave frequencies and wave guides. Therefore, microwave drying could not be used for rapid drying of the small shells.

Other drying schemes were considered along with process and dispersion compositional changes that would provide faster drying for the free-falling spheres. Dispersion of powders in a high volatility organic fluid was the most attractive alternative for several reasons. For example, acetone has a much larger vapor pressure, smaller heat of vaporization, and a lower surface tension and density than water. Initial testing of Al_2O_3 powders dispersed in acetone demonstrated that a very uniform stream of spheres could be blown for short periods at room temperature, although the high fluid evaporation rate lead to clogging of

the coaxial blowing nozzle.

The merits of dispersions made with acetone was readily apparent when water-based spheres splattered on impact on a soft landing surface after 30 to 40 feet of free-fall; whereas, similar acetone-based shells dried sufficiently to bounce. Recovery of the partially dried acetone based bubble streams was attempted using a variety of methods including: deflection off inclined surfaces, horizontal air jets to blow spheres for roll-out on flat surfaces, and heating using an infrared furnace. All of the spheres collected using these approaches experienced damage on collision with adjacent spheres and/or impact with a solid surface.

Success was achieved by designing an updraft drying and recovery system consisting of a vertical tube tower, approximately 3.2 meters tall and 30cm in diameter, combined with an air blower and sphere forming nozzle assembly. The system was constructed and tested. When the updraft air velocity and sphere diameter and weight are properly balanced, the residence time necessary for adequate drying (4 to 5 sec) can be maintained in the tower and a "soft landing" is achieved without mechanical damage to the shells. Recent runs using this facility have produced the best defect-free high strength thin-walled Al_2O_3 spheres achieved to date.

The major efforts of this program have been 1) analysis of the rheology of alumina/acetone dispersions containing varying amounts of methylmethacrylate which act as

disperants and binders, 2) development of a sphere recovery system which provides adequate residence time and a soft landing, and 3) characterization of the geometry of spheres provided by the system.

The following sections describe the procedures and terminology used to characterize the pseudoplasticity and Newtonian behavior of the acetone-based slips, the influence of the organic binder on slip rheology, the recovery system that yielded virtually "flaw-free" high strength thin-walled Al_2O_3 spheres, and finally, the geometrical characterization of thin wall hollow spheres which have a size uniformity seldom achieved by high volume manufacturing processes.

CHARACTERIZATION OF ACETONE-BASED DISPERSIONS

The rheology of alumina/acetone slips has been investigated to provide suitable dispersions for production of hollow polycrystalline spheres. It is necessary that the alumina powder be well dispersed to yield a reproducible process and to permit a high solids volume content which minimizes the quantity of solvent to be removed. In addition, the slips must possess a viscoelastic and film forming character sufficient for blowing and the hollow spheres formed must be strong enough for recovery. For these purposes, methylmethacrylate, DUPONT Elvacite, resins were added to the dispersions. Elvacite #2008 was added as a dispersant and a binder, while #2041 served as a binder and a rheology modifier. To characterize the rheology of

these dispersions, the viscosity was measured with Brookfield LV Viscometer at shear rate between 0.1-50 sec^{-1}.

Due to the use of organic polymers, the dispersions exhibit pseudoplasticity. This property can be described by the power law (also known as Ostwald-deWaele equation),

$$\tau = K\gamma^n \qquad (1)$$

where τ is shear stress, γ is shear rate, K is the consistency index and n is the flow behavior index. The value of n is less than 1 for pseudoplastic flow, and decreases as the degree of pseudoplasticity increases. If n is close to 1, the liquid is Newtonian. The power law equation can be related to viscosity, η, by:

$$\eta = K\gamma^{(n-1)} \qquad (2)$$

Transformed for linear plotting, this equation is rewritten as

$$\log \eta = \log K + (n-1) \log \gamma \qquad (3)$$

The value of γ is not accurately known since γ varies with distance from the rotating spindle thus causing a variation of η, for non-Newtonian liquids. However, to a first approximation, γ can be treated as in a Newtonian liquid so that

$$\gamma = \frac{2\pi rR}{dr} = 2\pi R, \qquad (4)$$

where r is the radius at which γ is desired to be known and R is the rotational speed of the spindle. Therefore equation (3) can be transformed to

$$\log \eta = \log K + (n-1) \log 2o + (n-1) \log R. \qquad (5)$$

The rheology of additional alumina/acetone slips as well as additional ceramic materials have been and will be studied by characterizing η and n for various compositions in order to improve the quality of the thin walled spheres.

Slip Viscosity Measurement Procedures

As stated above, the materials used for slip preparation were ALCOA XA-3000 Al_2O_3, acetone, plus Elvacite 2008 and Elvacite 2041. Used as a slip casting alumina, XA-3000 Al_2O_3 powder has a mean particle size of 3 μm, and a broad particle size distribution designed for slips. Elvacite 2008 is a low molecular weight binder and dispersant, which provides low viscosity at high solids content. Elvacite, 2041 is a very high molecular weight binder which increases viscosity with small additions.
The dispersions investigated had a fixed Al_2O_3 content of 51v/o based on the acetone plus alumina volumes. The slips were designated according to type of powder, solvent, and weight concentration of polymers based on powder content, i.e. A-A-0.6 indicates Al_2O_3 as the powder, acetone as the solvent, and 0.6 w/o of 2008, or A-A-1.2-0.67 indicates the same powder and solvent, but 1.2 w/o of 2008 and 0.67 w/o of 2041.

After weighing, Al_2O_3, acetone and 2008 were mixed by rolling with alumina cylinders in a polyethylene jar on a ball mill rack at 70-90 RPM for 24 hours. Then 2041 was added to the slip if needed and milled for an additional 24 hours. Viscosity was measured with a Brookfield LV

viscometer using proper spindles at rotational speeds of 1.5 to 60 RPM.

Rheology Measurements of Alumina/Acetone Slips

The viscosities of dispersions were plotted as log η vs. log R as shown in Figures 1,2,3, and 4 in accordance with equation 5. All slips were pseudoplastic as shown by the negative slope, (n-1), in Figures 1-4. The flow behavior as indicated by n values, were calculated and are listed in Table 1 along with viscosities at 30 RPM. It can be seen that n values increase with 2008 concentration indicating that the slips approach a Newtonian fluid as the powder becomes well dispersed.

The effect of 2008 concentration on viscosity is shown in Figure 5. These viscosity curves all show minimum viscosity around 1.7-2.0w/o 2008. This minimum point is indicative of monolayer adsorption of the polymer on the alumina particles. For slips without 2041, the increase of viscosity as the 2008 content was increased beyond the minimum may be due to excess 2008 going to solution. The rate of viscosity increase in this range should be equal to the rate of viscosity increase for a powder free 2008/acetone solution. Therefore, viscosities of 2008/acetone solutions were measured for comparison to slip viscosities, Table 2. A comparison between slips and solutions was made by converting the 2008 concentration in the slips to a w/o concentration based on solvent content. The viscosity increase rate, $[(\log \eta_1 - \log \eta_2)/(C_1 - C_2)]$, for

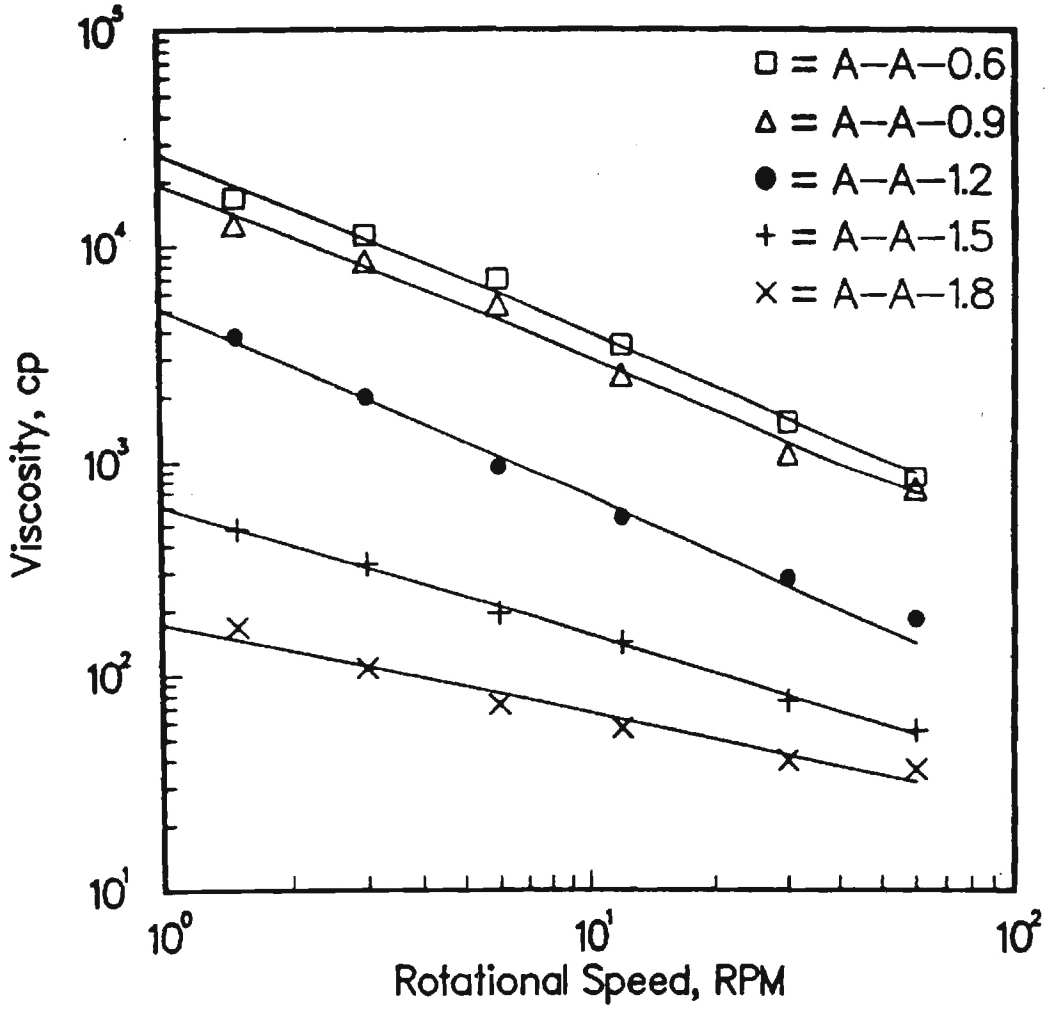

Fig. 1. Viscosity of Alumina/Acetone Slips vs Rotational Speed for Various PMMA Concentrations of 2008 Polymer.

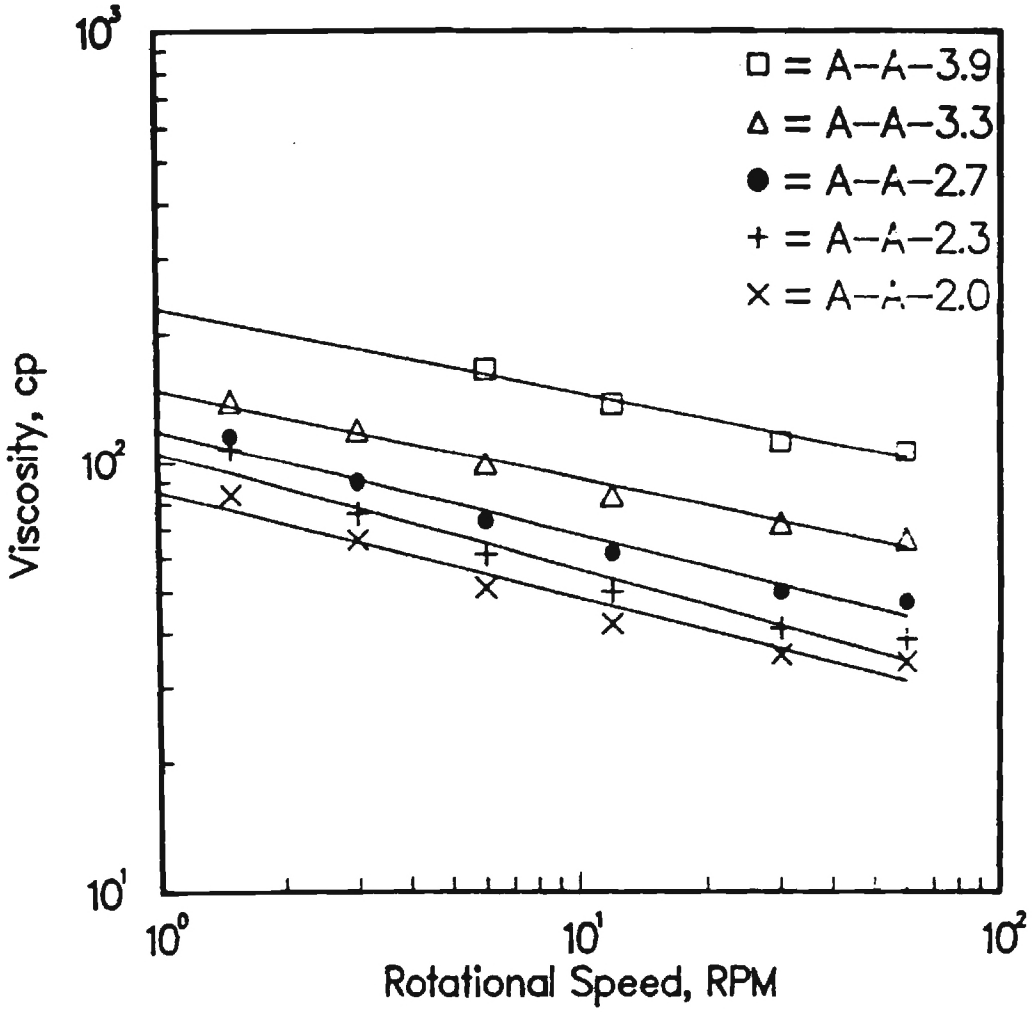

Fig. 2. Viscosity of Alumina/Acetone Slips vs Rotational Speed for Various PMMA Concentrations of 2008 Polymer.

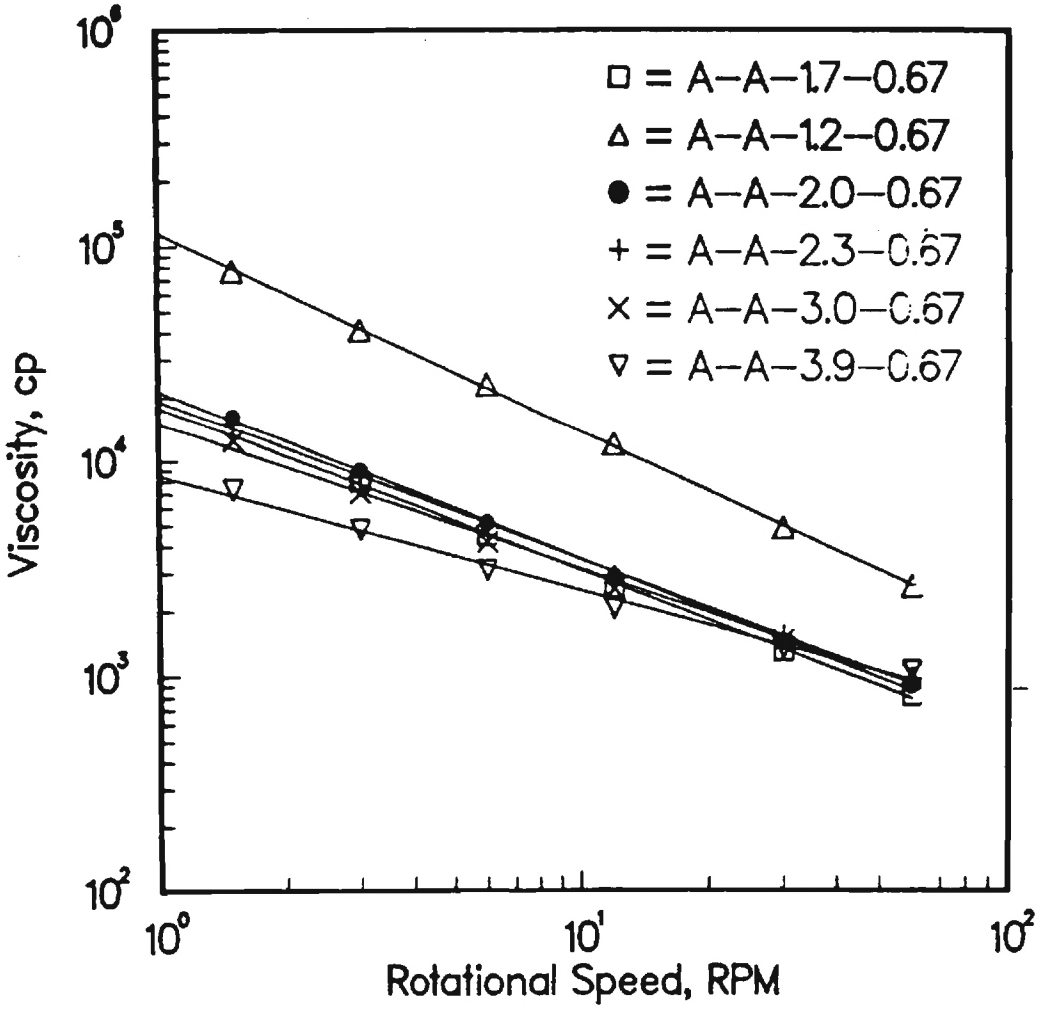

Fig. 3. Viscosity of Alumina/Acetone Slips vs Rotational Speed for Various PMMA 2008 Concentrations at a 2041 Concentration of 0.67 v/o.

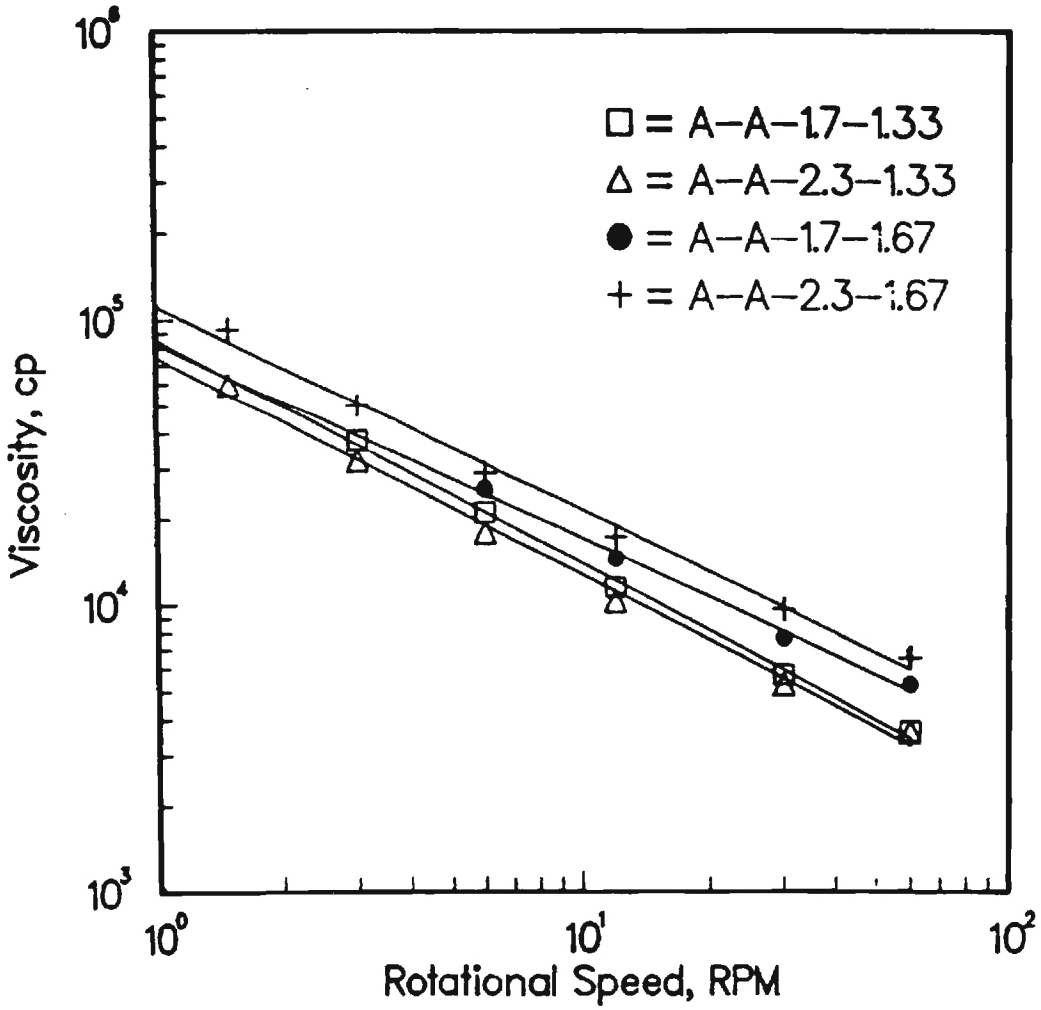

Fig 4. Viscosity of Alumina/Acetone Slips vs Rotational Speed for Various PMMA 2008 Concentrations at 2041 Concentrations of 1.33 & 1.67 w/o.

Table 1. Rheology of Alumina/Acetone Slips.

Sample	Viscosity[b] (cp)		n[c]
A-A-0.6	1528	(#3)[a]	0.05
A-A-0.9	1092	(#3)	0.02
A-A-1.2	284	(#2)	0.25
A-A-1.5	76	(#2)	0.41
A-A-1.8	40	(#1)	0.63
A-A-2.0	36	(#1)	0.78
A-A-2.3	41	(#1)	0.75
A-A-2.7	50	(#1)	0.76
A-A-3.3	72	(#1)	0.80
A-A-3.9	112	(#2)	0.76
A-A-1.2-0.67	4860	(#4)	0.03
A-A-1.7-0.67	1310	(#4)	0.23
A-A-2.0-0.67	1440	(#3)	0.21
A-A-2.3-0.67	1512	(#3)	0.26
A-A-3.0-0.67	1456	(#3)	0.35
A-A-3.9-0.67	1340	(#3)	0.45
A-A-1.7-1.33	5680	(#3)	0.19
A-A-2.3-1.33	5260	(#4)	0.24
A-A-1.7-1.67	7620	(#4)	0.25
A-A-2.3-1.67	9600	(#4)	0.32

a Numbers in parentheses indicate spindles used.

b Viscosities reported were at 30 RPM with a Brookfield LV Viscometer.

c n is the flow behavior index from the power-law equation.

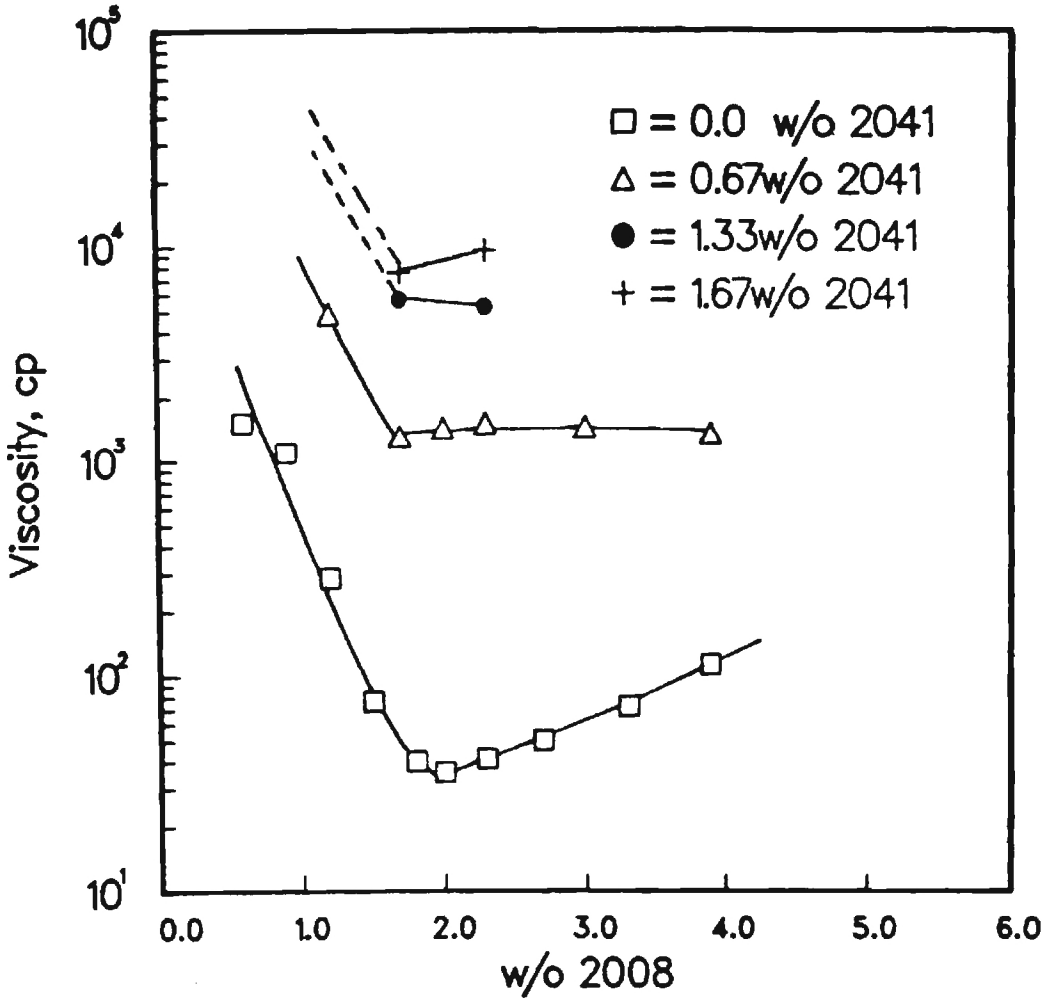

Fig. 5. Plot of Viscosity at 30 RPM vs Elvacite 2008 Concentration Based on Solids Content.

Table 2. Comparison of Viscosities of 2008/Acetone Solutions and Alumina/Acetone Slips Containing 2008 Polymer.

2008 w/o in Slips Based on Acetone	2008/Acetone Solutions	Alumina/acetone Slips
9.56	---	40
10.62	---	36
12.21	---	41
14.34	---	50
17.52	---	72
20.00	12	---
20.71	---	112
30.00	56	---
40.00	588	---
50.00	8320	---

the alumina/acetone slip in the range of 12.21-20.71w/o 2008 was 0.051 and for the 2008/acetone solutions in the range of 20-30 w/o 2008, the rate was 0.067. There is reasonable agreement between the two rates which indicates that after monolayer adsorption on the powder has been achieved, additional 2008 in solution increases the viscosity of slip at the same rate as for powder free acetone.

For fixed 2008 concentrations, the additions of 2041 produced large viscosity increases as would be expected for a high molecular weight polymer, Figure 6. Addition of 0.67 w/o 2041 to the slips raised viscosity about one order of magnitude, but this effect was not linear as more 2041 polymer was added. If comparison of n for slips at the same 2008 content are made, it is evident that the 2041 also increases the pseudoplasticity along with the viscosity.

Sphere Recovery System

This section describes the continuing evaluation of a sphere recovery (SR) system capable of high volume collection. The SR techniques evaluated reported below have all utilized upward flowing air in an effort to increase the residency time for drying the free-falling rate of descent to enable a "soft damage-free landing" for the thin-walled product. The most successful design tested to date consists of a 3.2m tall stack of three plexiglass tubes (30cm in diameter) joined on the upper end with a chamber containing the coaxial sphere forming nozzle, a smaller diameter tube to contain a saturated acetone atmosphere to facilitate

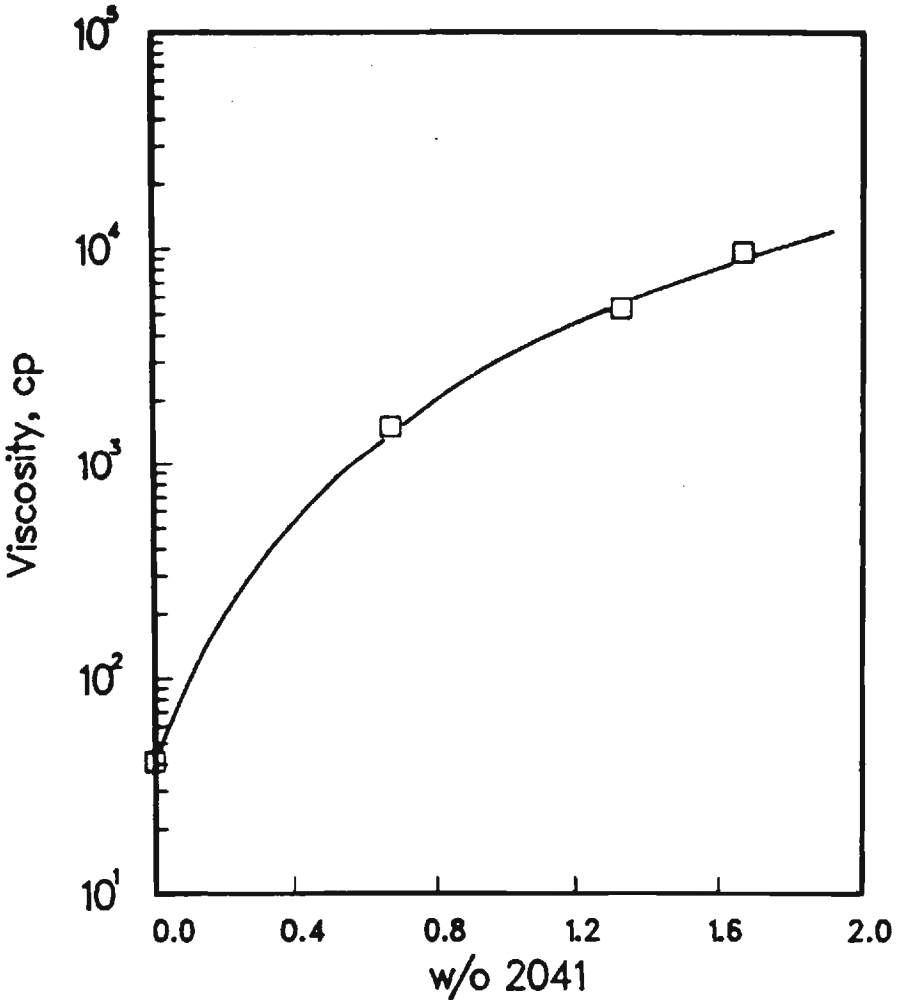

Fig. 6. Effect of 2041 Content on Viscosity (30RPM) of Alumina/Acetone Dispersions with 2008 Concentration Fixed at 2.3 w/o.

sphere formation and ducting to a high volume air blower. A photograph of the components at the top of the recovery tower is shown in Figure 7. Air is drawn in at the base of the tower to develop the updraft necessary to retard the decent rate of the free-falling spheres. At the base of the tower the sufficiently dried spheres land on an inclined screen, Figure 8, and roll into a simple collection box Figure 9. A process diagram describing the major steps for the manufacture of fired hollow ceramic sphere is shown schematically in Figure 10.

The updraft drying and recovery system described above has produced the most symmetrical damage-free thin-walled microspheres produced to date. Future modifications planned for this system include:

i. A larger capacity blower to increase the updraft air velocity to handle wider ranges of sphere diameters and densities,

ii. An improved air intake geometry to provide more laminar flow inside the tube

iii. A larger diameter (low air velocity) chamber between the drying tower and blower to "drop-out" the fine light weight Al_2O_3 particles carried to the blower and

iv. The evaluation of intake deflectors (wings) at the base of the tower that will generate a mild vortex motion in the raising air to help contain the spheres in the center of the tower.

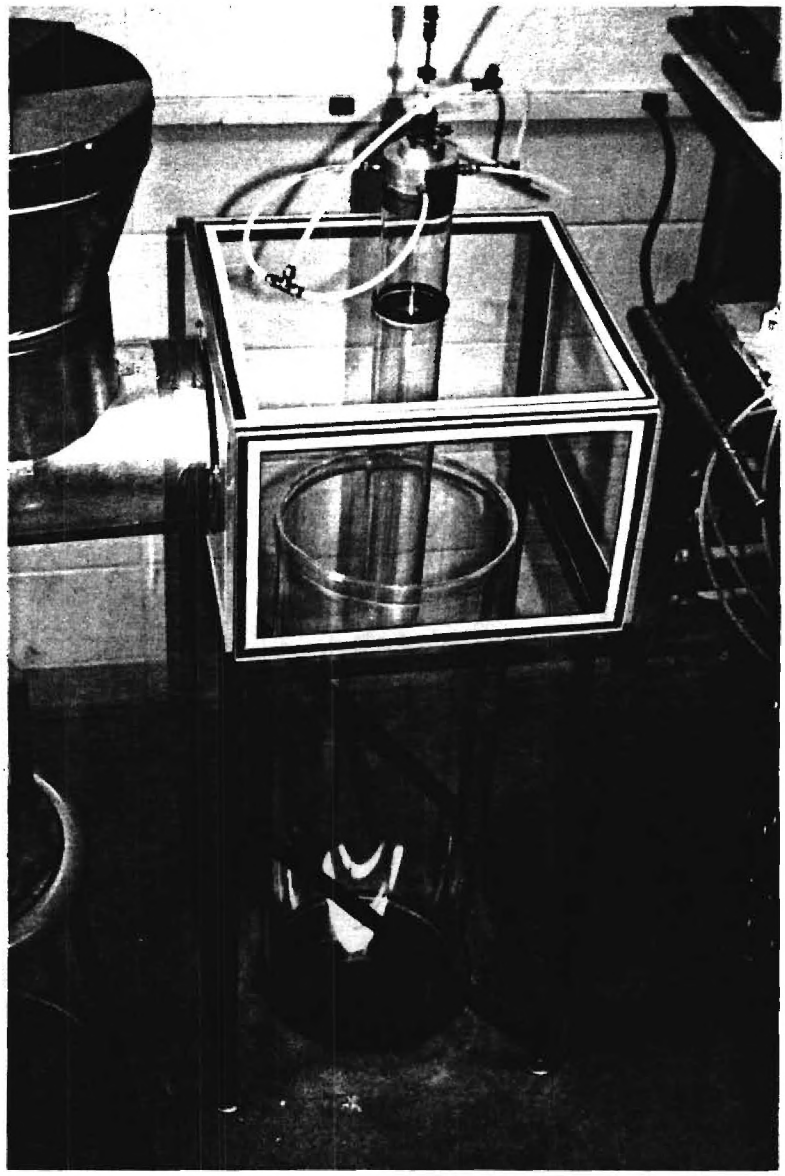

Fig. 7. Photograph of Components at the Top of the Sphere Recovery Tower.

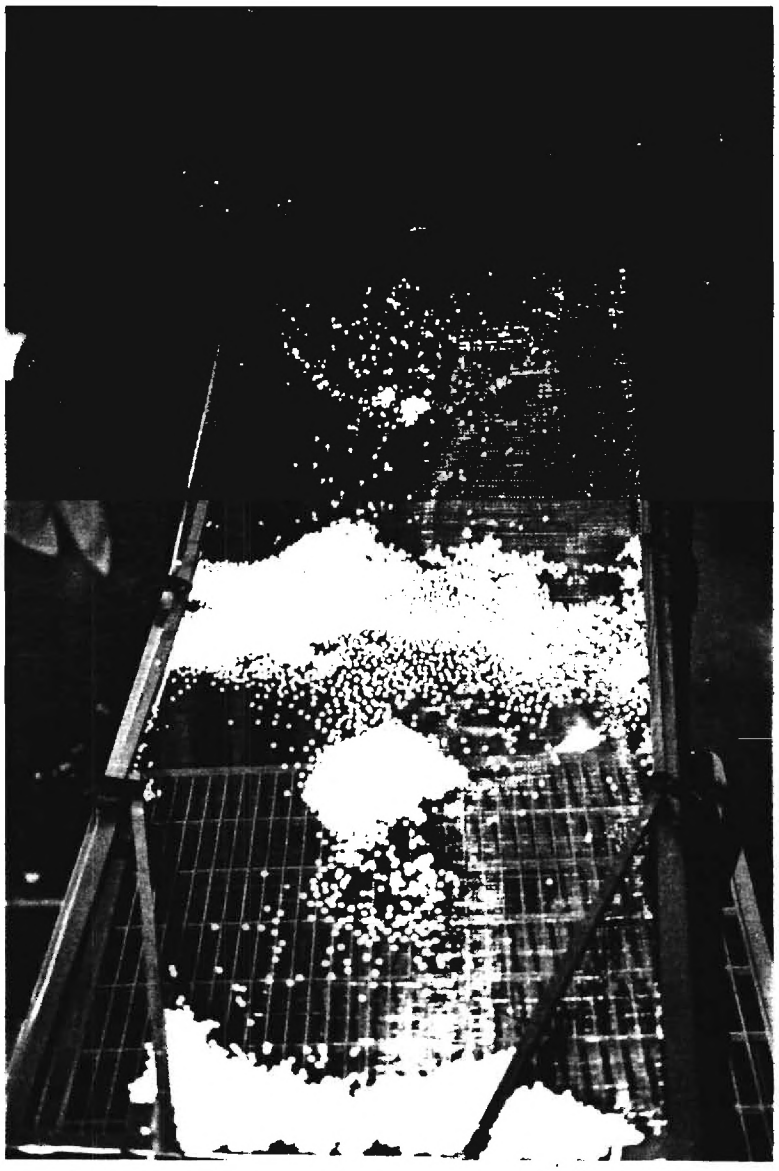

Fig. 8. Photograph of Decending Dried Spheres Landing on Inclined Screen.

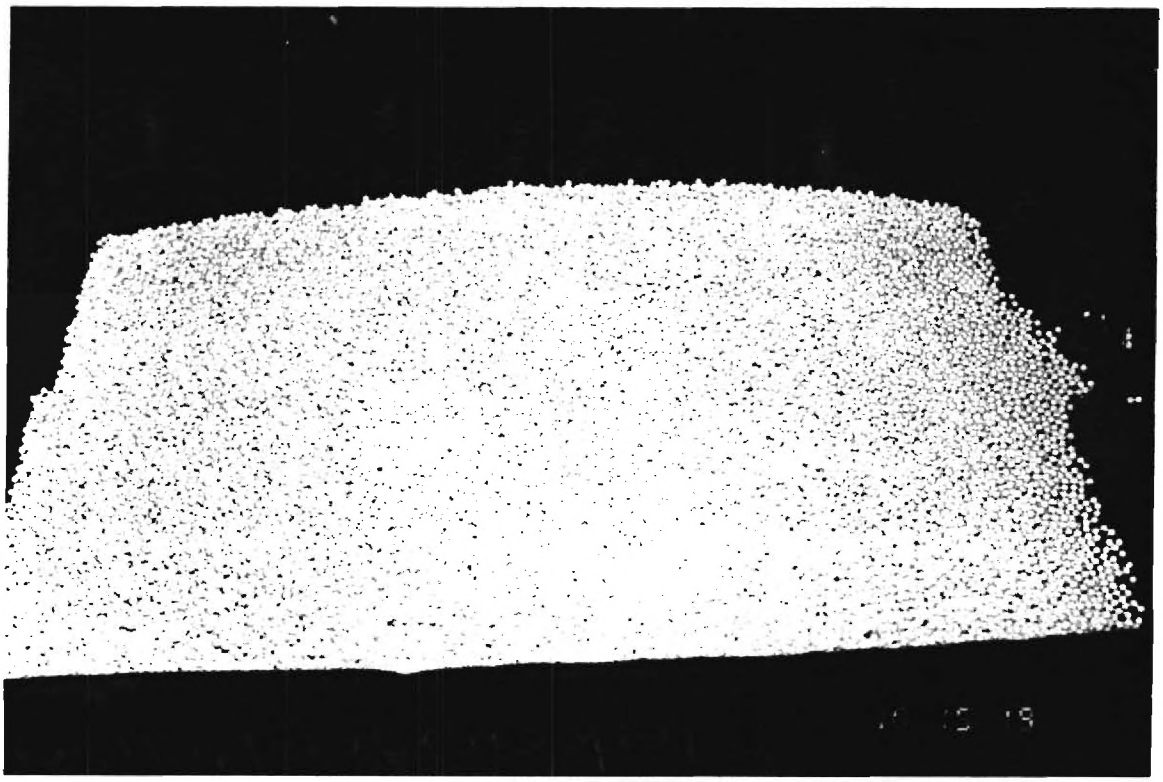

Fig. 9. Photograph of Dried Hollow Spheres Collected from Recovery Tower in 15 minutes of Operation.

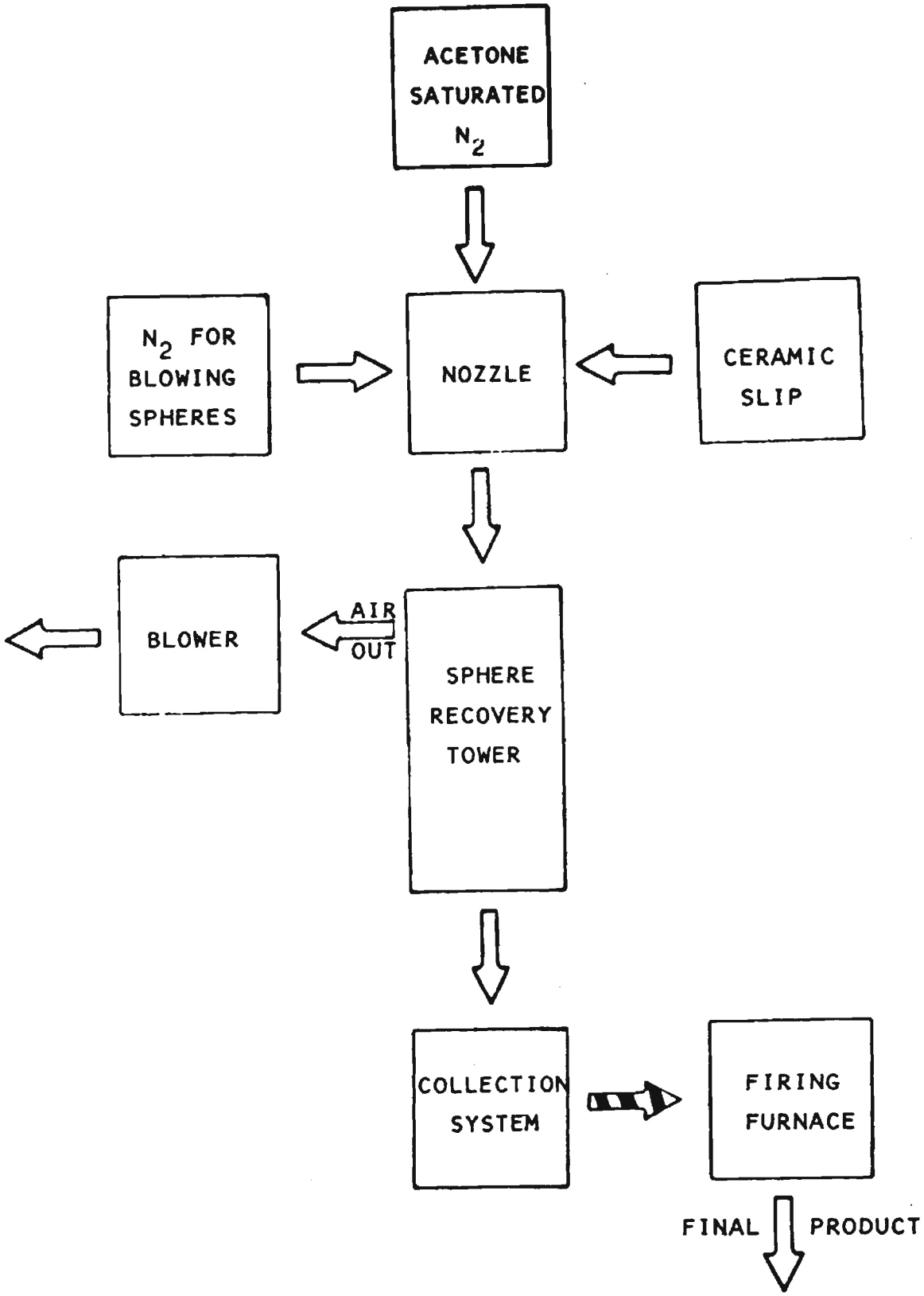

Fig. 10. Schematic Process Diagram, Incorporating the 3.2 m Tall Sphere Recovery Tower, for the Manufacture of Low Density Ceramic Spheres.

GEOMETRICAL CHARACTERISTICS OF THIN WALL HOLLOW SPHERES

To demonstrate the capabilities of the process, spheres were blown from the same slip under two sets of conditons; (1) 40 psi on the slip and 20 cc/min blowing gas flow rate (40-20) and (2) 20 psi with a blowing gas rate of 40 cc/min (20-40). Note that the ranges for both these variables is much greater than those values used here. The hollow sphere parameters presented below, Table 3, are not the limitations of the process but are presented to demonstrate the degree of perfection of size distribution and spherodicity achievable at this time. As the process continues to improve, degree of perfection will increase. The measurements and distributions presented are for randomly selected spheres from the two conditions.

For the higher slip pressure (or liquid flow rate) and lower blowing gas flow rate (40-20) spheres of smaller size were produced compared to a lower slip flow rate and higher gas flow rate (20-40) as shown in Figure 11. As the ratio of gas to slip flow rate increased, spheres were larger and had a smaller wall thickness as would be expected, Figure 12. After recovery and drying, the bulk density of the green product as measured by weighing ~100cc of tapped spheres was 0.51 and 0.20 g/cc or 31.8 and 12.5 lb/ft^3, respectively. After firing at 1650°C for 2 hours, the XA-3000 alumina sphere walls were impervious and the spheres increased in bulk density to 0.61 and 0.25 g/cc or 38.1 and

Table 3. Characteristics of Thin Wall Hollow Spheres Fabricated Under Two Blowing Conditions.

Parameter	Blowing Conditions 40-20	20-40
Green Bulk Density (g/cc)	0.51	0.20
Fired Bulk Density	0.61	0.25
Fired Sphere Density	1.07	0.41
Wall Thickness Fired (μm)	112	56
Diameter (μm)	2502 ± 71	3169 ± 83
Aspect Ratio *	1.11 ± 0.05	1.08 ± 0.02
Shape Factor !	1.04 ± 0.02	1.03 ± 0.02

* Due to measurement error, the aspect ratio (max dia/min dia) for perfect spheres was 1.05 for 40-20 and 1.04 for 20-40.

! Shape Factor = $P^2/4\pi A$ where P = perimeter and A= area. Shape Factor for Spheres = 1.00, Hexagons = 1.10, Squares = 1.27 and Triangles 1.65.

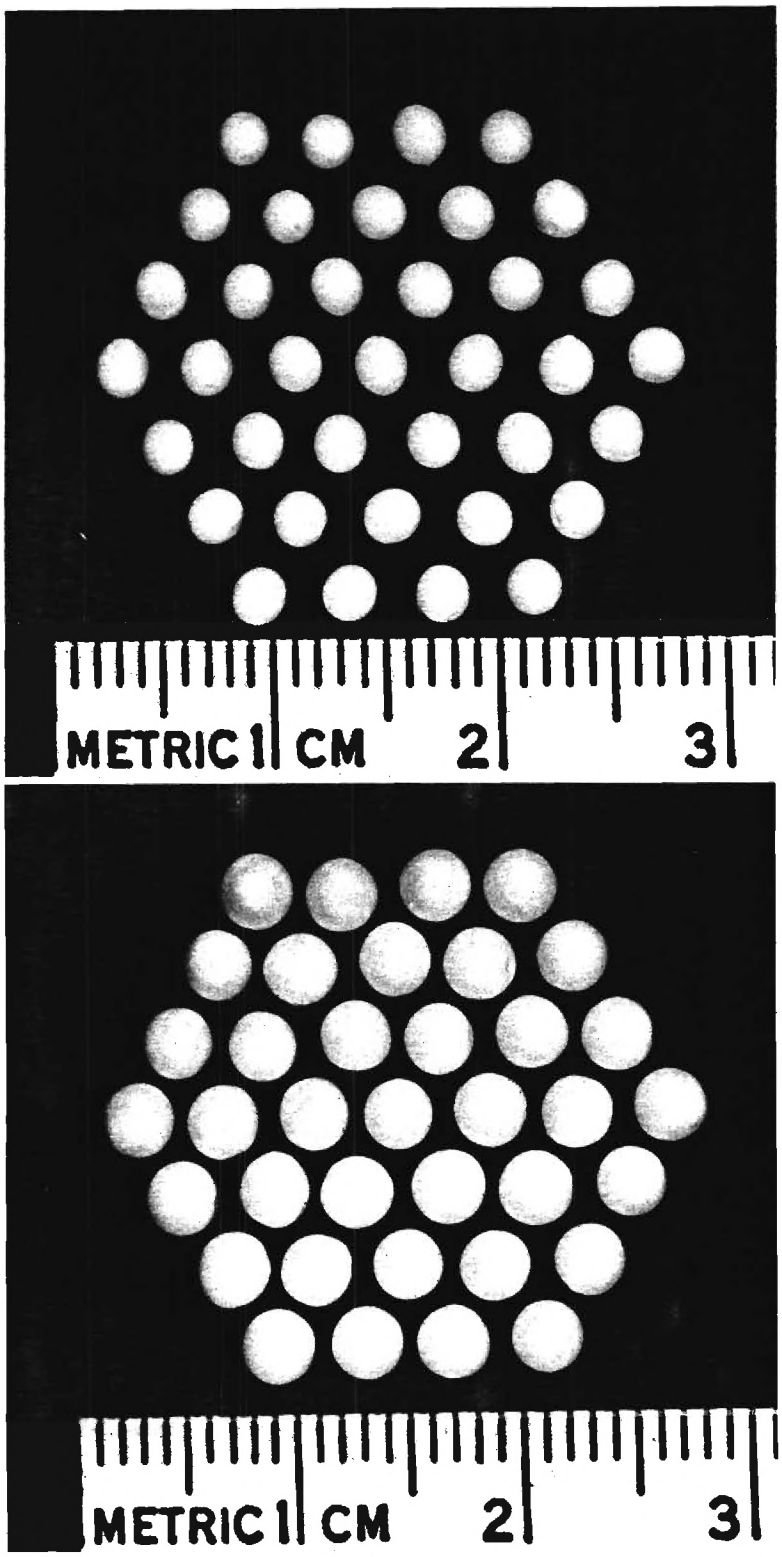

Fig. 11. Photographs of Fired, Thin-Wall, Alumina, Spheres Formed at Blowing Conditions (a) 40-20 and (b) 20-40.

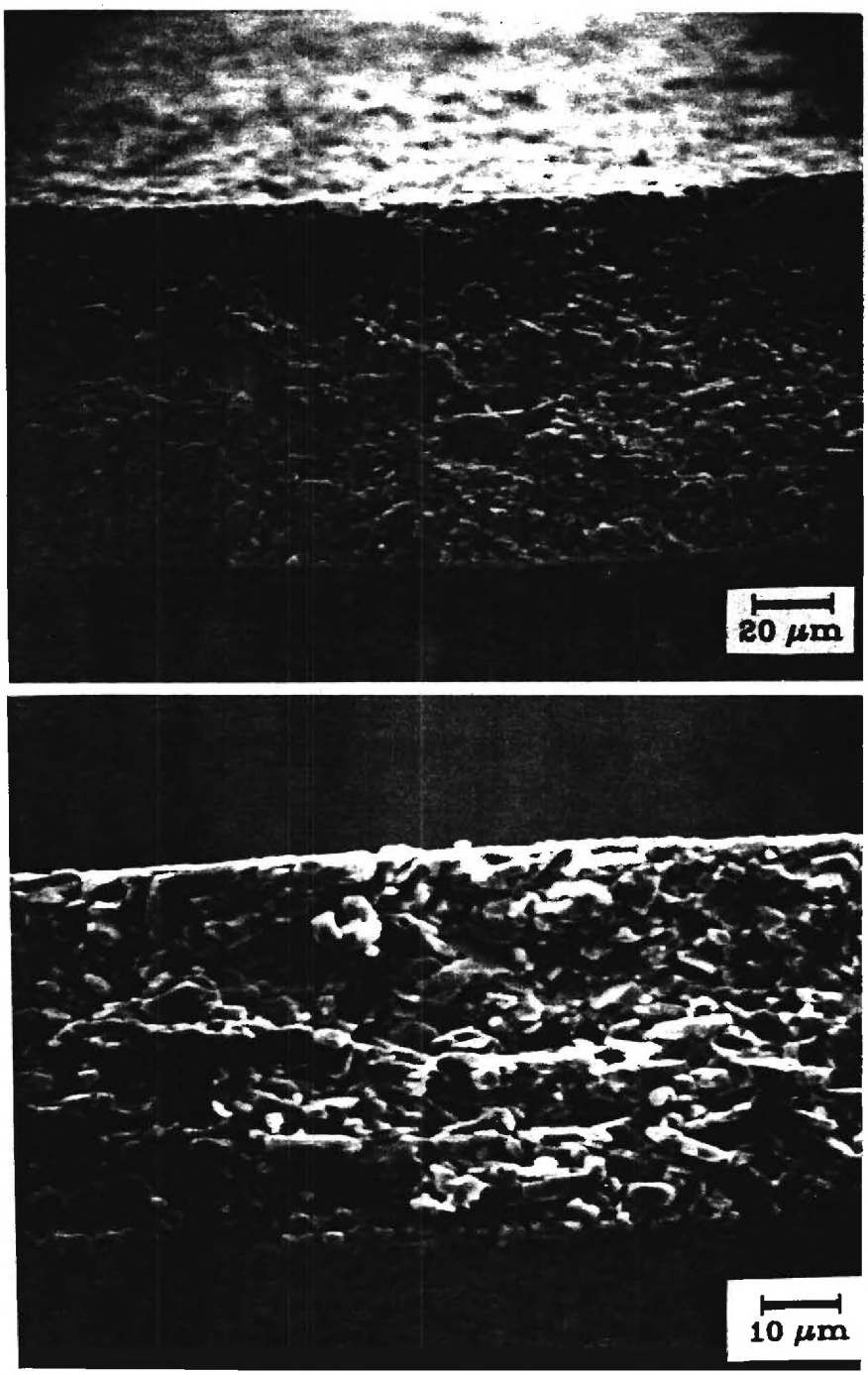

Fig. 12. Crossection of Sphere Walls for Polycrystalline Alumina Spheres Fired at 1650°C, (a) 40-20 and (b) 20-40.

15.6 lb/ft^3, respectively.

Sphere diameters, aspect ratios, and shape factors were measured using a video camera interfaced to an image analyzer. At a magnification of 11 x, four spheres at a time could be measured. For each sphere, the diameter in eight directions, the perimeter, and the crossectional area were recorded. For each blowing condition, 64 randomly selected spheres were quantified. As reported in Table 3 and shown in Figure 13, the average diameters for the two conditions were 2.50 and 3.17 mm with one standard deviation for the distributions of 2.8% and 2.6% respectively. This provides a 3σ limit of ~8% which is well under the 10% target for diameter variation suggested in the work statement.

Spherodicity was measured with two techniques by the image analyzer; aspect ratio and shape factor. The aspect ratio measured for each sphere was the maximum of the eight diameters divided by the minimum diameter. Because the sphere image was digitized from a video camera, the viewed area was divided into 256 x 256 pixals. Each diameter measurement had an error of $\pm$ 1 pixal. This provided a diameter measurement error of 2.5% for the small spheres and 2.0% for the large spheres. Because of the error, perfect spheres would have average aspect ratios of 1.05 and 1.04 for the small and large spheres respectively. The measured average aspect ratios for 40-20 and 20-40 were 1.11 and 1.08, respectively, Figure 14, which provided deviations of

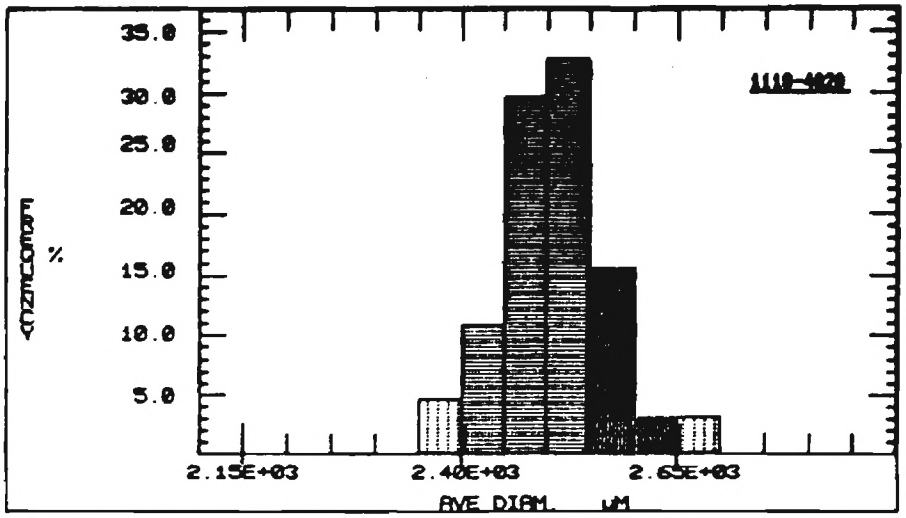

(a) Blowing Condition 40-20

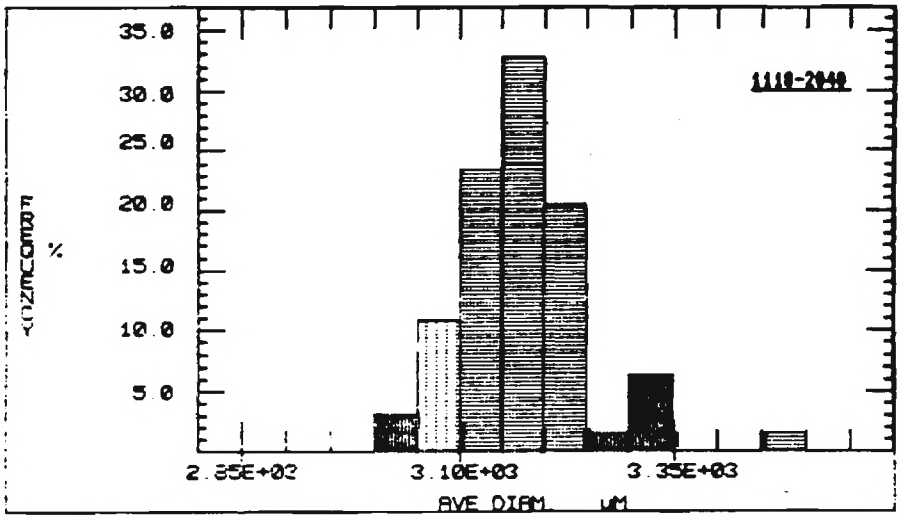

(b) Blowing Condition 20-40

Fig. 13. Diameter Distributions for 64 Randomly Selected Thin Wall Hollow Alumina Spheres.

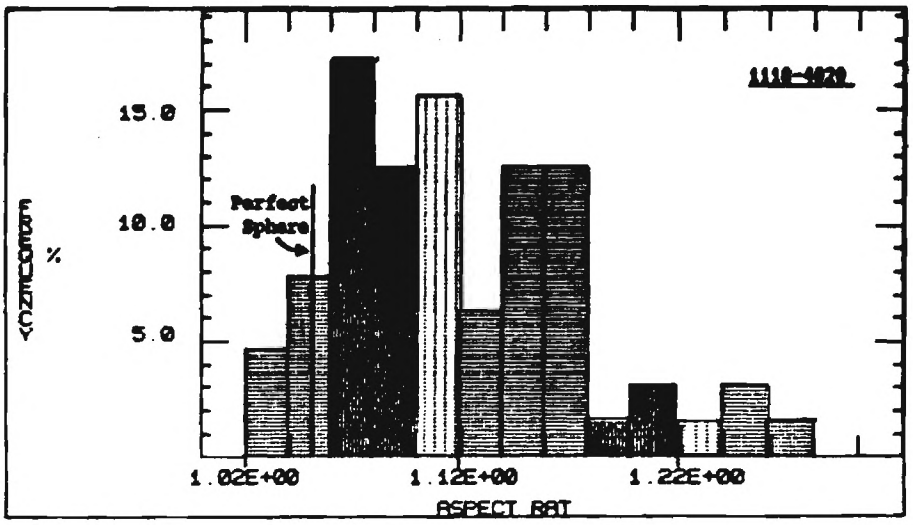

(a) Blowing Conditions 40-20

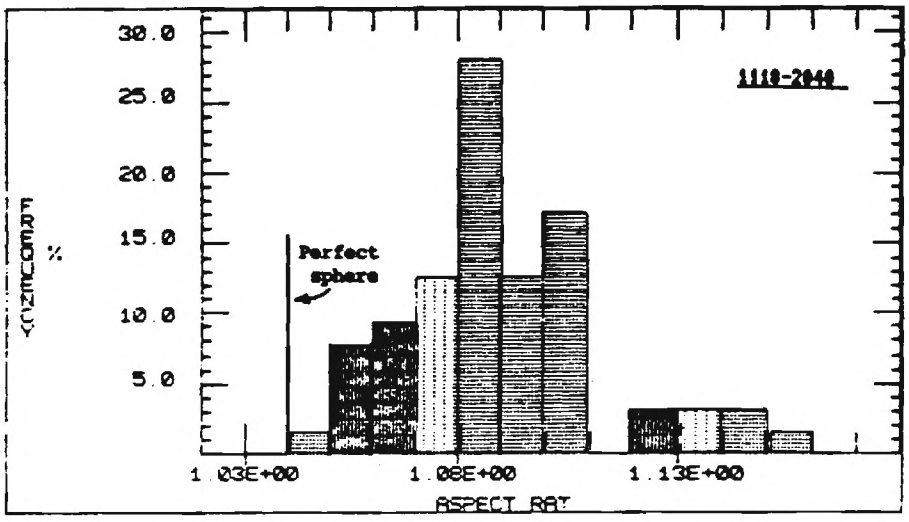

(b) Blowing Condition 20-40

Fig. 14. Aspect Ratio Distributions for 64 Randomly Selected Thin Wall Hollow Alumina Spheres.

6% and 4% from spherodicity, respectively. Although, the 6% and 4% deviations are above the desired value of 2%, it must be noted that aspect ratio is the most sever measurement of spherodicity that can be applied. As residence time in the recovery tower is increased, so also should sperodicity.

A more moderate measure of spherodicity was the shape factor which is $P^2/4\pi A$ where P is the measured perimeter and A the crossectional area of the projected sphere. Shape factor for a perfect sphere is 1.00; for a hexagon, it is 1.10; and a square has a factor of 1.27. Shape factors on average were 1.04 and 1.03 for the small and large spheres, respectively, Figure 15. Standard deviations for the shape factors were only 2%. By this techniques, deviations from spherodicity were minimal.

Using the average diameter for each distribution to calculate individual sphere volume and the average individual sphere weight from 100 spheres, the true sphere density was calculated to be 1.07 and 0.41 g/cc for the small and large spheres, Table 3. Based on an alumina wall density of 3.98, the average wall thickness calculated to be 112 and 56 μm, respectively, Table 3. The thicknesses from the wall crossection micrographs of Figure 11 agree well with these values. Statistical analysis of wall thickness variation has not yet been completed but techniques using the image analyzer are under development.

From the above analysis, it can be seen that the thin walled spheres being produced by the coaxial nozzle process

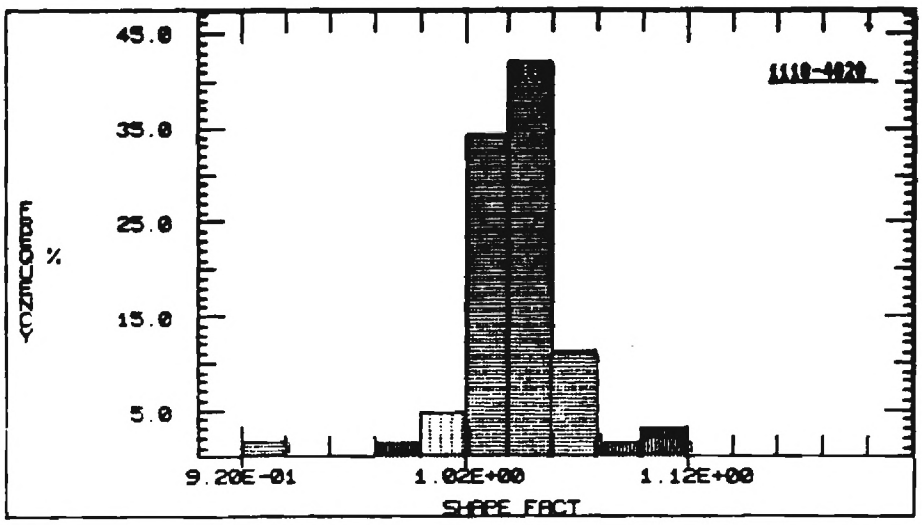

(a) Blowing Conditions 40-20

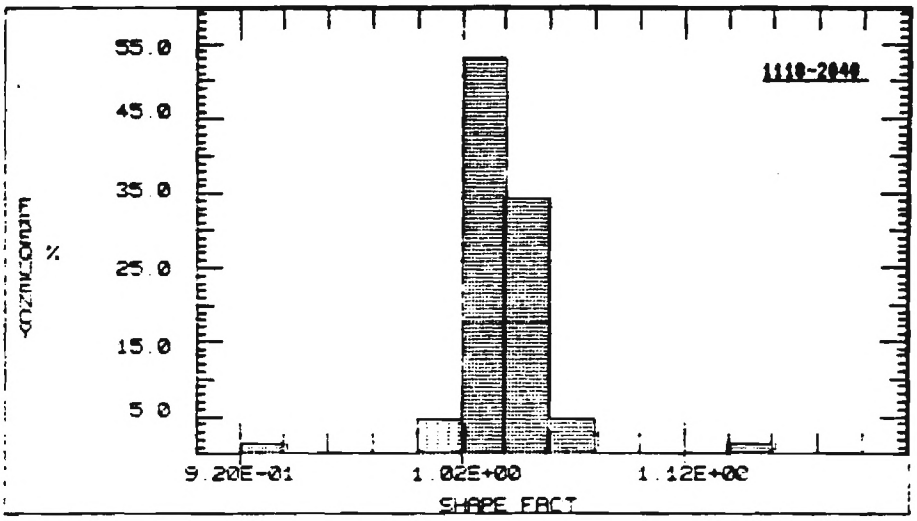

(b) Blowing Conditions 20-40

Figure 15. Shape Factor Distributions for 64 Randomly Selected Thin Wall Hollow Alumina Spheres.

have a uniformity seldom achieved by a bulk production process. As process controls are varied and improved, not only will the range of diameter and densities increase but distributions and deviations from spherodicity will approach a true monodispersed state.

FUTURE EFFORTS

Phase I has been successfully completed to the extent that test quantities of high quality thin-wall macrospheres may be collected. Naturally, obvious system alterations which improve the quality of the spheres will be made. However, sphere perfection is at the stage that Phase II should be implemented and the majority of the next year should be spent on Investigation of Process Parameters to deliniate the range of sphere diameters, wall thicknesses, and densities that one selectable within the context of the system.

The degree of sphere perfection and reproducibility that has been achieved in the first year is considerably better than was anticipated at the begining of the program. Therefore it is requested that a portion of Phase III effort also be initiated during the second year. At least initial attempts at other compositions (clay based, partially stabilized zirconia (PSZ), and SiC) should be implemented in the next year. In the area of properties, consultation should be initiated with thermal conductivity experts at ORNL to determine the most advantageous means of testing the

ceramic macrosphere for low conductivity applications. Finally, physical properties such as crush strength on both individual spheres plus monoliths bonded in several ways would be desirealbe. Both of the properties areas would serve as master's theses for two graduate students added to the program in the last quarter. Both students are supported on fellowships from the office of the Vice President for Research. Therefore no additional funds are requested. Being able to develop background and test techniques on property determination during year two would greatly advance efforts in the third year of the program.

Thin-Wall Hollow Ceramic Microspheres from Slurries

by

A. T. Chapman, J. K. Cochran, J. M. Britt, T. J. Hwang
M. K. Adicks, and M. Shapiro

School of Materials Engineering
Georgia Institute of Technology
Atlanta, Georgia 30332-0245

ORNL Subcontract 86X-22043C

ABSTRACT

During Phase I of this program the objective was to develop a process for fabricating thin-wall hollow spheres from powder slurries using the coaxial nozzle fabrication method. This objective was successfully met by utilizing alumina powders dispersed in organic liquids, where the individual spheres could be blown between 30 to 60 per second, and dropped into an updraft column to provide time sufficient for drying. The dried spheres had the strength necessary to survive landing and collection on a hard surface. Based on the success during Phase I, the work statement for Phase II was revised to emphasize the assessment of the potential structural and insulation applications for the spheres and modeling the sphere formation process. This report describes the preliminary analysis of the mechanical properties of loose spheres, the fabrication of samples for thermal conductivity measurements at the Oak Ridge National Laboratory, and the initial efforts of modeling the sphere forming process.

INTRODUCTION

The overall objective of this effort is to develop a process for economically fabricating thin-wall hollow ceramic spheres from conventional ceramic powders using dispersions. Thin-wall hollow ceramic spheres of small (one to five millimeter) diameter might have numerous novel applications as high-temperature insulation or even light structural materials.

Small solid spheres, and in a few cases, even thin-wall

hollow spheres of ceramics have been made either from the melt or from sol-gel processes. This limits the production to either the lower temperature melting ceramics, such as glass, or those that can be made from solutions, such as alumina. Small diameter spheres of SiC or Si_3N_4 have not been made. The basic approach in the present work is to use a recently developed and patented process whereby the sphere can be made from powder dispersions or slurries, thereby permitting the use of virtually any ceramic composition. During this reporting period, January 1 through March 31, 1987, the Phase I effort was completed and work was initiated in the revised Phase II work where structural and insulation potential for these unique particles will be emphasized.

DISCUSSION OF CURRENT ACTIVITIES

Assessment of Structural Potential

When an unrestricted sphere is loaded uniaxially, a compressive force exists along the axis and tensile force is placed on the exterior of the sphere at the equator[1]. For thin-wall spheres, failure does not occur at the points of contact due to Hertzian stress but results from exceeding the material tensile stress due to the bending of the wall at the equator. When this occurs, a circumferential crack forms around the equator, splitting the sphere in half. The stress on the surface at failure is [1]

(1) $$\sigma_c = \frac{3F_c(d/3)}{2\pi dt^2} = \frac{F_c}{2\pi t^2}$$

or,

(2) $$F_c = 2\pi t^2 \sigma_c$$

where F_c is the critical force at fracture, σ_c is the critical strength of wall material, t is the sphere wall

thickness, and d the sphere diameter.

In order to test the validity of the model, three different batches of spheres, produced over a five (5) month period, were characterized. The critical force at fracture, F_c, was determined by crushing 50 individual spheres from each lot on an Instron testing machine. The critical load, P_c, was applied uniaxially using hardened steel platens.

The wall thickness, t, was calculated from individual sphere density, ρ. The sphere density is related to the wall thickness by the equation

$$\frac{\rho}{\rho_o} = \frac{3t}{r} - 3\left(\frac{t}{r}\right)^2 + \left(\frac{t}{r}\right)^3 \qquad (3)$$

where ρ_o is the theoretical density of the sphere material. Because the walls are very thin the equation effectively reduces to

$$\frac{\rho}{\rho_o} = \frac{3t}{r} \qquad (4)$$

The density of individual spheres must first be determined from the sphere weight and volume. Image analysis, as reported in the 1986 Final Report, was used to measure the diameters of 64 spheres in each batch and an average was obtained. Similarly, 100 spheres were weighed and an average sphere weight was calculated. The average individual sphere density was calculated from the average weight and volume based on diameter. Finally, using this data, an average wall thickness for each batch was calculated. These values are given in Table I.

Assuming the strength model is correct, a plot of the average critical load, P_c, (note: $F_c = P_c g$ where g is the acceleration of gravity) versus the average thickness squared, t^2, should be a straight line passing through the origin. Figure 1 shows that if a σ_c of 310 MPa is assumed for the tensile strength of the alumina sphere wall, at the two lower wall thickness samples, Equation 2 agrees with the experimental results. Certainly the 310 MPa used for σ_c is a

Table I. PROPERTIES OF POLYCRYSTALLINE ALUMINA THIN WALL HOLLOW SPHERES AND STRENGTH DURING UNIAXIAL LOADING

Sample Number	Diameter (μm)	Density* (g/cc)	Wall (μm)	P_c (Uniaxial) (grams)	σ_c (MPa)	Weibull Modulus (m)
11186	3168 $\pm$ 83	0.44	58	650 $\pm$ 440	298 $\pm$ 201	1.82
02057	3096 $\pm$ 279	0.91	117	2120 $\pm$ 790	240 $\pm$ 89	2.99
03247	3320 $\pm$ 126	0.59	82	1340 $\pm$ 400	310 $\pm$ 92	3.44

* This represents sphere density and not bulk density.

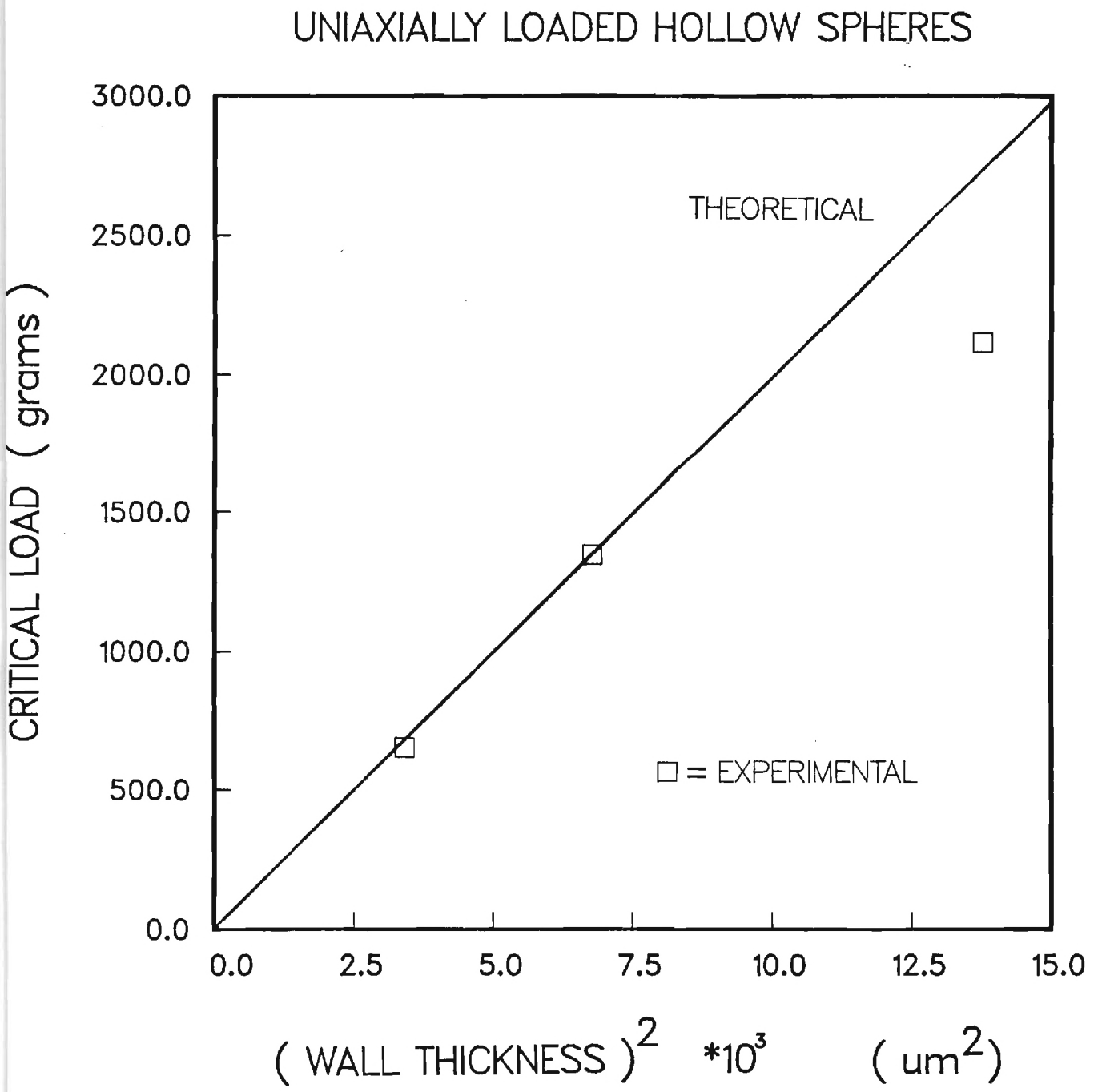

Figure 1. Comprison of Critical Load vs. Wall Thickness Calculated From Equation 2 (Theoretical) and Experimental Values From Table I.

typical value for Al_2O_3 with a grain size of 3-5μm. Due to the variation in wall thickness which causes some of the spheres to fail at the top or bottom poles rather than at the equator, the spheres with the greater wall thicknesses had strengths less than predicted. A Weibull plot of the probability of failure versus the applied load is shown in Figure 2. The slope of the best-fit line is equal to the Weibull modulul, m, which describes the flaw size distribution and thus the data scatter. The m values, shown in Table I, indicate that the spheres from Run No. 03247 have the least amount of scatter. Interestingly, this group has the highest σ_c, emphasizing the importance of wall thickness uniformity on the strength of the sphere.

Assessment of Insulation Potential

During recent discussions with ORNL personnel, a cooperative effort was initiated to assess the insulation potential of the thin-wall spheres. The theoretical modeling and experimental measurements of the thermal conductivity will be performed at ORNL. Georgia Tech will fabricate product for experimental evaluation, both to verify the model and to document the insulation potential of the product. In addition, an M.S. student, Michael Shapiro, will work at ORNL for three months this summer.

Preparation of samples needed for conductivity measurements is underway. Spheres of Al_2O_3 + 7w/o Cr_2O_3 have been successfully blown and fired. A porcelain enamel frit containing TiO_2 for light scattering and reflection has been received and a very preliminary trial indicated that the much larger particle size (avg. = 20 μm) distribution of the frit was unsuitable for sphere formation using existing nozzle dimensions and slip parameters. A rheology study has been initiated on blending fine grained ZrO_2 (average diameter < 1μm) with acetone and binder (see rheology section of this report) to form ZrO_2-based dispersions suitable for sphere production. Two trials with ZrO_2-based slips suggest

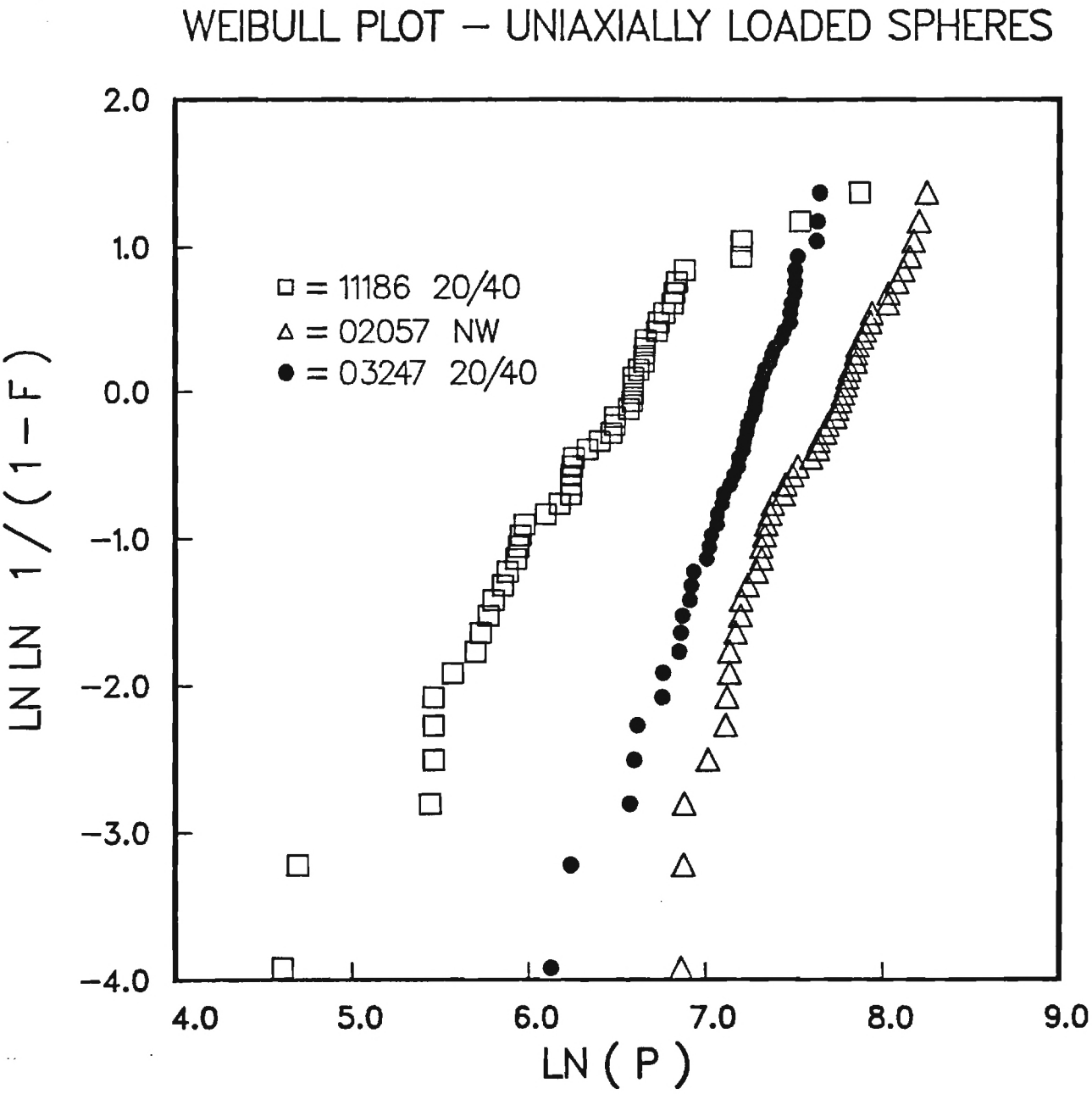

Figure 2. Weibull Plot of Uniaxially Loaded Thin-Wall Spheres.

sphere formation in this system is achievable.

Based on the encouraging results with Al_2O_3-Cr_2O_3 and ZrO_2 trials, the candidate shells of varying composition desirable for T/C measurements at ORNL should be available this summer.

Sphere Formation Model

During the next two years an effort will be made to develop mathematical expressions which describe various stages of the very complex sphere formation process occurring as powders dispersed in fluids are forced through the concentric nozzle assembly. We hope to arrive at a model that may be used to correlate and predict the findings of the concurrent experimental parameter study to be initiated shortly. An important first step in the model is establishing the factors controlling the rheology of powders and binders dispersed in acetone. In this area, an absorption isotherm for Elvacite 2008 interaction with a fine grained ZrO_2 powder is reported. The flow of the slip through the concentric tubes controls the delivery rate and geometrical conditions as blowing is initiated. Pertinent information abstracted from the literature describing flow through annuli are presented and compared with experimentally measured flow rates of Al_2O_3-based slips.

Rheology Study - Absorption Isotherm

In this reporting period a partially stabilized zirconia (PSZ) powder*, Elvacite 2008** dispersant and acetone were milled together for 24 hours at room temperature. The zirconia concentration was fixed at 30% by volume and the polymer concentration was varied from 1 to 9% by weight of the zirconia content. After milling, the viscosity of the resultant slip was measured. Additional samples were centrifuged and the supernatant solutions decanted for analysis of the polymer content.

To determine the absorption isotherm, the index of refraction of the supernatant liquid was compared with the

index values of previously prepared standards of appropriate dispersant-acetone composition. The equilibrium concentration of polymer remaining in the solvent was converted to weight and subtracted from the initial amount in the slip to calculate the quantity (grams of polymer per 100 grams of solid) absorbed on the PSZ particles. These data are plotted in Figure 3 where the numbers 1 through 9 at the data points on the graph refer to the initial polymer content in w/o of PSZ. The data in Figure 3 suggest the PSZ particles are coated with a monolayer of polymer when ~ 3 grams of polymer are added per 100 grams of powder. Interestingly, the viscosity measurements, Figure 4, also display a minimum value at 3 w/o polymer content. While this information is most helpful in understanding the rheology of solids and binders dispersed and dissolved in organic liquids, the selection of a polymer content suitable for the total sphere formation and collection process must reflect other requirements, i.e., drying rate, fluid drainage in flight, adequate strength for landing, etc.

Fluid Flow in Coaxial Nozzle

The initial boundary condidtions prior to sphere formation is dictated by the slip flow through the coaxial nozzle. Fluid flow in concentric tubes is described by the expression[2]

$$Q = \frac{\pi \Delta_p R_2^4}{8 \eta L} \left[(1 - k^4) - \frac{(1 - k^2)^2}{\ln (1/k)} \right]$$

where $K = R_1/R_2$

R_1 = radius of inner tube

R_2 = radius of outer tube

L = length of annuli

η = viscosity of fluid

Δ_p = pressure drop across length L

Q = fluid delivery rate

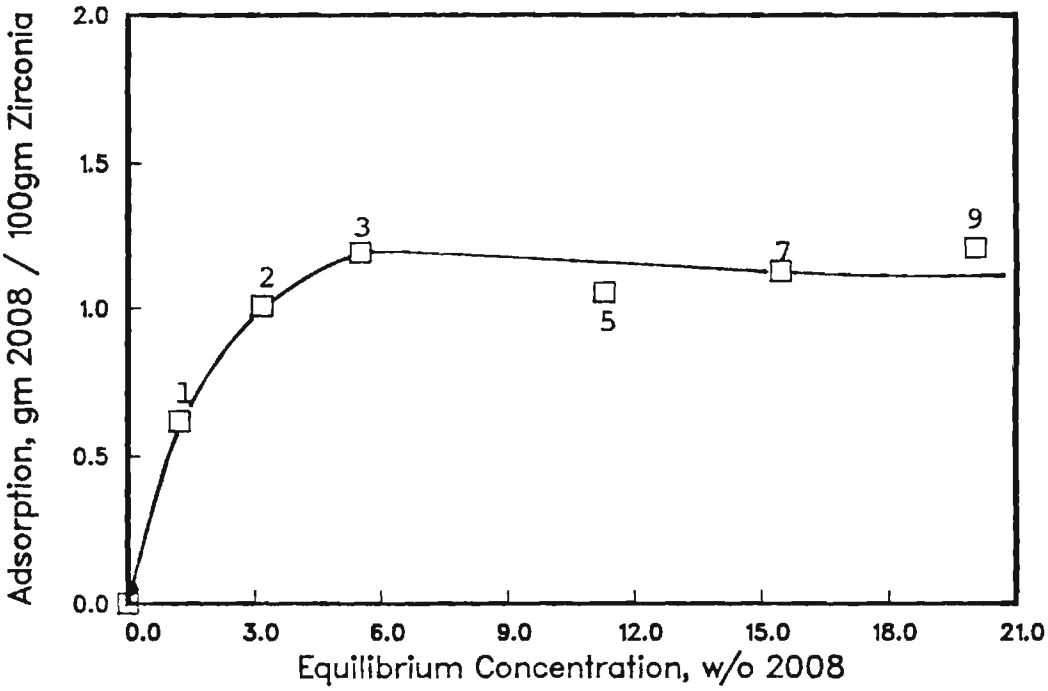

Figure 3. Absorption Isotherm for PSZ Powder* (Type H5Y3) Mixed With Elvacite 2008** and Acetone.

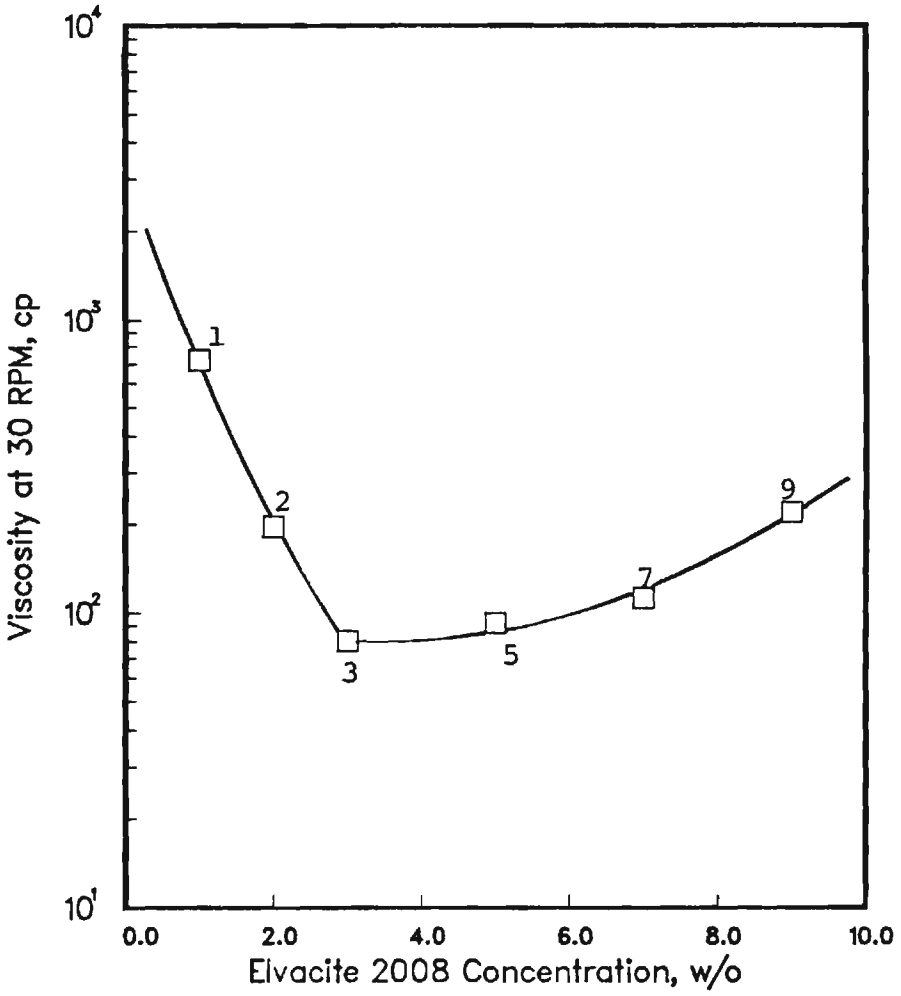

Figure 4. Viscosity of PSZ-Acetone Slip With Varying Concentration of Dispersant, Elvacite 2008**.

Preliminary comparisons of measured Al_2O_3-based slip flow rates with calculated values from this expression show the calculated values to be low by a factor of two to three. Probable reasons for this discrepancy include: (1) In the derivation of this equation the length, L, was assumed to be much larger than the radius, R_2, and thus entrance and exit effects could be ignored, this is certainly not the case with existing nozzle designs, and (2) the existing slips are pseudoplastic in nature and the high shear rate in the nozzle may be significantly less than that measured by conventional viscometers. Efforts will be made to provide suitable correction factors so that this equation will fit the flow in present and future nozzle designs. Literature and computer searches are planned to find previous attempts to model the film forming process as the liquid tube expands and pinches off during sphere formation.

References and Footnotes

1. P. W. Pratt, J. P. Cummion, and B. D. Spivack, "Mechanical Testing of Glass Hollow Microspheres," in Advances in Materials Characterization, Ed. D. R. Rossington et. al., Plemun Press, N. Y., 441-448, 1983.

2. A. G. Fredrickson and B. B. Bird, "Non-Newtonian Flow in Annuli," Ind. and Eng. Chem., vol. 50, No. 3, 347-52, 1958.

* Manufactured by Daiichi Kigenso, Osaka, Japan Powder No. H5Y-3.0.

** Manufactured by E. I. DuPont, Wilmington, Delaware.

ATC

THIN-WALL HOLLOW CERAMIC MICROSPHERES FROM SLURRIES

by

A. T. Chapman, J. K. Cochran, G. J. Simitses, R. Riff, J.M. Britt, T. J. Hwang, M. K. Adicks, and M. Shapiro

School of Materials Engineering
Georgia Institute of Technology
Atlanta, Georgia 30332-0245

ORNL Subcontract 86X-22043C

ABSTRACT

The overall objective of this effort is to develop a process for economically fabricating thin-wall hollow ceramic spheres from conventional ceramic powders using dispersions. Thin-wall hollow ceramic spheres of small (one to five millimeter) diameter might have numerous novel applications as high-temperature insulation or even light structural materials.

Small solid spheres, and in a few cases, even thin-wall hollow spheres of ceramics have been made either from the melt or from sol-gel processes. This limits the production to either the lower temperature melting ceramics, such as glass, or those that can be made from solutions, such as alumina. Small diameter spheres of SiC or Si_3N_4 have not been made. The basic approach in the present work is to use a recently developed and patented process whereby the sphere can be made from powder dispersions or slurries, thereby permitting the use of virtually any ceramic composition.

During Phase I of this program the objective was to develop a process for fabricating thin-wall hollow spheres from powder slurries using the coaxial nozzle fabrication method. This objective was successfully met by utilizing alumina powders dispersed in organic liquids, where the individual spheres could be blown between 30 to 100 per second, and dropped into a heated updraft air column to provide time sufficient for drying. The dried spheres had the strength necessary to survive landing and collection on a hard surface. Based on the success during Phase I, the work statement for Phase II was revised to emphasize the assessment of the potential structural and insulation applications for the spheres and modeling the sphere formation process.

Analytical methods have been employed to predict the buckling strength using thin shell theory as well as crushing of the material under two point and isostatic loads. A finite element code has been written to predict

sphere strengths for samples possessing uniform, as well as variable wall thickness. The strength of alumina spheres have been measured in two point loading and the experimental results are in reasonable agreement with the finite element modeling work. The thermal conductivity of a series of thin-walled spheres fabricated at Georgia Tech were measured at the Oak Ridge National Laboratory. This information is being used to help develop a computer model to predict thermal conductivity of this unique material. The modeling of the spheres formation process is currently underway with the evaluation of sphere fabrication parameters on sphere size, density and frequency of formation. This report summarizes the information obtained during the first two reporting periods of Phase II activity, January through June, 1987 and details the results obtained July through October, 1987.

THIN-WALL HOLLOW CERAMIC MICROSPHERES FROM SLURRIES

by

A. T. Chapman, J. K. Cochran, G. J. Simitses, R. Riff,
J.M. Britt, T. J. Hwang, M. K. Adicks, and M. Shapiro

School of Materials Engineering
Georgia Institute of Technology
Atlanta, Georgia 30332-0245

ORNL Subcontract 86X-22043C

INTRODUCTION

The overall objective of this effort is to develop a process for economically fabricating thin-wall hollow ceramic spheres from conventional ceramic powders using dispersions. Thin-wall hollow ceramic spheres of small (one to five millimeter) diameter might have numerous novel applications as high-temperature insulation or even light structural materials.

Small solid spheres, and in a few cases, even thin-wall hollow spheres of ceramics have been made either from the melt or from sol-gel processes. This limits the production to either the lower temperature melting ceramics, such as glass, or those that can be made from solutions, such as alumina. Small diameter spheres of SiC or Si_3N_4 have not been made. The basic approach in the present work is to use a recently developed and patented process whereby the sphere can be made from powder dispersions or slurries, thereby permitting the use of virtually any ceramic composition.

This is the interim report for Phase II activities covering the period January 1, to September 30, 1987 with emphasis on the accomplishments for the third quarter of Phase II work, July 1 to September 30, 1987. The major objectives of Phase II are to assess the structural and insulation potential of the spheres and to continue the on-going analysis and modeling of the sphere formation process. In the structural area an effort is underway to develop models to calculate the ranges of stiffness and strength possible for the thin-wall ceramic spheres both as individual spheres as well as bonded monoliths. Computer codes to predict the strength of individual spheres in two point and isostatic loads have been developed. Very preliminary testing of the spheres under isostatic loading indicated failure pressures much less than predicted by an analytical model for thin-wall shells of uniform wall thickness. The probable cause of this discrepancy is the nonuniformity in wall thickness of the "real" spheres as presently fabricated. A finite element code was developed to include variations in the wall thickness of an individual sphere in the calculation of mechanical strength. This program was employed with an approximation of the "real" wall geometry of a specific sample of spheres to predict the uniaxial two-point failure loads. The resultant calculated strengths were in good agreement with the average measured uniaxial loads necessary to fracture this sample of thin-wall Al_2O_3 shells. Efforts to measure

the isostatic strength of individual spheres and the correlation with failure pressures predicted using the infinite element code are continuing and will be described in subsequent reports. Improvements in sphere wall uniformity must be made if the potential strength of the spheres, especially under isostatic loads, are to be achieved.

The initial evaluation of the thermal conductivity (T/C) of beds of spheres of variable geometry and different compositions was performed at ORNL. These results are being utilized by ORNL personnel in the development of an analytical model to predict thermal conduction of future spheres, and to direct sphere fabrication efforts toward forming the optimum sphere geometry and composition to yield low T/C material. The room temperature T/C measurements documented the need to employ low density sphere beds composed of low conductivity solids to minimize conduction. The lowest T/C material tested was relatively dense ZrO_2 spheres. Simple extrapolation suggested if the walls of the ZrO_2 sample could be reduced in half (from 120μm to 60 μm) this material would approach the T/C of glass fiber insulation. The T/C of several sphere compositions was measured from room temperature to 1000°K and during this temperature interval the T/C showed a 2 to 2½ fold increase. Interestingly, silica based refractory fiber insulation shows a 5 fold increase during this same interval. This behavior suggests selected sphere

compositions may be competitive with refractory fibers, especially at and above the upper use temperature of the fibers.

An effort is underway to develop mathematical expressions which describe various stages of the very complex sphere formation process occurring as powders dispersed in fluids are forced through the concentric nozzle assembly. An objective of this model is to predict the probable upper and lower limits of sphere diameter and wall thickness expected from this technology. An important first step in the model is establishing the factors controlling the rheology of powders and binders dispersed in liquids. Adsorption isotherms were employed to evaluate powder dispersibility and binder distribution in a variety of slip compositions. The effectiveness of different binder/dispersant compositions for forming stable suspensions is also underway.

A systematic experimental study of the process parameters that control the sphere diameter, wall thickness and sphere forming rate is ongoing. During this work spheres between 1.6 and 4.5mm in diameter have been successfully formed, collected and densified. Future parameters to be included in the sphere forming study include slip rheology with emphasis on resultant sphere wall uniformity.

DISCUSSION OF CURRENT ACTIVITIES

Assessment of Structural Potential

In this section the development of models useful in predicting the mechanical strength of the thin-wall Al_2O_3 spheres, the actual measurements of sphere strength under two-point loads and the probable causes of disagreements between predicted and measured strengths are presented. The initial modeling work used thin shell relationships from the literature to predict the isostatic strength of spherical and ellipsoidal spheres possessing uniform wall thickness. Very preliminary evaluation of isostatic strengths of the spheres (to be described in future reports) indicated the measured hydrostatic strength was much less than the predicted value. The probable cause for this discrepancy is the variable wall thickness present the spheres as presently fabricated. A finite element code was developed to predict the mechanical strength of spheres of virtually any geometry under all types of loads. The compressive uniaxial strength of 22 batches of spheres made under varying forming parameters was measured and one set of spheres was carefully examined to provide a realistic approximation of the "real" variation in wall thickness. Whereas the predicted and measured isostatic strength were in major disagreement, the uniaxial modeled and measured strengths agree remarkedly well once the "real" sphere geometry was employed in the code. The experimentally measured uniaxial fracture load for the Al_2O_3 spheres was

used to calculate the tensile strength of the sphere wall and these values agreed reasonably well with the flexural strength of Al_2O_3 bars sintered under equivalent conditions as the spheres. The information in this section describes the initial efforts to develop models capable of predicting the strength of the thin-walled spheres, and strongly endorses the need to improve the wall thickness uniformity if the structural potential of these thin shells are to be realized.

Model of Mechanical Properties

Analytical solutions are presented for the buckling strength of spherical and ellipsoidal thin-wall shells. In addition, failure by crushing of the material is also predicted analytically. In both cases the shell is assumed to be of constant thickness and free of initial geometric imperfections. To treat the case of shells possessing nonuniform walls a finite element code was developed to predict failure strength under all types of loads.

First, the geometry of the shells and the ranges of the geometric parameters are presented, as well as the material properties. Subsequently the analytical results are computed and discussed, and finally a comparison with experimental results is presented.

Structural Geometry

The geometry of a thin ellipsoidal shell of revolution and the designated geometric parameters are shown in Figure 1. The uniform thickness is denoted by t, and the major and

minor diameters are given by d_1 and d_2, respectively. If one assumes that the ellipsoidal is generated by rotating the ellipse about the x-axis, see Figure 1, then R_1 denotes the radius of the cross-section at x = 0, while R_2 denotes the radius of an oscillating circle tangent to the ellipse at x = 0.

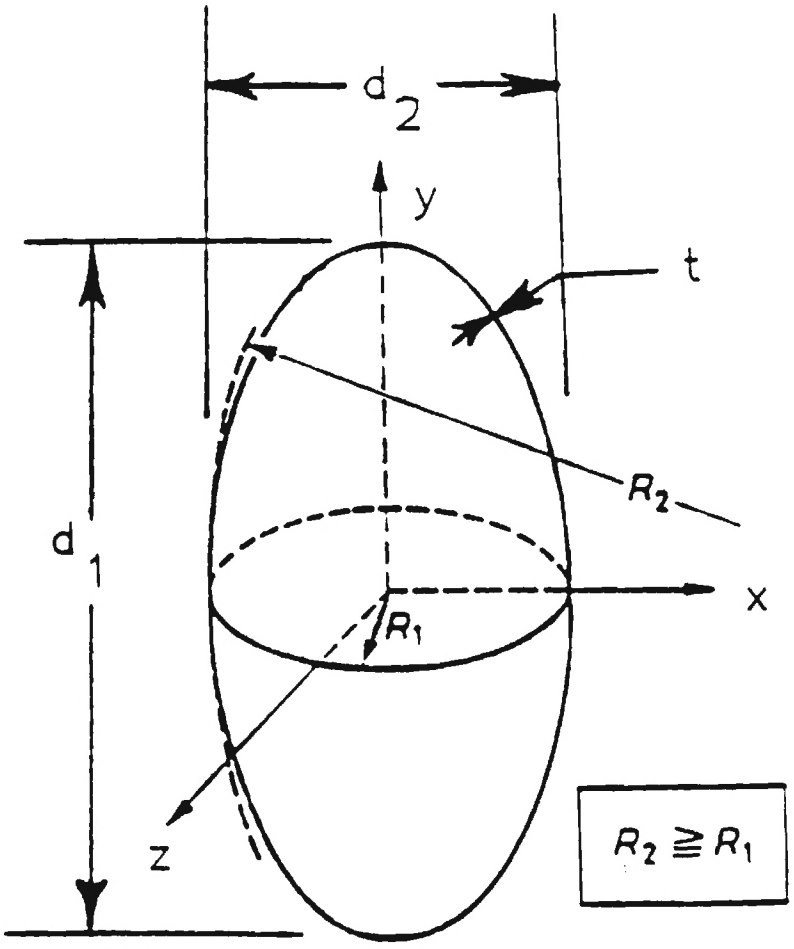

Figure 1. Geometry of a Thin Ellipsoidal Shell

In terms of d_1 and d_2, the radii R_1 and R_2 are:

$$R_1 = d_2/2;\ R_2 = \frac{d_2}{2}\left(\frac{d_1}{d_2}\right)^2 \qquad (1)$$

The best estimates of the material properties of the sintered alumina forming the thin sphere walls are:

Elastic Modulus

$$E_t = E_c = 380 \times 10^9 \text{ Pa} \qquad (2a)$$
$$= 55.1 \times 10^6 \text{ psi}$$

Poissons Ratio

$$\nu = 0.26 \qquad (2b)$$

Tensile Strengtn

$$\sigma_{ult_t} = 0.345 \times 10^9 \text{ Pa}$$
$$= 50{,}000 \text{ psi} \qquad (3a)$$

Compressive Strength

$$\sigma_{ult_c} = 6.89 \times 10^9 \text{ Pa} \qquad (3b)$$
$$= 10^6 \text{ psi}$$

The compressive ultimate strength is needed in order to establish whether the failure is by buckling or crushing of the material. Finally, the range of interest for the geometrical parameters is given by:

$$1\text{mm} < d_2 < 4\text{mm}\ ; \qquad (4a)$$

$$5 < \frac{d_2}{2t} = \frac{R_1}{t} < 50; \qquad (4b)$$

and

$$1 < \frac{d_1}{d_2} < 4 \qquad (4c)$$

Isostatic Buckling Load For A Thin Spherical Shell

The classical critical pressure, P_{cl}, for a thin spherical shell of constant thickness under hydrostatic load is given by [1,2]:

$$P_{cl} = \frac{2E}{\sqrt{3(1-\nu^2)}} \left(\frac{t}{R}\right)^2 \tag{5}$$

Using 0.26 for Poissims ratio this equation reduces to:

$$P_{cl} = 1.196\ E \left(\frac{t}{R}\right)^2 \tag{6}$$

The corresponding classical critical stress is given by

$$\sigma_{cl} = P_{cl}\ R/2t = 0.598\ E \left(\frac{t}{R}\right) \tag{7}$$

Experimental results on all classes of materials point out that the buckling pressure is considerably smaller than the analytically predicted critical pressure, given by Eg (6). Nonlinear analysis reveal [3] that thin spherical shells are imperfection sensitive, and in order to relate analytical predictions, P_{cr}, to experimental results a factor must be used in conjunction with Eg (6).

$$P_{cr} = \Lambda\ P_{cl} \tag{8}$$

where P_{cl}, the classical prediction is given by Eg (6) and Λ is a factor known as the "knockdown factor". This knockdown factor is dependent, among other parameters, on the radius to thickness ratio. For the range of interest, [See Eg (4)], a reasonable value to use for this factor is 0.6 [2,3].

Thus,

$$P_{cr} = 0.718\ E\ (\frac{t}{R})^2 \text{ and} \tag{9a}$$

$$\sigma_{cr} = 0.359\ E\ (t/R) \tag{9b}$$

Note that in order for the shell to fail by buckling, the stress in the sphere wall must be less than 6.89 GPa (10^6 psi), the compressive strength, or

$$0.359\ E\ \frac{t}{R} \leq 6.89 \times 10^9 \text{ Pa } (10^6 \text{ psi}) \tag{10}$$

This occurs when $R/t \geq 20$. For R/t values less than 20, representing smaller diameter and thicker walled spheres, the relationships predict the spheres should fail by crushing. In Table I the first three rows of data (R/t values of 5, 10 and 15) show the ultimate crushing strength as the failure stress., Subsequent data (R/t values 20 or greater) represent calculated stresses and pressures where buckling is the mode of failure.

Isostatic Buckling Load for Ellipsoidal Thin Shells

There exist several approximate expressions for analytically predicting the critical pressure for thin ellipsoidal shells of constant thickness [2,4]. According to Eg. (4.27) of [2] and the discussion on p.95 of [2], the expression for the critical pressure is given by

$$P^E_{cr} = C\ E\ \frac{t^2}{R_1 R_2} \tag{12}$$

where P^E_{cr} denotes the critical pressure for the ellipsoid, C

Table I. Failure Pressure & Stresses (Complete Spherical Shell)

			σ fail = $\frac{PR}{2t}$		$P_{failure}$	
R/t	t/R	$(t/R)^2$ 10^4	in Pa x 10^{-9}	in psi x 10^{-6}	in Pa x 10^{-9}	in psi x 10^{-6}
5	0.2000	400.00	6.895	1.000	2.758	0.4000
10	0.1000	100.00	6.895	1.000	1.379	0.2000
15	0.0667	44.44	6.895	1.000	0.919	0.1333
20	0.0500	25.00	6.821	0.989	0.682	0.0989
25	0.0400	16.00	5.457	0.791	0.437	0.0633
30	0.0333	11.11	4.547	0.659	0.303	0.0439
35	0.0286	8.18	3.901	0.566	0.223	0.0324
40	0.0250	6.25	3.411	0.494	0.171	0.0247
45	0.0222	4.93	3.032	0.440	0.135	0.0196
50	0.0200	4.00	2.728	0.396	0.109	0.0158

is the knockdown factor Λ, E is the Young's modulus for the shell material, t is the shell thickness, and R_1 and R_2 are defined by Eqs. (1). The critical pressure for the ellipsoid can be expressed in terms of that of a sphere, P^S_{cr} with $R_1 = R = d_2/2$,

or

$$P^E_{cr} = E \left(\frac{t}{R_1}\right)^2 \left(\frac{R_1}{R_2}\right) = P^S_{cr} \frac{R_1}{R_2} \tag{13}$$

In terms of d_1 and d_2, then

$$P^E_{cr} = P^S_{cr} \left(\frac{d_2}{d_1}\right)^2 \tag{14}$$

Moreover, according to Eqs (4.28) of [2], the compressive (max.) stress resultants, N_1 and N_2, in the two principal directions are given by

$$N_1 = - P \frac{R_1}{2} \left(2 - \frac{R_1}{R_2}\right) \tag{15a}$$

$$\text{and } N_2 = P \frac{R_1}{2} \tag{15b}$$

Thus, since

$$N_i = \sigma_i h; \; i = 1,2 \tag{16}$$

then,

$$\sigma_1 = - P \frac{R_1}{2t} \left(2 - \frac{R_1}{R_2}\right) \tag{17}$$

$$\sigma_2 = - P R_1/2t$$

and in terms of the major and minor diameters

$$\sigma_1 = - P \frac{d_2}{4t} \left[2 - \left(\frac{d_2}{d_1}\right)^2\right] \qquad (18)$$

$$\sigma_2 = - P\, d_2/4t$$

Next, one must establish the range of R_1/t values for which buckling failure will occur as opposed to failure by crushing. In order to establish failure due to excessive stresses (crushing), the Von Mises failure criteria [5] is employed. If σ_1 and σ_2 denote principal stresses the Von Mises criteria yields

$$\sigma_1^2 + \sigma_2^2 - \sigma_1\sigma_2 \leq \sigma_o^2 = \sigma^2 ult_c \qquad (19)$$

The value of σ_o corresponds to yielding, but for this brittle material (alumina), σ_o represents the ultimate compressive strength. Then substitution of Egs. (18), (14) and (9) into Eg (19) yields that:

$$0.359\, E \left(\frac{2t}{d_2}\right) \left(\frac{d_2}{d_1}\right)^2 \left\{2 - \left(\frac{d_2}{d_1}\right)^2\right\}^2 + 1 - \left\{2 - \left(\frac{d_2}{d_1}\right)^2\right\}\Big]^{\frac{1}{2}} \leq \sigma\, ult_c \qquad (20)$$

is the condition for buckling failure to occur before crushing.

From Eg. (20), buckling will first occur if

$$\left(\frac{d_2}{2t}\right) = \left(\frac{R_1}{t}\right) > 20 \left(\frac{d_2}{d_1}\right)^2 \left[3 - 3\left(\frac{d_2}{d_1}\right)^2 + \left(\frac{d_2}{d_1}\right)^4\right]^{\frac{1}{2}} \qquad (21)$$

If $d_1/d_2 = 2$, 3, and 4, then $d_2/2t > 7.6$, 3.6, and 2.1, respectively.

Valves of critical pressure and stress are presented both in tabular form and graphically, in Table II and Figure 2, for $5 < \frac{R_1}{t} < 50$ and $2 < d_1/d_2 < 4$. Note that when $d_1/d_2 = 1$ (sphere) the corresponding critical strength valves are given on Table I. All critical values in Table II denote failure by buckling except for the values in the first row that denote crushing.

It is suggested (see last paragraph on p. 95 of [2]) that if $0<R_1/R_2<0.5$ or $0<d_2/d_1 < 0.707$, the P^E_{cr} is better approximated by

$$P^E_{cr} = P^S_{cr}/2 \tag{22}$$

The curve corresponding to $d_1/d_2 = \sqrt{2} = (0.707)^{-1}$ is shown also in Figure 2. If this suggestion is valid then, the curves corresponding to $d_1/d_2 = 2, 3, 4$ are primarily academic.

Table II. Failure Pressures and Stresses for Isostatic Loading of Ellipsoidal Shells.

$\frac{R_1}{t} = \frac{d_2}{2t}$	d_1/d_2	σ_1 fail		σ_2 fail		P fail	
		in Pa x10^{-9}	in psi (10^{-6})	Pa x 10^{-9}	psi x 10^{-6}	Pa x 10^{-9}	psi x 10^{-6}
5	2	7.9336	1.1506	4.5335	0.6575	1.8134	0.26300
	3	5.7248	0.8303	3.0308	0.4396	1.2123	0.17583
	4	3.3030	0.4790	1.7048	0.2473	0.6819	0.09890
10	2	5.9669	0.8654	3.4095	0.4945	0.6819	0.09890
	3	2.8656	0.4156	1.5169	0.2200	0.3034	0.04400
	4	1.6500	0.2393	0.8515	0.1235	0.1703	0.02470
20	2	2.9807	0.4323	1.7031	0.2470	0.1703	0.02470
	3	1.4300	0.2074	.7571	0.1098	0.0757	0.01098
	4	1.6500	0.2393	0.8515	0.1703	0.2470	0.02470
30	2	1.9871	0.2882	1.1356	0.1647	0.0757	0.01098
	3	0.9536	0.1383	0.5047	0.0732	0.0337	0.00488
	4	0.5488	0.0796	0.2834	0.0411	0.0189	0.00274
40	2	1.4941	0.2167	0.8534	0.1238	0.0426	0.00618
	3	0.7136	0.1035	0.3778	0.0548	0.0189	0.00274
	4	0.4247	0.0616	0.2124	0.0308	0.0106	0.00154
50	2	1.1921	0.1729	0.6812	0.0988	0.0272	0.00395
	3	0.5730	0.0831	0.3034	0.0440	0.0121	0.00176
	4	0.3316	0.0481	0.1710	0.0248	0.0068	0.00099

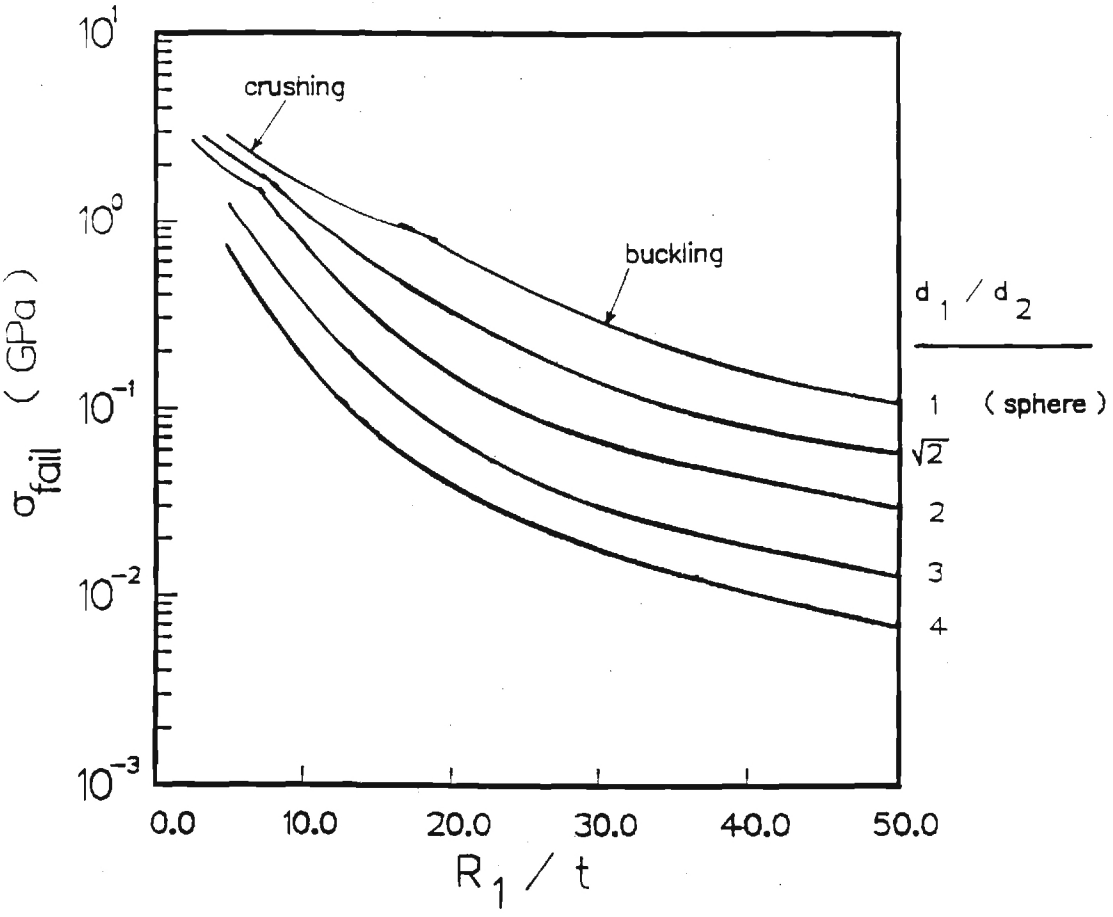

Figure 2. Predicted Failure Pressure for Spherical and Ellipsoidal Shells, from Table I and II.

Finite Element Model For Predicting Sphere Failure

The preceding analysis predicts a 3 mm diameter Al_2O_3 sphere with a wall thickness of 50, 85, and 120 μm should withstand isostatic pressures of approximately 50,000,100,000 and 150,000 psi, respectively. Preliminary isostatic strength measurements (to be described next reporting period) on spheres of these geometries failed at average pressures between about 2000 to 8000 psi. The spheres, as presently fabricated, have major variations in wall thickness and an analytical method capable of including this nonuniform geometry was needed to predict critical pressures.

A finite element code was developed to analyze the strength of both the "ideal" uniform thickness geometry as well as the "real" nonuniform spherical shell under hydrostatic pressure and under a uniaxial two point self equilibrated load. The finite element code is capable of predicting critical (buckling) loads as well as stress states and displacements for thin shells of revolution with, in general, non-uniform thickness. The loading can be virtually of any type, i.e. uniform and non-uniform pressure, and many-point "self-equilibrated" concentrated loads.

Predicted Uniaxial Strength Using Finite Element Model

To evaluate the capability of the finite element code to predict sphere strengths the geometry of a specific set of spheres (Run 05287-31/10 reported in Table III) was

examinated in detail. The cross section of this "real" nonuniform sphere along with the geometry of the "ideal" uniform thickness sphere is shown in Figure 3 and the appropriate dimensions and material properties for the Al_2O_3 sphere are listed below:

R_o = 1158 μm; t_1 = 125 μm; t_2 = 50 μm; $t_{av.}$ = 102μm

R_1 = 1056 μm; R_{av}/t_{av} = 10.85

E = 380GPa; ν = 0.26,

σ_{ultt} = 310 MPa (measured flexure strength of equivalent Al_2O_3 bars)

An imperfection (out of sphericity) was employed in the analysis with a very small amplitude (1.15 μm). This amplitude is extremely small (one percent of the total thickness). Use of higher amplitudes will lower the buckling load. The code was used to calculate the two-point load necessary to fracture the "ideal" uniform wall sphere and the "real" nonuniform thickness sample.

A: "Ideal" uniform wall sphere

The failure of the uniform wall sphere occurs at the equator where the tensile stress exceeds the critical tensile strength. The corresponding value of the two-point load, P, is:

$$\underline{P}_{fail} = 55.7N \ (5.680 \text{ kg})$$

The critical load $\underline{P}$ (to cause buckling) is much higher, 4290N (438 kg).

B: "Real" nonuniform wall sphere

Two cases were considered for this geometry, (Figure 3) with regard to the points of load application.

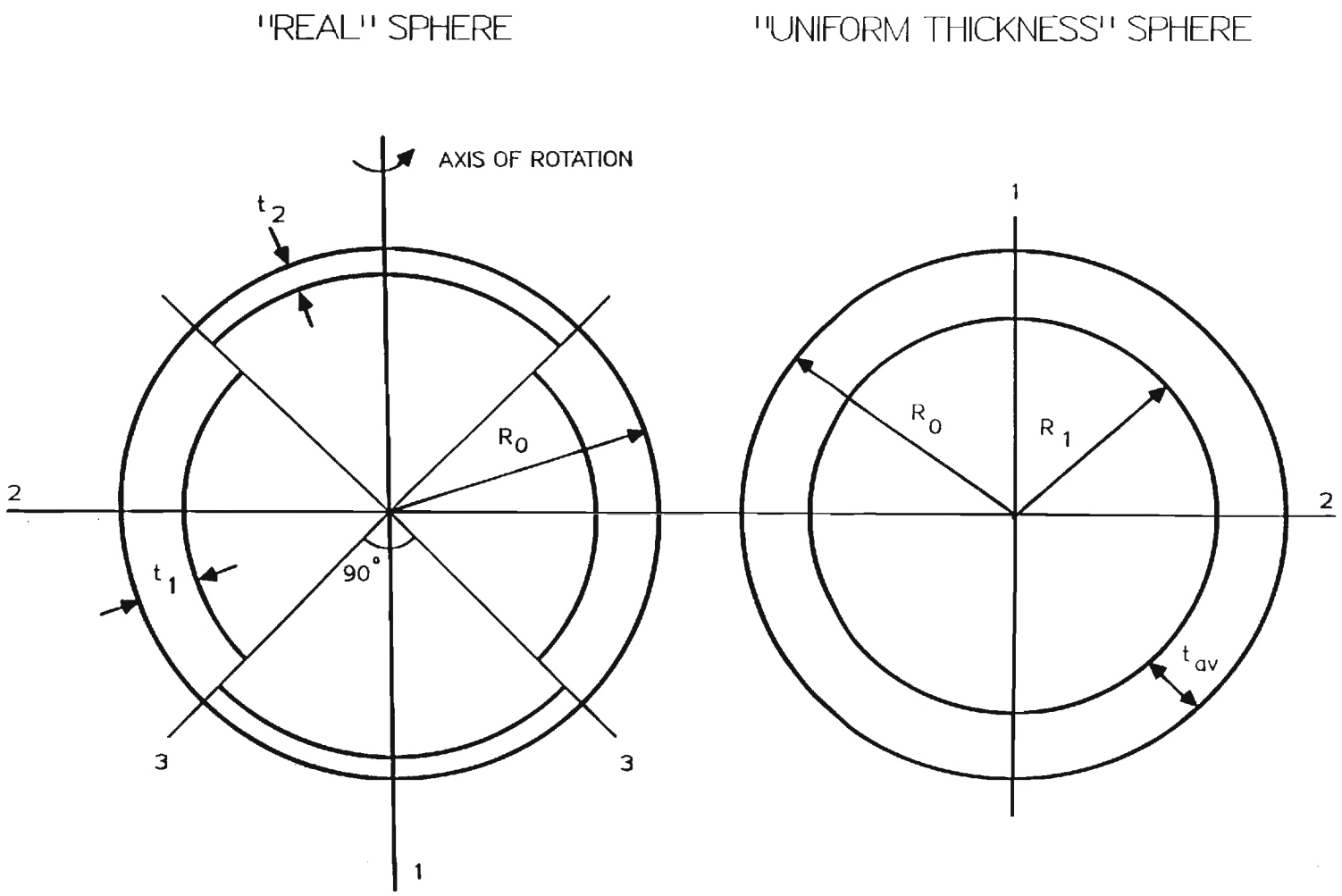

Figure 3. Section of "Real" Nonuniform Wall Sphere and Uniform Wall Sphere.

C: Load on the Thick Wall

The failure is due to the high tensile stress developed in the thin section, and the corresponding "failure" load is:

$\underline{P}_{fail}$ 46.8N (4.77 kg)

The critical (buckling) load for this orientation is also much higher than the "failure" load, 3910N (398 kg).

D: Load on the Thin Wall

In this case, also the failure is due to high tensile stresses in the thin walled section under the load. The corresponding "failure" load is

$\underline{P}_{fail}$ 14.6N (1.49 kg)

The critical (buckling) load for this orientation is 900N (92 kg).

Comparison of Predicted and Measured Uniaxial Strength

The average uniaxial load necessary to fracture the Al_2O_3 spheres formed during Run 05287 - 31/10 was measured as 19.95 N with a one standard deviation of ± 9.09 N as reported in Table IV of the next section. The infinite element code predicted fracture loads between 14.6 and 46.8N depending on orientation of the sphere during testing. Considering the uncertainty of accurately modeling the geometry of the wall thickness variations of the "real" sphere and the probable variability in the repeatability of "real" sphere wall symmetry, this agreement between predicted and measured uniaxial strength is remarkably close. As with typical strength measurements

of ceramic materials a wide distribution of sphere strength was encountered and the experimental values included the high and low load values predicted by the model. Perhaps most importantly this comparison shows the coaxial nozzle sphere forming method produces geometries of sufficient uniformity to enable reasonable modeling of anticipated mechanical strength. Additionally, the model indicates any modification to the sphere forming process that can improve the uniformity of the wall thickness will increase the strength. As noted in the next sections, an effort has been initiated to document the degree of wall nonuniformity in individual runs in order to address the process parameters that influence variations in wall thickness.

Uniaxial Compressive Strength

As reported above, finite element modeling has provided initial uniaxial strength estimates for spheres of specific geometries. These strength estimates agreed well with measured uniaxial strengths the details of which will be reported below. In future efforts, the finite element model will be used to produce a parametric model where effects of sphere diameter, density, wall thickness and wall thickness uniformity on uniaxial strength will be analyzed. At the present time, however, this is not available and uniaxial compressive strengths will be analyzed below using the model presented by Bratt, et al (6).

When an unrestricted sphere is loaded uniaxially, a compressive force exists along the loading axis and tensile force is placed on the exterior of the sphere at the equator (6). For thin-wall spheres, failure does not occur at the points of contact due to Hertzian stress but results from exceeding the material tensile stress due to bending of the sphere wall at the equator. When this occurs, a circumferential crack forms around the equator, splitting the sphere in half. The stress on the surface at failure is (6)

$$\sigma_c = \frac{3F_c(d/3)}{2\pi dt^2} = \frac{F_c}{2\pi t^2} \qquad (23)$$

or,

$$F_c = 2\pi t^2 \sigma_c \qquad (24)$$

where F_c is the critical force at fracture, σ_c is the critical strength of wall material and t is the wall thickness. Another sphere strength value, σ_s, is also reported, where σ_s represents the strength per unit area for a sphere based on its diameter and is given as follows:

$$\sigma_s = \frac{F_c}{\pi r^2} = \frac{2\pi t^2}{\pi r^2}\sigma_c \qquad (25)$$

or

$$\sigma_s = \frac{2}{9}\sigma_c (\rho_s/\rho_o)^2 \qquad (26)$$

since $\rho_s/\rho_o = \frac{3t}{r} - 3\left(\frac{t}{r}\right)^2 + \left(\frac{t}{r}\right)^3$ (27)

which effectively reduces to

$$\rho_s/\rho_o \cong \frac{3t}{r} \qquad (28)$$

because the walls are very thin. In equations (27) and (28) r is the sphere radius, ρ_s is the overall density of the sphere and ρ_o the theoretical density of the wall material (3.98 gm/cc for Al_2O_3).

In order to test the validity of the model by Bratt et al (6), twenty-two groups of hollow spheres from seven different runs were characterized under uniaxial compression. The critical force at fracture, F_c, was determined by crushing at least 25 individual spheres from each group on an Instron testing machine. The critical load, P_c, was applied uniaxially using hardened steel platens.

The density of individual spheres was determined from the sphere weight and volume. Average sphere weight was determined by weighing 100 spheres and the diameter was measured with a dial gauge. The average individual sphere density was calculated from the average weight and volume based on diameter. Finally, using this data, an average wall thickness of each batch was calculated from equation (28) and these values are reported in Table III.

The average uniaxial compressive strength of the twenty-two groups of spheres are shown in Table IV. Sphere strength, σ_s, and strength of the wall materials, σ_c, were calculated from equation (25). The error values reported with each value in Table IV are one standard deviation. To test Bratt's relationship, sphere strength was plotted against relative density squared for both the Al_2O_3

TABLE III. Geometry and Density of Al_2O_3 and Cr_2O_3-Doped Al_2O_3 Thin-Wall Hollow Spheres

Run-Group	Diameter (d) (μm)	Sphere Density (p_s) (gm/cc)	Relative Density (p_s/p_o)	Wall Thickness (um)
11186-	3275 ± 89	0.938	0.100	54.6
02057-	3158 ± 71	0.853	0.214	112.8
03247-	3244 ± 68	0.634	0.159	86.1
05077-				
30/10	2419 ± 37	1.160	0.291	117.5
30/30	2897 ± 44	0.811	0.204	98.4
30/60	3583 ± 64	0.479	0.120	71.9
30/102	3685 ± 76	0.432	0.109	66.7
05287 -				
30/2	1974 ± 24	2.000	0.503	165.3
31/4	2134 ± 77	1.430	0.359	127.8
31/4	2197 ± 36	1.346	0.338	123.8
31/10	2316 ± 33	0.917	0.230	89.0
40/10	2174 ± 29	1.157	0.291	105.3
31/20	2946 ± 24	0.655	0.165	80.8
60/40	2996 ± 36	0.848	0.213	106.4
20/40	3594 ± 81	0.358	0.090	69.0
08267 -				
70/40	3734 ± 233	0.441	0.111	69.0

Table III (con't)

Run-Group	Diameter (d) (μm)	Sphere Density (ρ_s) (gm/cc)	Relative Density (ρ_σ/ρ_o)	Wall Thickness (μm)
05147 - Cr_2O_3 Doped Al_2O_3				
30/10	2710 ± 114	1.096	0.271	122.5
30/20	3099 ± 122	0.831	0.206	106.2
30/30	2939 ± 76	0.683	0.169	82.8
30/60	3637 ± 58	0.423	0.105	63.5
60/20	2969 ± 114	1.143	0.283	140.0
60/100	4419 ± 72	0.444	0.110	80

Table IV. Uniaxial Compressive Strength of Al_2O_3 and Al_2O_3-7w/o Cr_2O_3 Spheres

	Breaking Load (P_c) (grams)	Breaking Force (F_c) (N)	Sphere Strength (σ_s) (MPa)	Sphere Wall Strength (σ_c) (MPa)
11186-	650 ± 440	6.38 ± 4.31	0.757 ± 0.512	341 ± 230
02057-	2120 ± 790	20.73 ± 7.71	2.647 ± 0.984	259 ± 96
03247-	1340 ± 400	13.17 ± 3.91	1.594 ± 0.473	283 ± 84
05077-				
30/10	2120 ± 1340	20.75 ± 13.10	4.514 ± 2.850	239 ± 151
30/30	2200 ± 1040	21.60 ± 10.21	3.276 ± 1.549	355 ± 168
30/60	680 ± 360	6.72 ± 3.53	0.666 ± 0.350	207 ± 109
30/102	4205 ± 130	4.09 ± 1.25	0.383 ± 0.118	146 ± 45
05287 -				
30/2	6060 ± 3640	59.44 ± 35.71	19.42 ± 11.67	346 ± 208
31/4	3670 ± 1510	35.97 ± 14.81	10.06 ± 4.140	350 ± 144
31/4	3270 ± 1360	32.07 ± 13.31	8.459 ± 3.510	333 ± 138
31/10	2030 ± 930	19.95 ± 9.09	4.735 ± 2.158	401 ± 182
40/10	2800 ± 1460	27.50 ± 14.35	7.408 ± 3.865	395 ± 205
31/20	340 ± 370	3.30 ± 3.67	0.485 ± 0.538	81 ± 89
60/40	2160 ± 1220	21.19 ± 11.94	3.006 ± 1.694	298 ± 168
20/40	290 ± 150	2.84 ± 1.49	0.280 ± 0.147	156 ± 82
08267 -				
70/40	951 ± 390	9.33 ± 3.83	0.852 ± 0.350	312 ± 128

Table IV (con't.)

	Breaking Load (P_c) (grams)	Breaking Force (F_c) (N)	Sphere Strength (σ_s) (MPa)	Sphere Wall Strength (σ_c) (Ma)
05147 -	Cr_2O_3 Doped Al_2O_3			
30/10	3230 ± 1606	31.68 ± 15.74	5.492 ± 2.730	336 ± 167
30/20	1778 ± 952	17.43 ± 9.34	2.518 ± 1.349	246 ± 118
30/30	1576 ± 856	15.45 ± 8.39	2.278 ± 1.237	359 ± 195
30/60	708 ± 256	6.94 ± 2.51	0.668 ± 0.242	274 ± 99
60/20	1504 ± 727	14.75 ± 7.13	2.130 ± 1.030	120 ± 58
60/100	1755 ± 896	17.21 ± 8.69	1.122 ± 0.566	418 ± 211

spheres, Figure 4 and the Al_2O_3-7w/o Cr_2O_3 samples, Figure 5. As indicated by equation (26), this should give a straight line with a slope proportional to $\frac{2}{9}\sigma_c$. The best fit least squares lines, as calculated for this data, is presented as the solid lines in both Figure 4 and 5. Two points were omitted (05287-31/20 and 05077-30/10) for the Al_2O_3 and one was omitted for the Al_2O_3-7w/o Cr_2O_3 spheres (05147-60/20) because these strength values were well below the other data. These low strengths were thought to be caused by large variations in wall thickness which will be discussed below. As can be seen in Figures 4 and 5, the density squared relationship provides good linear correlation to uniaxial compressive strength. From the slope of the least square lines for the Al_2O_3 and Al_2O_3-7w/oCr_2O_3 spheres, flexure wall strengths, σ_c, of 365 and 326 MPa, respectively, were calculated.

In an attempt to independently determine the flexure strength of the XA-3000 Al_2O_3 used for the sphere wall material, bars 6.2 x 6.2 x 100 mm were dry pressed from the XA-3000 Al_2O_3. These bars were fired with the same firing schedule used for the spheres and were broken under three point load. An average flexure strength of 309 MPa resulted. This is reasonable agreement with the 365 MPa value calculated from Bratt's equation for the hollow sphere wall strength. The sphere might be expected to have less surface defects than the dry pressed bars because both the inside and outside surfaces of the spheres are formed

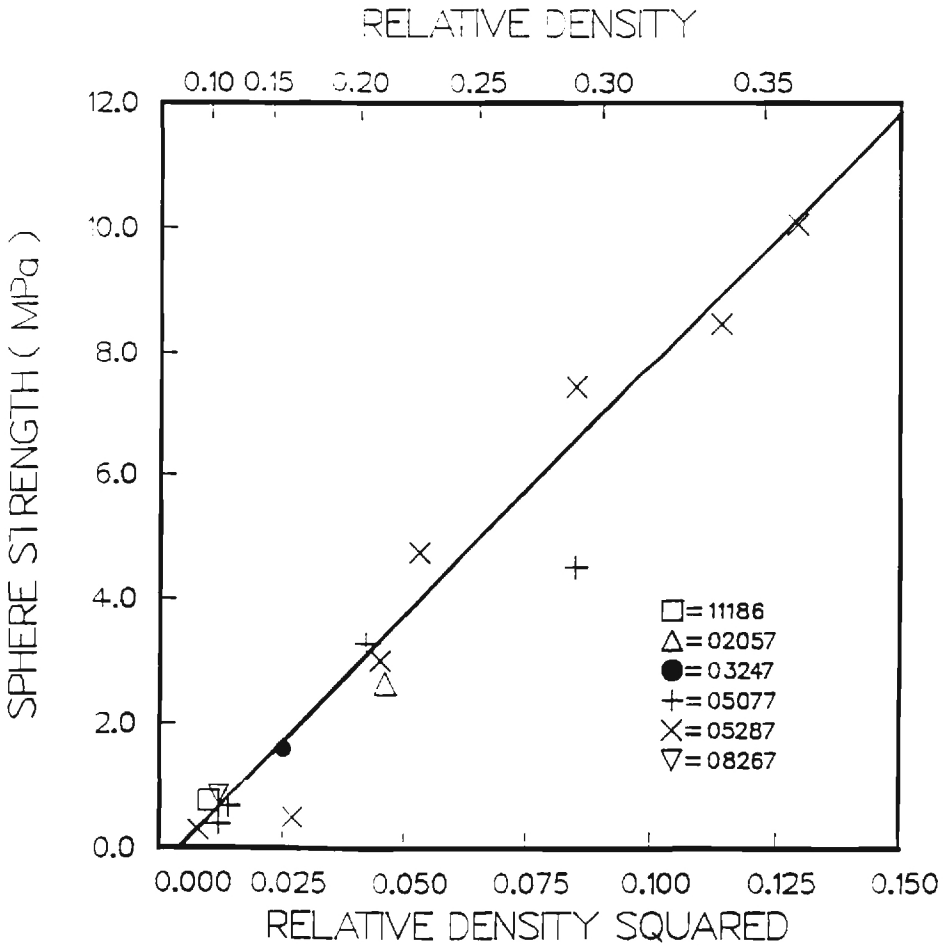

Figure 4. Uniaxial Sphere Strength vs Relative Density of Al_2O_3 Spheres, from Table III and IV.

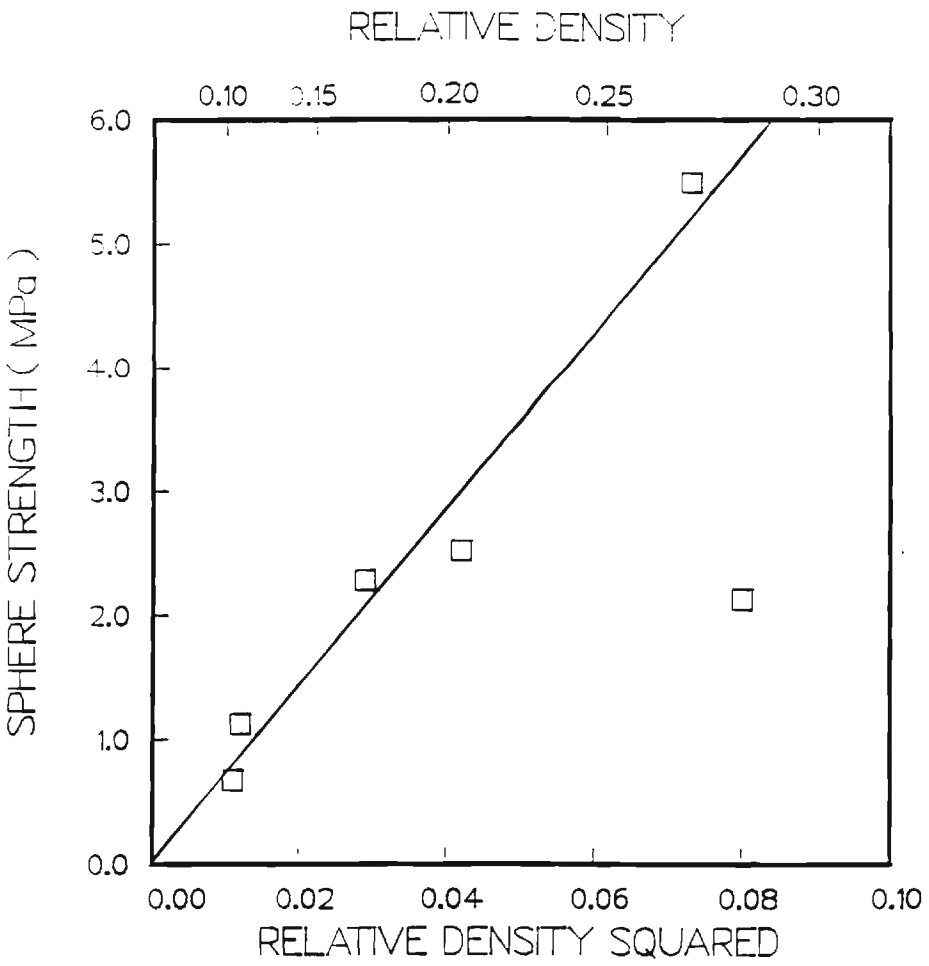

Figure 5. Uniaxial Strength vs Relative Density for Al_2O_3-7w/oCr_2O_3 Spheres, from Table III and IV.

from liquid surface tension forces. Whereas dry pressing tends to leave surface voids that produce critical defects and reduced strengths.

It is encouraging that Bratt's relationship fits the experimental data as well as it does and predicts a reasonable value for flexure strength of the wall material. Note that the density square relationship was linear over a wide range of sphere densities. In the future, this behavior will allow characterization of the strength of new sphere forming materials by only testing a relatively few groups of new spheres.

Uniaxial Strength and Wall Thickness Variation

Most of the variation in uniaxial strength reported above can be attributed to variations in the wall thickness. Although the production process results in spheres with very uniform outside diameters, the walls have thick and thin areas which greatly affect the strength. A typical sphere wall geometry includes a toroid of greater thickness with two thin caps on either side of the thicker toroid. This geometry is shown in Figure 3, and was used in the finite element model to predict strength variations as a function of loading orientation. If the spheres are uniaxially loaded on the thick stripe, a strength higher than average is expected and if loaded on the thin caps, lower strength should result.

Average wall thickness, based on relative density, was used for strength calculations in the preceding section. An attempt has been made to quantitatively measure the variations in wall thickness in six groups of spheres. Some samples had obvious large variations in wall thickness while others (such as a group made from high viscosity slip, No. 08267) were thought to have fairly uniform walls. Each group of spheres was mounted for examination by floating in epoxy and allowing the epoxy to harden. Each sample was ground to the mid section and then polished. Five spheres were chosen at random and the wall thickness was visually measured with a calibrated eyepiece at eight approximately 45° intervals around the circumference. The

thickness accuracy of this method is about ± 3 μm and the resulting thickness values are given in Table V. Each group shows a large range of values and high standard deviation. The ratio of thick to thin was as high as 5 to 1. As expected the group made from the high viscosity slip (No. 08267) had the most uniform walls with a thickness variation of approximately 2 to 1.

Table V. Hollow Sphere Wall Thickness Measurements and Variations.

Sample	Average Metallograph Thickness	Std Dev (μm)	% Std Dev	Range (μm)	Thickness From Density (μm), Table III
05147-60/100	76.7	38.0	49.5	32-145	80.9
05147-30/30	95.2	34.9	36.6	35-177	82.8
05287-31/10	104.9	43.1	41.0	38-170	89.0
05077-30/30	134.8	49.7	36.9	47-205	98.4
05287-60/40	81.1	22.7	28.0	38-142	106.4
08267-70/40	57.4	11.2	19.6	41-95	69.0

Several problems and sources of error exist with this wall thickness measurement technique. First, when the spheres are floated in the epoxy the center of gravity may produce preferential sphere orientation and, consequently, random sections through the spheres will not be exposed for measurement after polishing. Second, it is difficult to assure all the spheres are ground and polished at the mid point (equator) to provide wall sections perpendicular to the surfaces. Finally, these measurements are very time

consuming and, a very small sample size was used, thus the results cannot be considered statistically significant.

The average wall thickness visually measured using the metallograph (Table V) is plotted vs the thickness calculated from density (Table III) in Figure 6, and it is clear that there is little correlation between the directly measured and density calculated average. The line shown in Figure 6 has a slope of one (1) so that if the two methods yield the same value the data points would lie on this line. The density calculated average is based on a large sample size and therefore is believed to be more reliable. Because of the difficulties in directly measuring statistically significant average sphere wall thickness, it was decided to continue using the density-calculated average for the near term evaluation of sphere strength. However, efforts will continue to find a simple and convenient technique to measure wall geometry and to detect changes (improvements) in wall uniformity. A suitable method to assess wall uniformity is necessary for realistic predictions of mechanical strength and also to judge the effectiveness of varying sphere forming parameters on wall geometry.

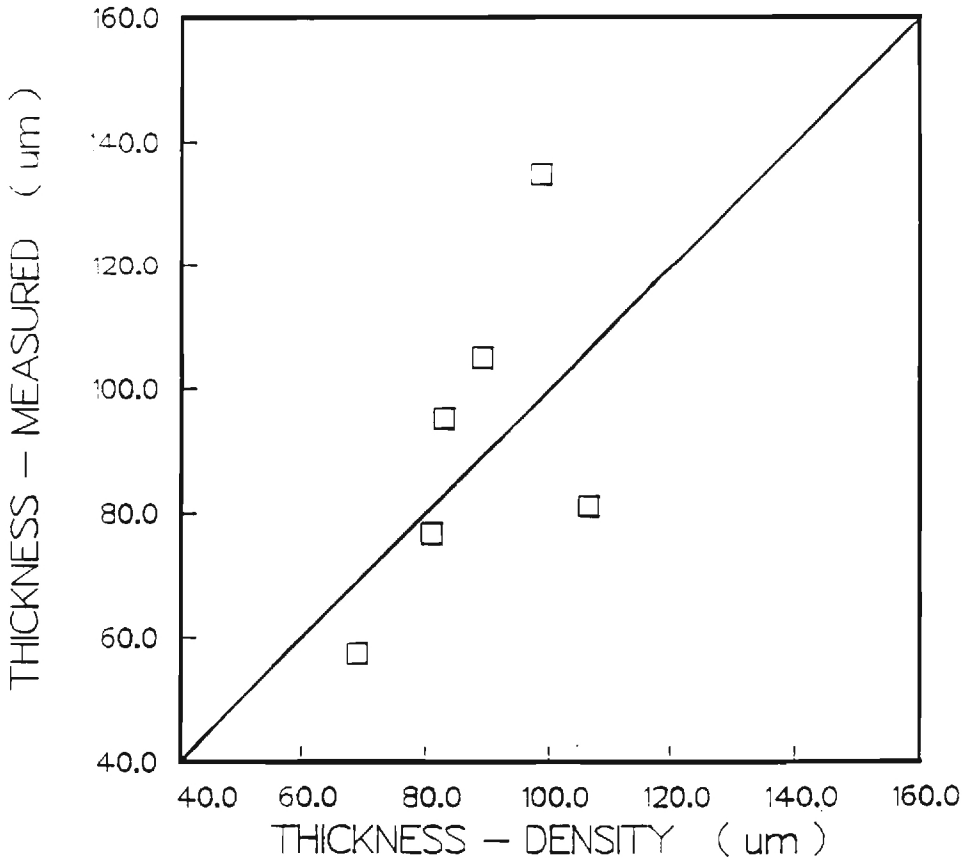

Figure 6. Graph showing poor correlation of wall thickness values determined by visual measurements and calculated from density (diameter and weight), Table V.

Assessment of Insulation Potential

The thermal conductivity (T/C) of sphere beds was studied this summer at ORNL. The material samples were characterized and tested in two radial heat flow devices. The variation of thermal conductivity was measured as a function of gas pressure, bed density, and temperature. The tests indicated that the spheres should be made of low conductivity material which can scatter and/or reflect radiation.

Characterization of Spheres Samples

Test spheres were fabricated at Georgia Tech and were composed of Al_2O_3, Al_2O_3-7 w/o Cr_2O_3, and partially stabilized ZrO_2. Sphere diameters varied between 2100 and 3500 μm with wall thickness of 80 to 160 μm. The resulting bed densities were between 260 to 900 $Kg.m_3$. The thermal conductivity of the bulk material ranged from 2 to 21 W/m*K. The specific properties of each sample are listed in Table VI.

Radial Heat Flow Devices

The thermal conductivity, k, of beds of the spheres was measured using the radial heat flow method in two different devices at ORNL. The first apparatus measured k in helium and nitrogen at pressures between 0.05 to 2 atm at 300°K. The second device measured the k of sphere beds in air from 300 to 1000°K. A repeatability error analysis was performed on each device.

The apparatus operating at room temperature, designated

Table VI. Measured material properties of the hollow ceramic spheres.

Sample	Composition	Diameter μm	Wall Thickness μm	Bed Density kg/m^3
11	Al_2O_3	3448	78	260
12	Al_2O_3	2809	104	480
13	Al_2O_3	2229	92	590
14	Al_2O_3	2289	132	790
15	Al_2O_3	2106	130	900
21	Al_2O_3-7%Cr_2O_3	2852	91	410
22	Al_2O_3-7%Cr_2O_3	3498	70	240
31	ZrO_2	2250	118	1089

Bulk Material	Thermal Conductivity
Al_2O_3	21.4 W/m.K
Al_2O_3-7%Cr_2O_3	10.8*
ZrO_2	2-3**

* Measured at ORNL on equivalent dry pressed materials sintered at 1600°C for 2 hrs. using a cut bar device described by Williams.

** Average values for ZrO_2 (PSZ) taken from the literature.

ORNL 7, is shown in Figure 7. The spheres were placed in the annulus created by the central stainless steel core heater and cooled brass cylinder. The chamber had a length to diameter ratio of 22.5 which minimized axial heat flow. The radial heat flow equation then applies:

$$k = \frac{EI(\ln r_o/r_i)}{2\pi L\ \Delta T} \qquad (29)$$

where EI/L is the power supplied to the core heater, r_o and r_i are the radial dimensions of the annulus, and ΔT is the radial temperature drop across the specimen. A repeatability error of 3% was calculated for this device. The error is composed of uncertainty in radial lengths, temperature readings, and power measurements.

The high temperature test facility, designated ORNL 8 and shown in Figure 8, measured bed conductivities up to 1000°K in air. The assembly was similar to ORNL 7 in that a core heater was used in the device. A cylindrical nichrome mesh screen heater encircled the core heater. The nichrome screen heater was typically operated about 100°K below the core heater to facilitate T/C measurements approaching 1000°K. The spheres (Aerospheres) to be tested were placed between these two heaters as well as between the screen heater and calcium silicate cylinder to serve as additional insulation. The length to diameter ratio in ORNL-8 was 17 which maximized radial heat flow. The total repeatability error for ORNL 8 was calculated to be ± 2.4%. Again length, temperature and power measurements all contributed to the error.

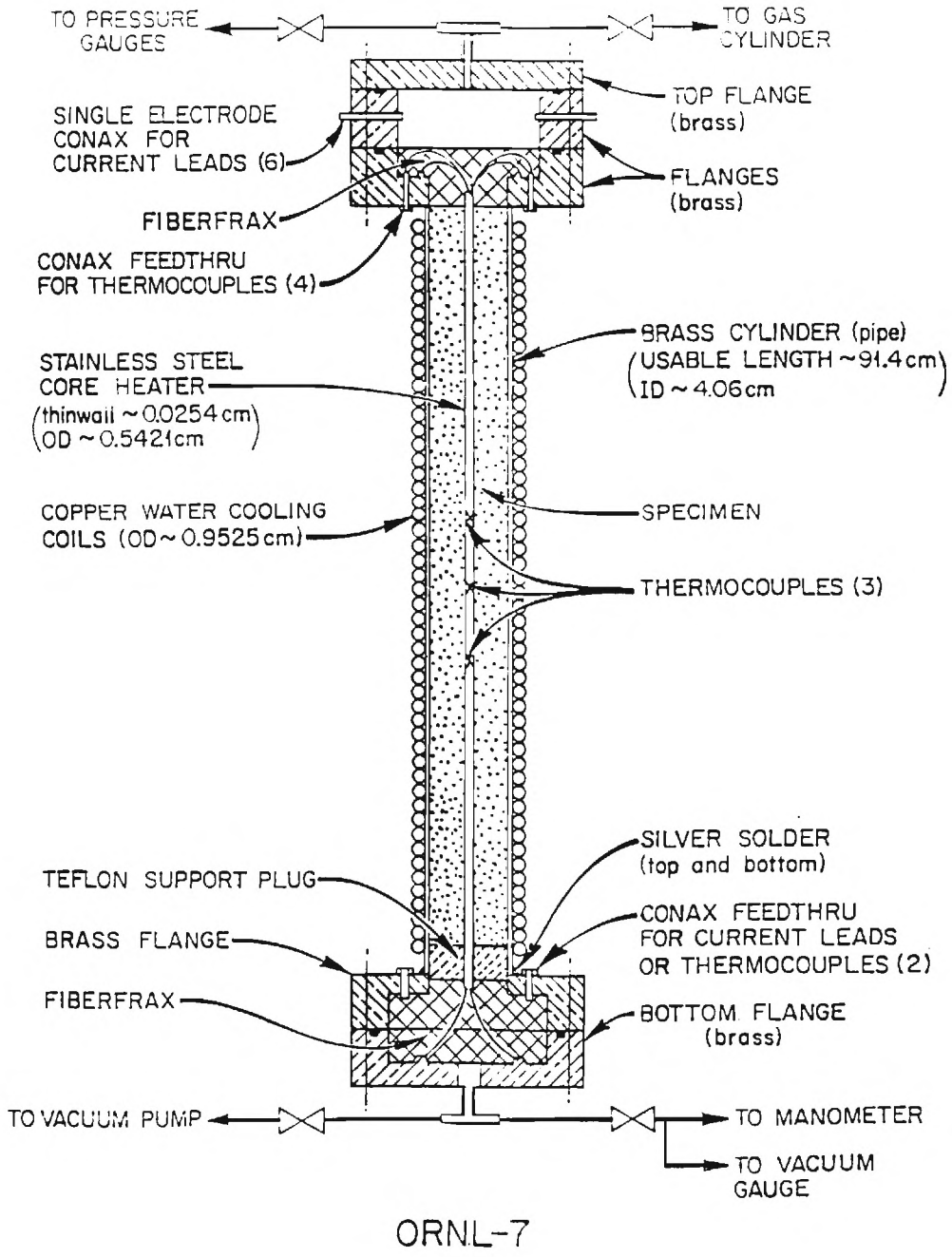

Figure 7. The Room Temperature Thermal Conductivity Apparatus, ORNL-7.

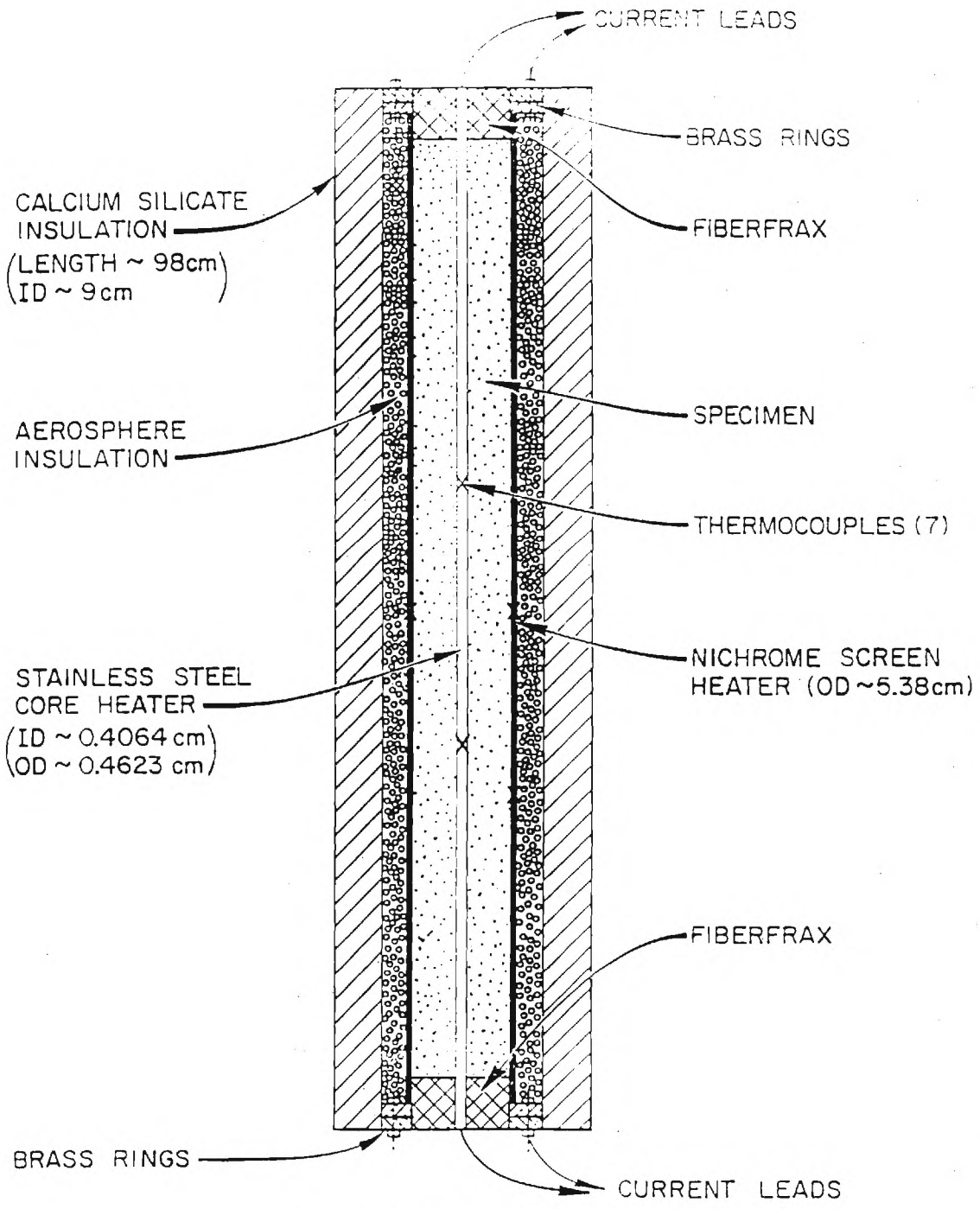

Figure 8. The High Temperature Thermal Conductivity Apparatus, ORNL-8.

Results of Thermal Conductivity Study

This section supplies values of thermal conductivity for the eight samples measured in ORNL 7 at a temperature of 300°K in various pressures of nitrogen and helium. The thermal conductivity of four samples in ORNL 8 at temperatures ranging from 300 to 1000°K is also supplied. The effect of radiation on these four samples is presented.

The T/C results from ORNL 7 are shown in Figures 9 (for nitrogen) and 10 (for helium). Sample 31, the partially stabilized zirconia, has been plotted separately in Figure 11. It should be noted that in these Figures the thermal resistance is plotted which is the inverse of thermal conductivity. The pressure dependent curves were plotted using a least squares fit of the data points. All curves fit the general equation:

$$1/k = a + b.P + c/P^3 \qquad (30)$$

where k is the thermal conductivity; P is pressure; and a, b, and c, are constants. All the samples displayed a decrease in thermal resistivity with increasing pressure. This behavior levels off at higher gas pressures. As expected the T/C of the sphere beds was significantly higher (about twice) in helium than in nitrogen.

First estimates of the effect of sphere geometry (i.e diameter, wall thickness and density) on T/C may be drawn from the data in Figures 9 and 10. Interestingly, the

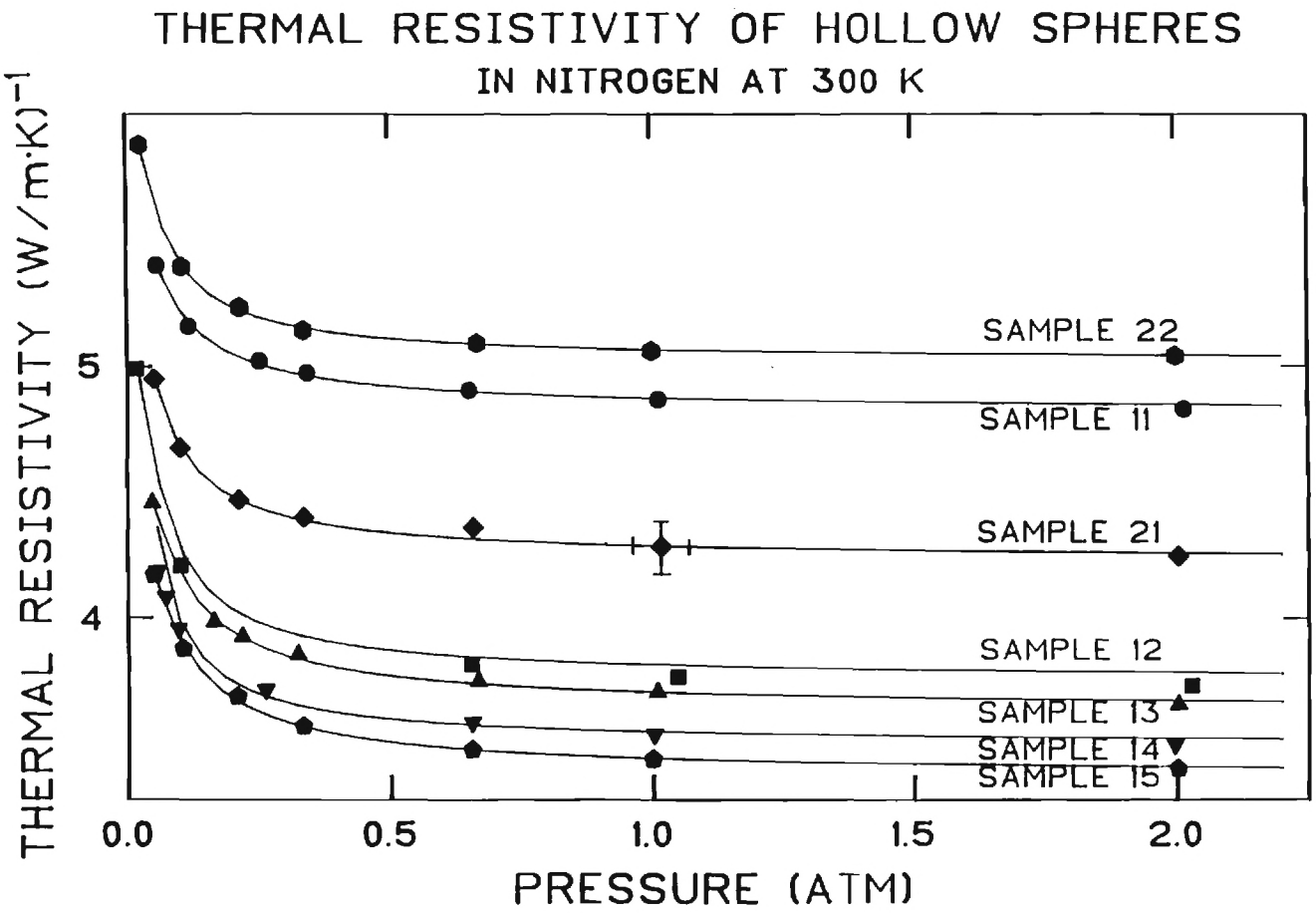

Figure 9. Pressure Dependence of Thermal Resistivity of Hollow Sphere Beds (Described in Table VI) at 300°K in N_2.

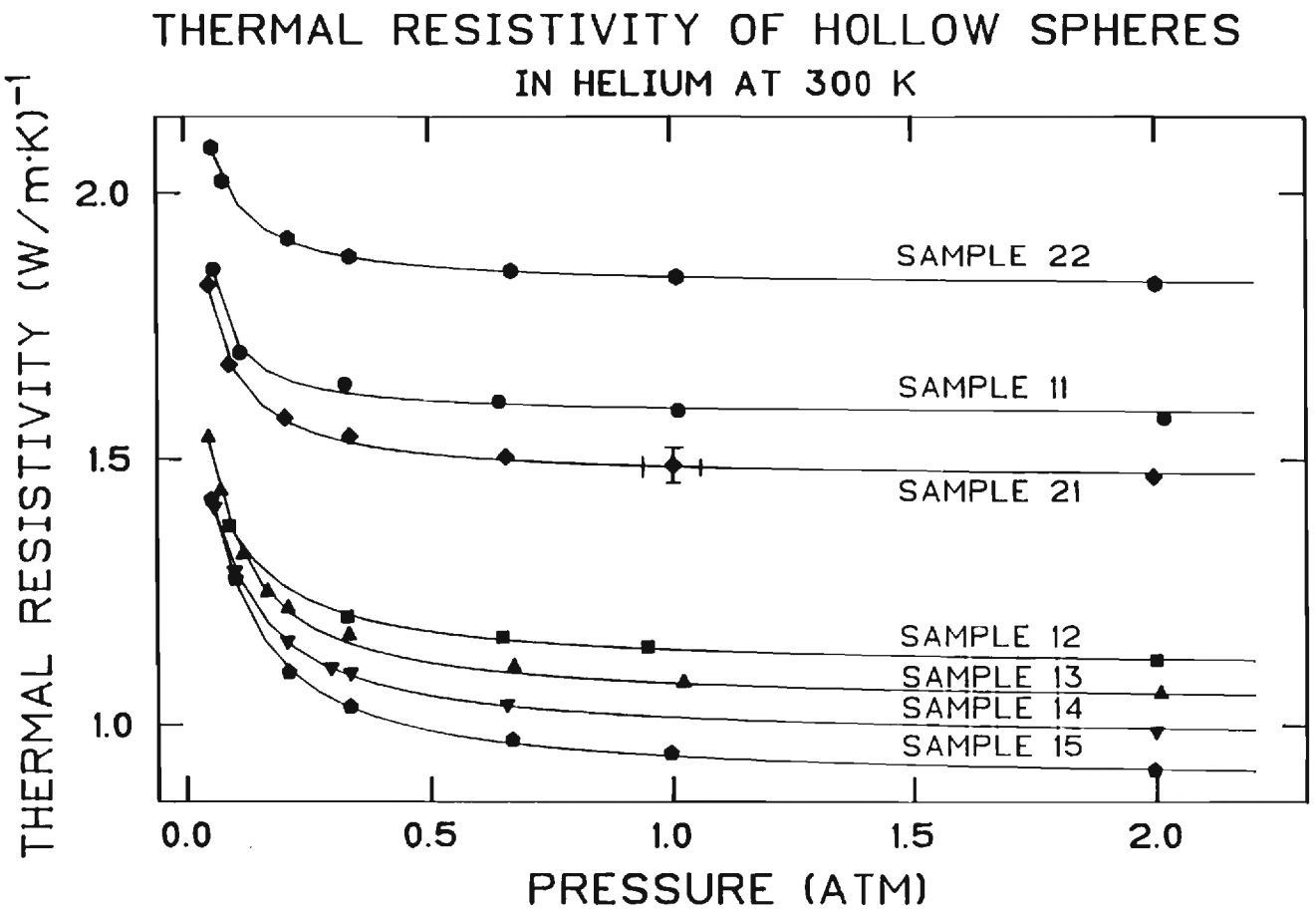

Figure 10. Pressure Dependence of Thermal Resistivity of Hollow Sphere Beds (Described in Table VI) at 300°K in He.

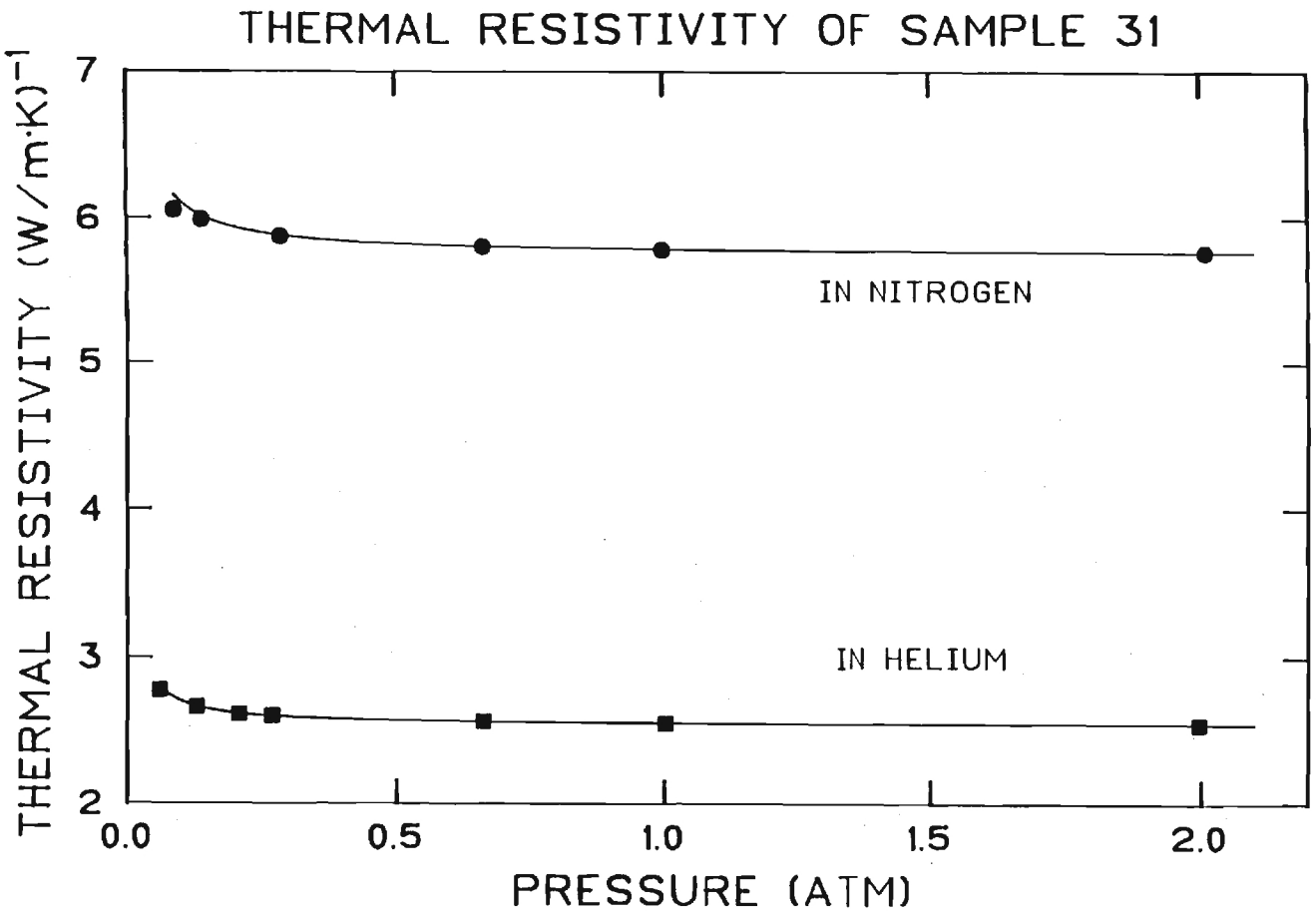

Figure 11. Pressure Dependence of Thermal Resistivity of Sample 31, ZrO_2 spheres, at 300°K in N_2 and He.

larger spheres and thin walls exhibit the low T/C. There is not enough data to inconclusively separate these two factors. The bed density of the pure Al_2O_3 samples versus thermal conductivity is plotted in Figure 12 and clearly demonstrates the value of low density beds.

The influence of composition on bed conduction is easily made by comparing the T/C of Al_2O_3 with the Al_2O_3-7%Cr_2O_3 and ZrO_2 samples. Reducing the T/C of Al_2O_3 by about one half with the Cr_2O_3 addition decreased the conduction of the bed about 6 to 10% (comparing samples 11 and 12 with 21 and 22).

Using ZrO_2 spheres with a T/C about one tenth that of Al_2O_3 the bed conductivity decreased about 13% compared to the lowest measured Al_2O_3-7^w/o Cr_2O_3 sample (No. 22). Clearly if ZrO_2 spheres can be fabricated with walls in the 50μm range, further decreases in T/C are expected. These comparisons suggest a low conduction glass would probably be the ideal sphere composition to provide room temperature insulation approaching that of fiberglass.

The temperature dependence of thermal conductivity of the four samples tested in ORNL 8 are shown in Figure 13. The hollow spheres show the typical increase in k with temperature characteristic of low density materials. Some interesting trends appear to be emerging from the high temperature data; 1) for the Al_2O_3-Cr_2O_3 compositions the small diameter sample (No. 21) displaying the higher room temperature k crosses the curve of the larger diameter

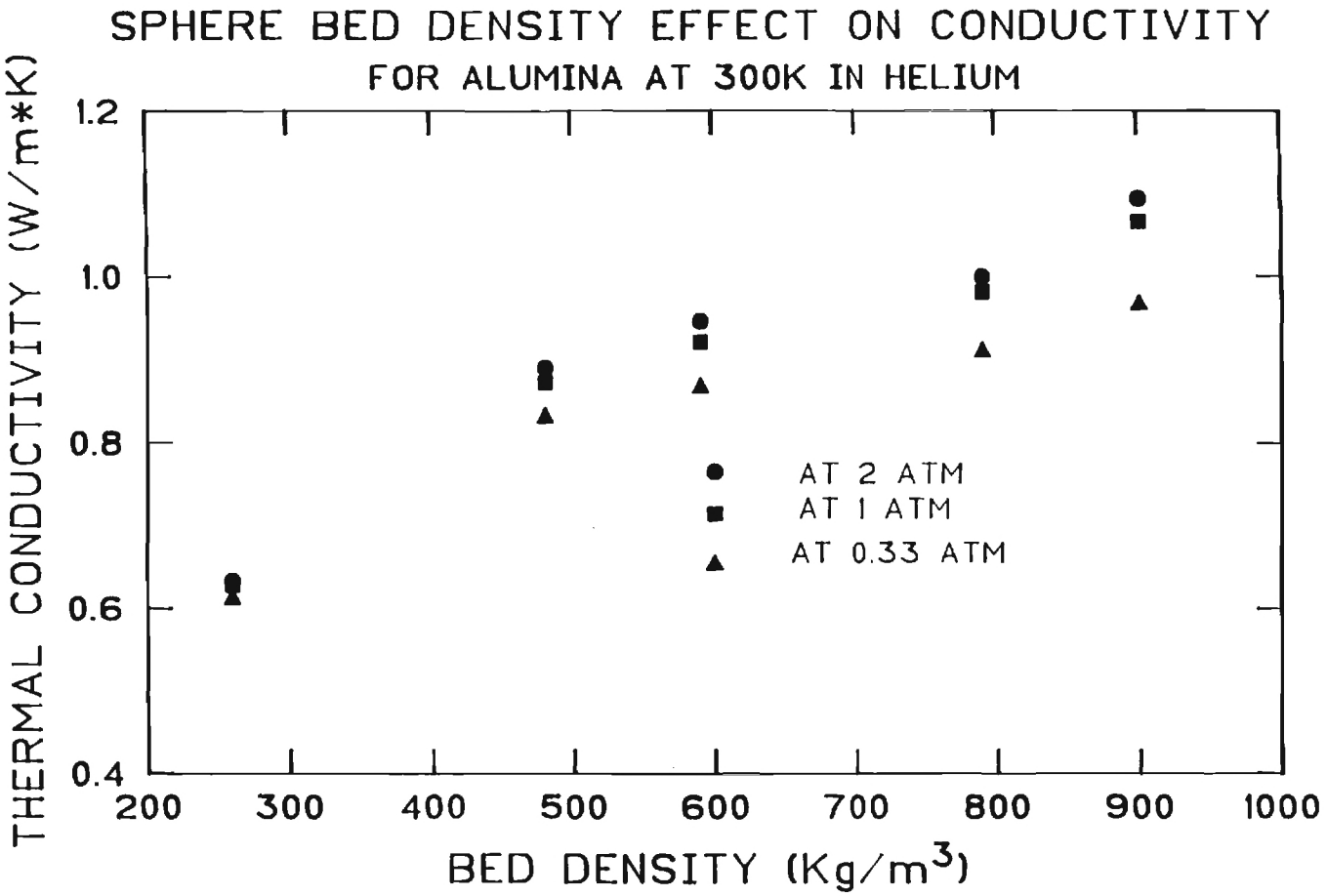

Figure 12. The Dependence of Thermal Conductivity on Sphere Bed Density for Samples 11, 12, 13, 14 and 15 (Table VI) measured at 300°K in He.

Al_2O_3-Cr_2O_3 sample (No. 22) at about 900°K, showing the effect of closer spaced surfaces in retarding radiation transfer and 2) the more transparent ZrO_2 spheres show a greater increase in conductivity with increasing temperature than the more opaque Al_2O_3 and Al_2O_3-7^w/o Cr_2O_3 specimens. Perhaps most importantly the k of the thin-wall spheres increase by a factor of 2 to 2.5 as the temperature increases to 1000°K whereas typical fiber insulation increases by a factor of 4 to 5 over the same temperature interval. This behavior suggests the spheres may be competitive with fiber insulation, especially at and above the upper use temperature range of silica based fibers. Obviously additional testing is needed to verify this projected performance.

Sphere Formation Model

An effort is underway to develop mathematical expressions which describe various stages of the very complex sphere formation process occurring as powders dispersed in fluids are forced through the concentric nozzle assembly. The objective of this activity is to arrive at a model that will correlate with the findings of the concurrent experimental parameter study. An important first step in the model is establishing the factors controlling the rheology of powders and binders dispersed in acetone. Adsorption isotherms were employed to evaluate powder dispersibility in liquids and the distribution of the binder between the amount absorbed on the powder surface and amount dissolved in the acetone. Additional parameters of interest include the viscosity of acetone as a function of binder content and type.

In the sphere forming process concentric nozzles are used, and a hollow cylinder of slip is delivered through the outer annuli and the blowing gas is fed through the inner annuli (inner jet). Pertinent equations describing the flow of fluids through annuli are presented and compared with experimentally measured flow rates of Al_2O_3-based slips. Several runs were performed to systematically vary slip delivery rate (cell pressure) and amount of blowing gas (inner jet flow rate) and assess changes in sphere diameter, density and wall thickness. The results from these runs are described in the last section of this

report.

Rheology Study

To provide prediction of slip rheology, a model for slip viscosity is being developed which is based on the following parameters: liquid media viscosity, solids content, thickness of adsorbed polymer layer on the powder, particle size, and critical particle volume concentration. It is hoped that the model will be sufficient to predict the rheology of powders of regular shape over a wide size range. Although some empiricism will be present, this will be limited as much as possible. The purpose of this model is to allow incorporation of rheology into liquid flow rates through the nozzle for the process formation model.

For the PMMA/acetone system in use, the PMMA both adsorbs on the powder and dissolves in the acetone solvent. The adsorption isotherm analysis provides qualitative prediction of the dispersibility of ceramic powder in the liquid, and quantitative distribution of the polymer in the liquid and on the powder. Because adsorption isotherms vary based on powder type and the surface area of powder, the concentrations of polymer in the liquid varies from powder to powder. Hence, the adsorption isotherms and the viscosities of PMMA/acetone solutions have been characterized for incorporation in the model.

Adsorption Isotherm

The adsorption isotherms of PMMA (elvacite 2008) on ceramic powders, including partially stabilized zirconia

(HSY3), alumina (XA3000 and XA1000) and fused silica (GP3-1), have been constructed by the following method: a ceramic powder, PMMA and acetone were mixed together by ball milling for 24 hours at room temperature. The samples were then centrifuged and the supernatant solutions decanted for analysis of the polymer concentration. The concentrations were determined by comparison of the refractive index with previously prepared standards of known concentrations. Finally the isotherms were plotted as weignt of PMMA adsorbed per 100 grams of oxides vs. equilibrium concentration of PMMA in solution, Figs. 14 and 15.

The isotherms can also be represented by their BET plots, Fig. 16. From the slopes and the intercepts of these curves, the values of monolayer adsorption, Nm, were calculated. The values of Nm can also be normalized as grams of PMMA adsorbed per unit surface area, Ns. In addition, from the BET plots the values of a parameter C (related to the heat of adsorption of the polymer on the powder) were calculated because C is a measure of the affinity of the polymer for the ceramic powder surface. These values are presented in Table VII.

Based on the analysis of adsorption isotherms, some conclusions can be drawn. First, for the same type of powder, XA3000 and XA1000, the adsorption amount is a function of surface area, thus the normalized monolayer adsorption amounts, Ns, are almost identical for both Al_2O_3

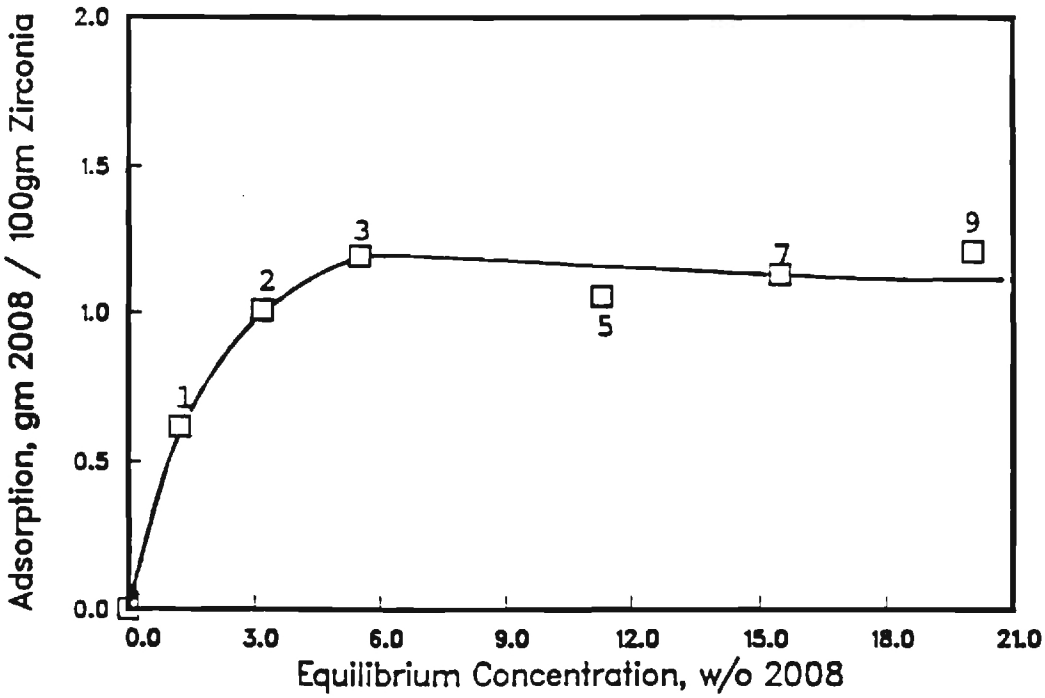

Figure 14. Absorption Isotherm for PSZ Powder (Type H5Y3) Mixed With Elvacite 2008 and Acetone.

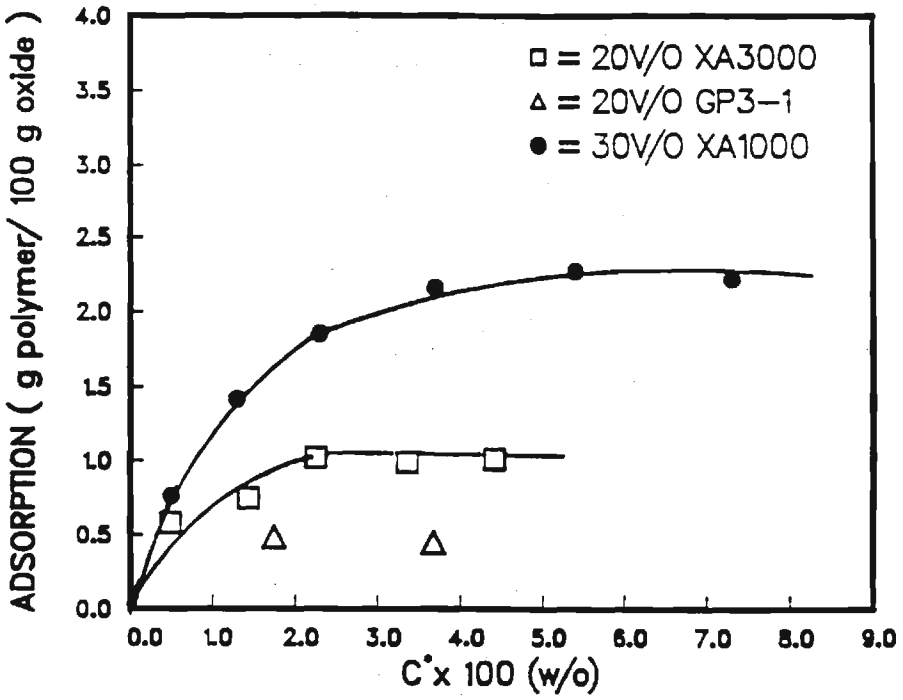

Figure 15. Absorption Isotherms for PMMA on Alumina and Silica Powders in Acetone.

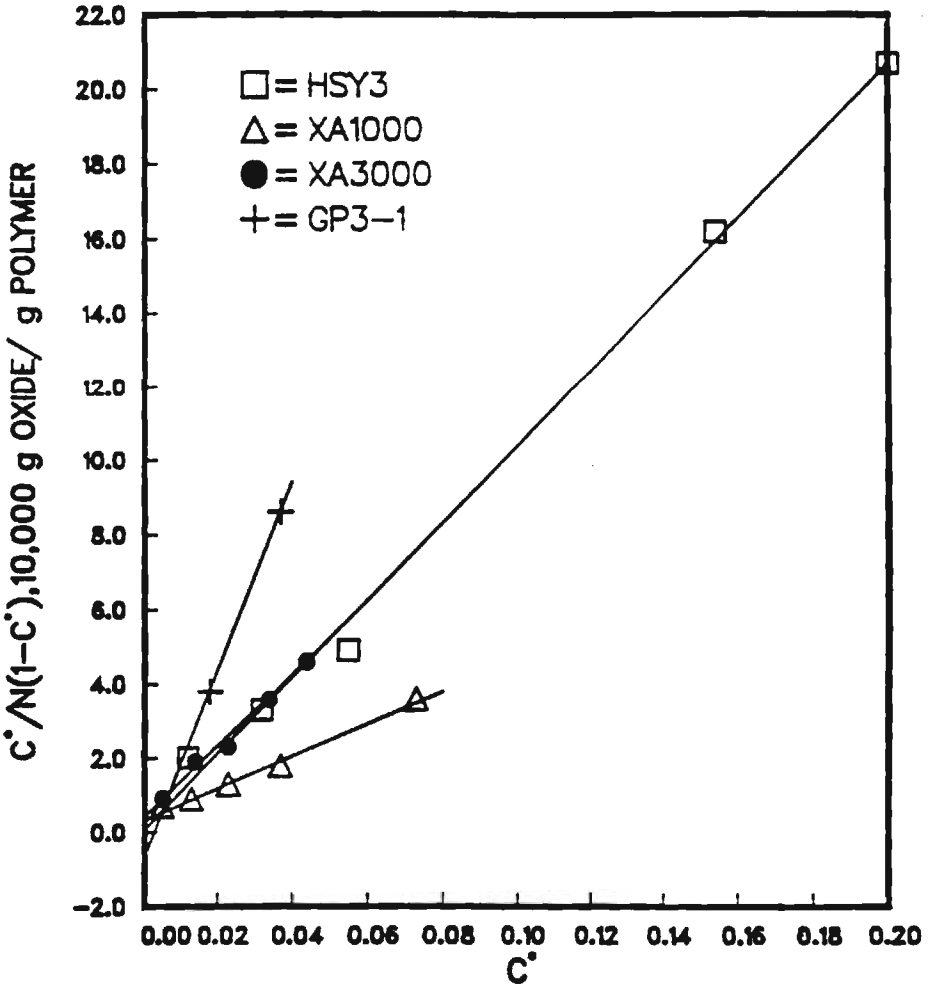

Figure 16. BET Plots from PMMA on Alumina, Zirconia and Silica Powders in Acetone.

powders. Second, the negative C value for GP3-1 silica explains the poor dispersibility of silica in a PMMA/acetone solution, therefore other dispersants rather than PMMA should be used for silica slips. Finally, the higher C value, i.e. stronger affinity of PMMA on HSY3 zirconia, probably indicates the long chain polymer is attached to the zirconia particles at more points that to the Al_2O_3. The adsorption per surface area values, N_s, in Table VII, also support more segmental adsorption of the polymer by ZrO_2 than Al_2O_3.

Viscosities of PMMA/Acetone Solutions

The viscosities of PMMA/acetone solutions were measured at PMMA weight fractions of .2, .3, .4, and .5, Figure 17. The rheology equation describing this relationship was determined by the least-square method to be:

$$\log \eta = -0.961 + 9.544\ C^* \qquad (31)$$

where η is viscosity in centipoise, and C^* is the concentration (weight fraction) of the polymer in solution. The practical concentrations of PMMA in solution of interest for sphere formation are usually in the concentration range that produces a viscosity of about .3 cp. A deviation from the equation above is present in the very low viscosity range, e.g. below 5 cp. Therefore, a rheology equation for the low viscosity range will soon be determined using the new Haake viscometer which provides low viscosity measurement capabilities not previously available.

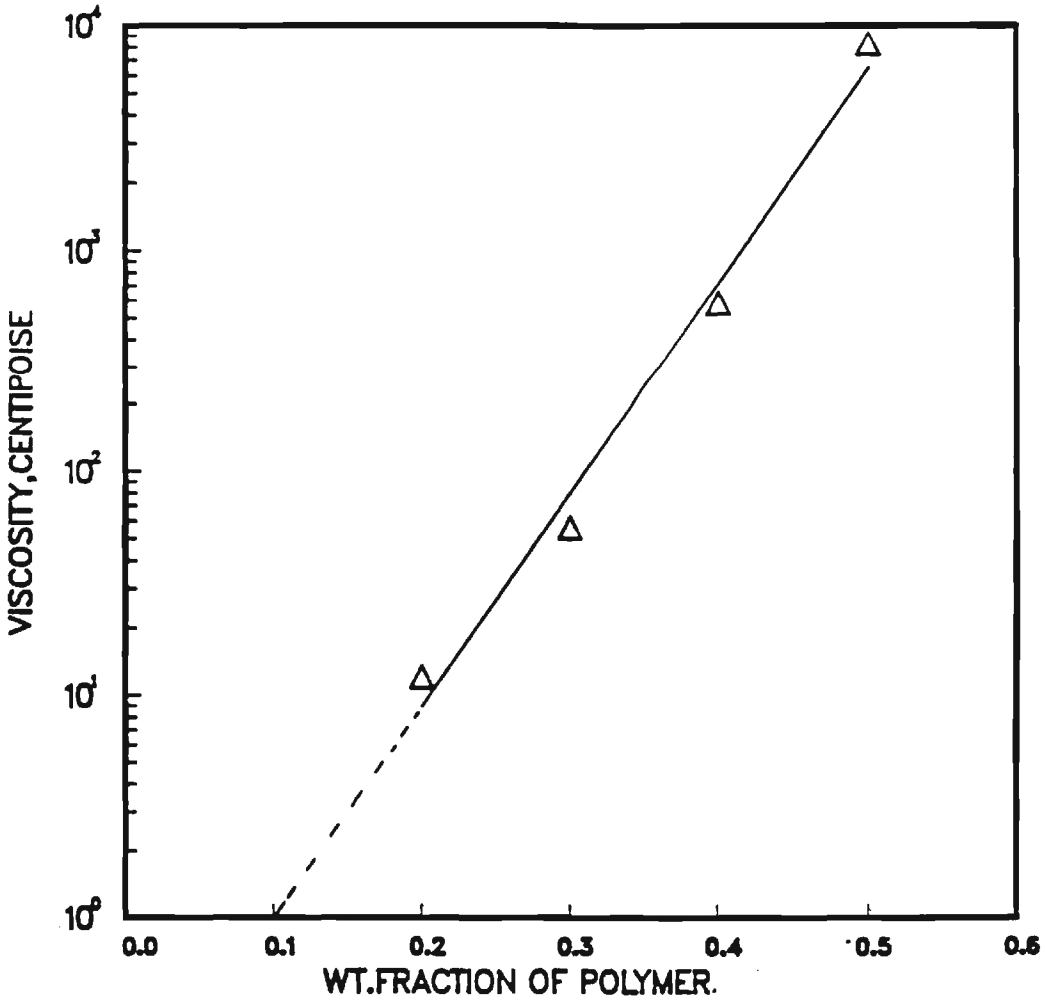

Figure 17. Viscosity of PMMA/Acetone Solutions

Table VII. Adsorption Parameters for PMMA/Acetone Suspensions

BET Parameters	Powder			
	XA3000	XA1000	HSY3	GP3-1
N_m(g/100g)	1.05	2.32	0.97	0.39
C	227	123	1948	-343
SA(m^2/g)	3.99	9.01	6.52	6.30
N_s(mg/m^2)	2.63	2.57	1.49	0.62

Experimental Parameter Study

The initial boundary conditions for the dispensionprior to sphere formation is dictated by the slip flow through the coaxial nozzle. Fluid flow in concentric tubes is described by the expression (7):

$$Q = \frac{\pi \Delta_p R_2^4}{8\eta L} (1-K^4) - \frac{(1-k^2)^2}{\ln (1/k)} \qquad (32)$$

where $K = R_1/R_2$

R_1 = radius of inner tube

R_2 = radius of outer tube

L = length of annuli

η = viscosity of fluid

Δ_p = pressure drop across length-L

Q = fluid delivery rate

Preliminary comparisons of measured Al_2O_3-based slip flow rates with calculated values from this expression show the

calculated values to be low by a factor of two to three. Probable reasons for this discrepancy include: (1) In the derivation of this equation the length, L, was assumed to be much larger than the radius, R_2, and thus entrance and exit effects could be ignored. This is certainly not the case with existing nozzle designs, and (2) The existing slips are pseudoplastic in nature and the high shear rate in the nozzle may be significantly greater than that measured by conventional viscometers. A new viscometer has been received that can measure viscosity at shear rates equivalent to that occurring in the nozzle, and hopefully this instrument will provide better viscosity data for use in equation (32).

In the evaluation of the many process variables controlling the geometry of the hollow spheres, the two major parameters were identified as: 1) cell pressure (controlling slip delivery rate) and 2) inner jet flow rate (controlling volume of sphere forming gas). Several runs were made using the "standard" Al_2O_3 slip where these two parameters were systematically varied. The weight and diameters of the resultant spheres were measured to characterize trends in sphere diameter, density and wall thickness. The diameter changed as a function of cell pressure and inner jet flow rate much as anticipated, and Figure 18 schematically presents this information. However, the variation of the wall thickness and density of the Al_2O_3 spheres was not as clear. Wide changes in the

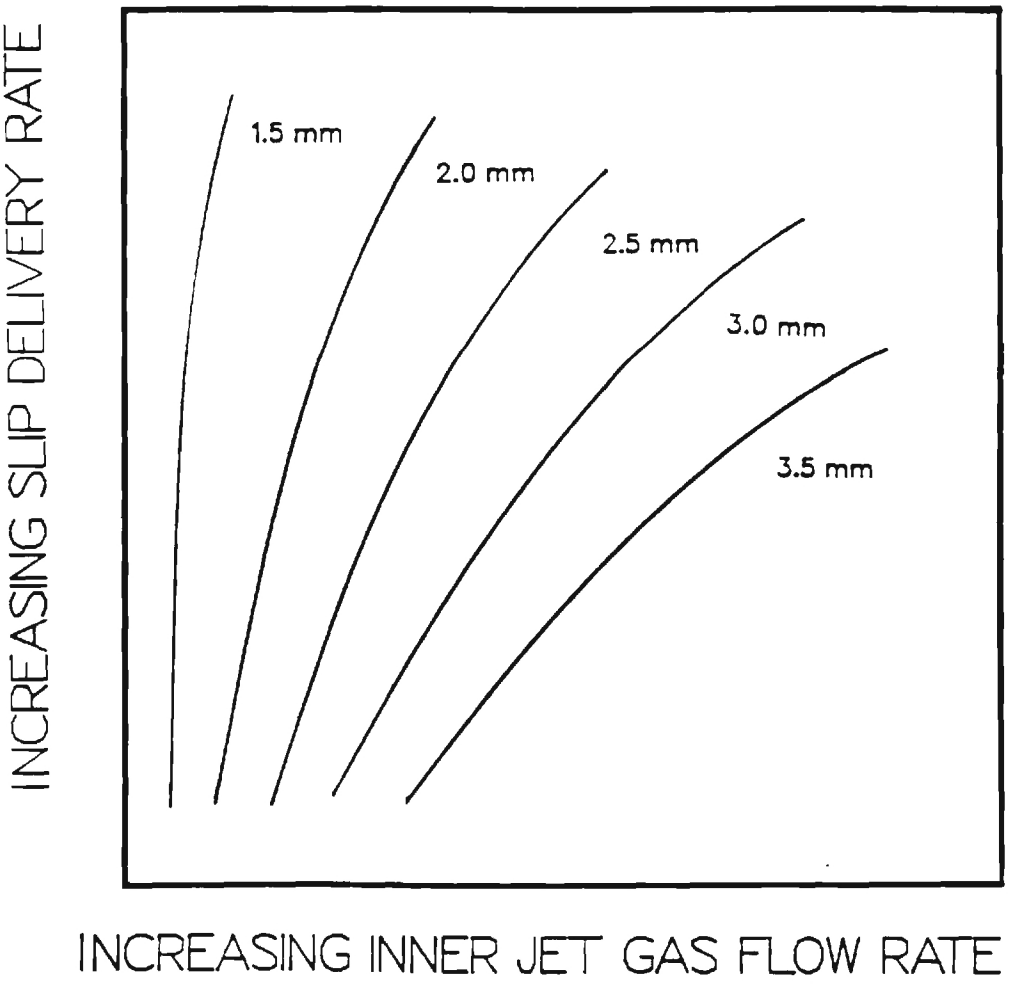

Figure 18. Schematic Diagram Showing Changes in Sphere Diameter with Slip Delivery Rate and Blowing Gas Rate.

frequency of sphere formation occurred especially as the cell pressure was changed. Subsequent experiments have documented the influence of slip delivery rate (cell pressure) on frequency of sphere formation. Combining this data with the blowing gas volume from the inner jet has produced relationships to calculate sphere diameter, density and wall thickness that agrees very well with measured values of the "real" spheres. This work provides some interesting insight into the limits of sphere size and density that can be expected from the existing slip rheology and nozzle configuration. Details of these calculations will be presented in the next report.

During the experimental study of the process parameters the smallest Al_2O_3 spheres achieved to date were formed ~1.6mm in diameter. In previous experiments Al_2O_3 - 7 w/o Cr_2O_3 spheres (fabricated for T/C measurements at ORNL) with diameters of about 4.5mm were blown, collected and successfully densified. Consequently the range of sphere sizes that may be fabricated using the present coaxial nozzle technology with Al_2O_3 based slips is between 1.6 to 4.5mm in diameter. Efforts to extend this range will continue.

REFERENCES

1. Timosnenlco, S.P., and Gere, J.M. Theory of Elastic Stability, Second Edition, McGraw-Hill Book Co., Inc. New York, 1961.

2. Kollar, L. And Dulacska, E., Buckling of Shells for Engineers, John Wiley and Sons, New York, 1984.

3. Kaplan, A., "Buckling of Spherical Shells" in Proceedings of the First Symposium on Naval Structural Mechanics, Edited by J.N. Goodier and N.J. Hoff, Pergamon Press, New York, 1960.

4. Hyman, B.I., and Healey, J.J. Buckling of Prolate Speroidal Shells Under Hydrostatic Pressure, AIAA J., Vol. 5, No. 8, 1967, pp. 1469-1477.

5. Hill, R., The Mathematical Theory of Plasticity, Oxford University Press, London, 1960.

6. P.W. Pratt, J.P. Cummion, and B.D. Spivack, "Mechanical Testing of Glass Hollow Microspheres,: in Advances in Materials Characterization, Ed. D.R. Rossington et. al., Plemun Press, N.Y., 441-448, 1983.

7. A.G. Fredrickson and B.B. Bird, "Non-Newtonian Flow in Annuli," Ind. and Eng. Chem., Vol. 50, No. 3, 347-52, 1958.

THIN-WALL HOLLOW CERAMIC MICROSPHERES FROM SLURRIES

by

A.T. Chapman, J.K. Cochran, G.J. Simitses, R. Riff,
T.J. Hwang, M.K. Adicks, and M. Shapiro

School of Materials Engineering
Georgia Institute of Technology

ORNL Subcontract 86X-22043C

ABSTRACT

During Phase I of this program the objective was to develop a process for fabricating thin-wall hollow spheres from powder slurries using the coaxial nozzle fabrication method. This objective was successfully met by utilizing alumina powders dispersed in organic liquids, where the individual spheres could be blown between 30 to 60 per second, and dropped into an updraft column to provide time sufficient for drying. The dried spheres had the strength necessary to survive landing and collection on a hard surface. Based on the success during Phase I, the work statement for Phase II was revised to emphasize the assessment of the potential structural and insulation applications for the spheres and modeling the sphere formation process. Work this reporting period concentrated on the sphere formation model. Information on the parameters controlling the viscosity of ceramic powders dispersed in acetone and experimental evaluation of the interrelationship between the frequency of sphere formation and slip delivery rate are presented.

INTRODUCTION

The overall objective of this effort is to develop a process for economically fabricating thin-wall hollow ceramic spheres from conventional ceramic powders using dispersions. Thin-wall hollow ceramic spheres of small (one to five millimeter) diameter might have numerous novel applications as high-temperature insulation or even light weight structural materials.

Small solid spheres, and in a few cases, even thin-wall hollow spheres of ceramics have been made either from the melt or from sol-gel processes. This limits the production to either the lower temperature melting ceramics, such as glass, or those that can be made from solutions, such as alumina. Small diameter spheres of SiC or Si_3N_4 have not been made. The basic approach in the present work is to use a recently developed and patented process whereby the sphere can be made from powder dispersions or slurries, thereby permitting the use of virtually any ceramic composition. During this reporting period October 1 through December 31, 1987 project activity in Phase II emphasized the development of a model to describe the various stages of the very complex sphere formation process occurring as powders dispersed in fluids are forced through the concentric nozzle assembly. Work on the model to predict the viscosity of powders dispersed in acetone and the experimental determination of parameters controlling the frequency of sphere formation are reported.

DISCUSSION OF CURRENT ACTIVITIES

Sphere Formation Model

An effort is underway to develop mathematical expressions which describe various stages of the very complex sphere formation process occurring as powders disperse in fluids are forced through concentric nozzle assembley. The objective of this activity is to arrive at a model that will correlate with the findings of the concurrent experimental parameter study. An important first step in this model is establishing the factors controlling the rheology of powders and binders dispersed and dissolved in acetone. Adsorption isotherms have been described in previous reports that evaluate the dispersibility of powders in liquids and the distribution of the binder and dispersant between the powder and the liquid. Using this information, a model is being evaluated to predict the viscosity of acetone dispersions and this model is outlined in the next section. The last section describes an experimental parameter study where the frequency of sphere formation and slip delivery rate was measured as a function of controllable parameters. These measurements were combined with simple geometrical calculations to predict ranges of sphere diameters and densities achievable with existing dispersions of Al_2O_3 powders in acetone.

Viscosity Model For Acetone Dispersions

The objective of this effort is to study and model the viscosity of non-aqueous steric stabilized dispersions of ceramic powders as a function of solids concentration and viscosity of the liquid phase. The effects of the particle size and/or surface area of the solid, the polymer layer adsorbed on the ceramic particle, and the maximum solid concentration will also be investigated. The ceramic powders to be used are aluminum oxide and zirconium oxide. These powders are dispersed in acetone solvent with the use of poly(methyl methacrylate), PMMA, to yield concentrated dispersions. The role of PMMA in the oxide-acetone system is not only that of a binder but also to provide steric stabilization of the dispersion through adsorption at the solid/liquid interface. Therefore, it will be necessary to determine the effects of adsorption behavior on the effective solids volume concentration and on the viscosity of the liquid phase. The results of this model will be used to predict the concentrations of ceramic powders and polymer required to produce a given viscosity of non-aqueous dispersions used in the fabrication of thin-wall ceramic hollow spheres.

The relationship between viscosity and solids volumetric concentration of suspensions has been studied since the publication of Einstein's basic analysis on

dilute suspension of rigid spheres in a viscous liquid. Numerous equations, empirical, theoretical or both, have been developed to extend Einstein's equation to suspensions of higher solid concentration. These models were developed for suspensions of rigid, spherical particles. They cannot adequately describe the rheological behavior of non-aqueous steric stabilized dispersions because adsorption of polymer at the interface of the solid can drastically increase the effective solids content and the fraction of polymer dissolved in the liquid can dominate liquid phase rheology. Therefore, several parameters in the analysis of the viscosity of non-aqueous dispersions must be modified or re-defined with regard to the adsorption behavior of the polymer.

To predict the concentration of polymer both adsorbed on the powder and dissolved in the liquid phase from the analysis of the polymer adsorption isotherms, it is assumed that (a) in dispersions, polymer molecules distribute either on the powder surface or in the liquid; (b) and adsorption of solvent on the powder surface has little effect on the concentration of existing liquid phase. Then, from the analysis of adsorption isotherms for a given polymer and powder, the equilibrium polymer concentration in the liquid phase can be calculated from the difference between the original polymer amount and

the amount adsorbed on the solid. Finally, the viscosity of the liquid phase can be determined by substituting the equilibrium concentration into equations that relate viscosity to concentration of polymer solutions.

The model for the viscosity of dispersions as a function of solids content will be of the form of the Mooney or the Eilers equations, which are mathematically described, respectively, as

$$\frac{\eta}{\eta_s} = \eta_r = \exp\left(\frac{\alpha_o \phi}{1 - k\phi}\right), \quad \text{or} \quad \left[1 + \frac{1.25\phi}{(1-\phi/\phi_{max})}\right]^2 \qquad (1)$$

The viscosity of the liquid phase can be calculated from the equilibrium concentration of the polymer by

$$\eta_s = \exp(kc), \text{ or } \eta_s = \eta_0 \{1+[\eta]c \exp(k'[\eta] c)\} \qquad (2)$$

where the equilibrium concentration as well as the amount of polymer adsorbed can be obtained from the analysis of the polymer adsorption isotherm. Since the adsorbed layer on the surface of the solid greatly increases the volume of the particle, the effective volume concentration of the solid used in modelling is defined as

$$\phi = [(D + 2\delta)/D]^3 \phi_o \qquad (3)$$

where the diameter of the particles should be a function

of the surface area with regard to the adsorption capability and the size distribution of the solid. Therefore, the size of the powder should be the surface-area average diameter. It can be approximated for spherical particles as

$$D = f(SA) \simeq \frac{6}{\rho(SA)} \qquad (4)$$

The thickness of the adsorbed layer used to modify the volume concentration of the solid can be approximated from,

$$\delta = \frac{V}{(SA)} \simeq \text{constant} \times (Mw [\eta] / \phi)^{1/3} \qquad (5)$$

where:

η viscosity of dispersion

η_s viscosity of liquid medium

η_r relative viscosity

ϕ effective or apparent volume fraction of solid

ϕ_o actual volume fraction of solid

α_o constant, $\simeq 2.504 \pm 0.046$

K constant, crowding factor, $\simeq 1/\phi_{max}$

ϕ_{max} maximum volume fraction of solid

k constant

c concentration of solution, in weight fraction

k' constant

D particle diameter

δ thickness of adsorbed polymer layer

SA specific surface area of solid

ρ particulate density

v volume of polymer adsorbed on solid

Mw weight average molecular weight of polymer

$[\eta]$ intrinsic viscosity of polymer solution

ϕ = 2.6×10^{22}, the Flory-Fox hydrodynamic parameter

It should be noted that the thickness of the adsorbed layer can be estimated by several other models and they will be evaluated.

Experiments are being conducted to test the above model and to determine which variation of the model agrees best with experimental data. It is anticipated six months will be required to complete testing of the experimental matrix. At the end, we should be in a position to calculate the quantity of powder and PMMA necessary to provide a dispersion of the correct viscosity to form aerospheres if we know the density, surface area, and a PMMA/acetone adsorption isotherm for the powder.

Experimental Parameter Study

At present, the least understood process occurring during the formation of the spheres is the parameter(s)

Page missing from report

controlling the frequency of sphere formation. For a given slip rheology and nozzle assembly, changes in cell pressure (controlling slip delivery rate) cause major variations in frequency, whereas changes in inner jet flow (sphere blowing gas) do not significantly effect frequency. Although blowing gas does not change frequency it greatly effects sphere size (diameter) and to some extent the quantity of slip retained as stringers (tails) between the spheres as initially formed.

An experimental study was undertaken to measure the frequency of sphere formation. Using the standard Al_2O_3 slip the cell pressure was systematically varied and the frequency of sphere formation and the slip flow rate were measured. With this information the resultant sphere diameter, density and wall thickness could be readily calculated. Unfortunately it has been noted that very small changes in the rheology of different dispersions cause major variations in the frequency of formation. Therefore any model able to accurately predict sphere properties must eventually address the changes in slip rheology as these fluids are forced through the narrow nozzle passages where very high shear rates are present.

The frequency of sphere formation and slip flow rate is presented in Figure 1. For these measurements the standard Al_2O_3 slip was employed and the slip was forced through an annulus about 0.25mm wide. The inner jet flow

rate was held constant at 30 cc/min during these measurements. Note, the frequency decreases with increasing mass flow rate and this behavior results in some interesting tends in sphere diameter and density as discussed below.

The following six equations represent the formation of thin-walled spheres based on the frequency of sphere formation, liquid and blowing gas flow rates. In these equations it is assumed all the liquid and blowing gas is used to form uniform wall thickness spheres. The density of the slip was measured at 2.50 gm/cm^3.

$$V_1 = \frac{M_1}{p\ F} = \frac{4}{3}\ \pi\left[\left(\frac{d}{2}\right)^3 - r^3\right] \tag{6}$$

$$V_g = \frac{Q_g}{F} = \frac{4}{3}\pi\ r^3 \tag{7}$$

combining equations (6) and (7), d can be calculated as

$$d = \left[\frac{6}{\pi}\left(V_1 + V_g\right)\right]^{1/3} \quad \text{or} \tag{8}$$

$$d = \left[\frac{6}{\pi}\left(\frac{M_1}{pF} + \frac{Qg}{F}\right)\right]^{1/3} \tag{9}$$

Thickness can be calculated by,

$$t = \frac{d}{2} - r = \frac{d}{2} - \left[V_g\ \frac{3}{4\ \pi}\right]^{1/3} = \frac{d}{2} - \left[\frac{3\ Q_g}{4\ \pi\ F}\right]^{1/3} \tag{10}$$

and sphere density was obtained by,

$$p_s = \frac{V_1 \; p}{\frac{4\pi}{3}\left[\frac{d}{2}\right]^3} \qquad (11)$$

where F = frequency, in spheres/min.

M_1 = liquid mass flow rate, in g/min.

Q_g = gas volume flow rate, in cm^3/min.

V_1 = volume of liquid per sphere, in cm^3.

V_g = volume of gas per sphere, in cm^3.

d = diameter of sphere.

ρ = liquid density

ρ_s = sphere density

t = sphere wall thickness

r = radius of sphere

Using the data from Figure 1 the expected sphere diameter and density at blowing gas rates between 0 and 100 cc/min are shown in Figures 2 and 3. The resultant sphere diameter versus density is given in Figure 4. Interestingly the nature of the curve in Figure 1 requires that the spheres formed at the high production rate (F = 7520/minute) have the largest diameter (and accompanying thick walls) at low gas flow rates; whereas the spheres formed at the lower production rate (F = 4270/minute) have the largest diameter (and accompanying

thin walls) at the higher blowing gas flow rates. Additional work is planned to further explore the process parameters that control the frequency of sphere formation.

To calculate the range of sphere geometries potentially available from the concentric nozzle forming process a series of graphs were generated from equations 1 through 6, assuming the frequency of sphere formation and slip delivery rate can be independently varied. Figures 5a,b,c and d display the possible sphere diameters and wall thickness available at sphere formation rates between 1000 to 5000 per second. More basic understanding of the process is necessary before it will be possible to approach the wide range of geometries presented in these graphs.

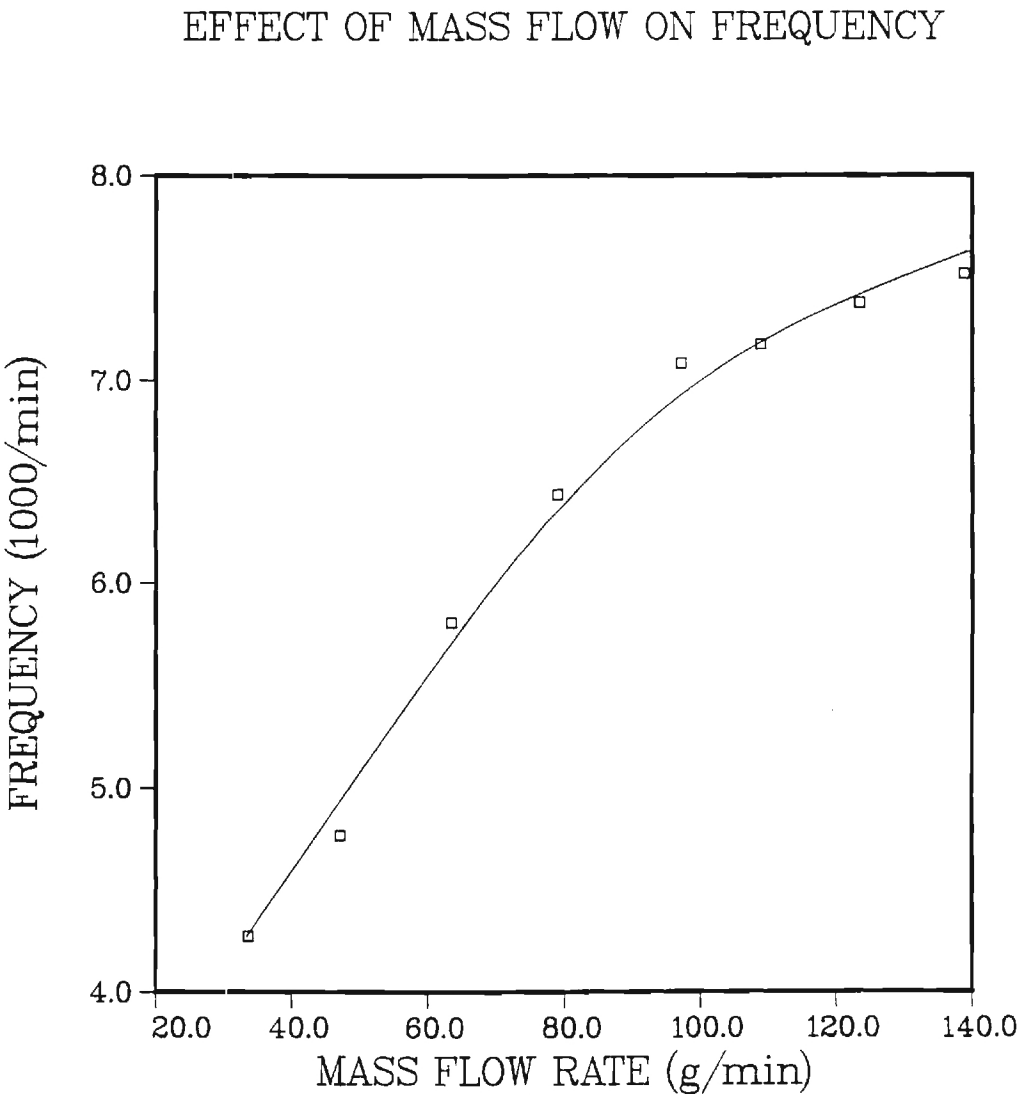

Figure 1. **Dependence of Frequency of Sphere Formation on Mass Flow Rate of Slip Through Blowing Nozzle.**

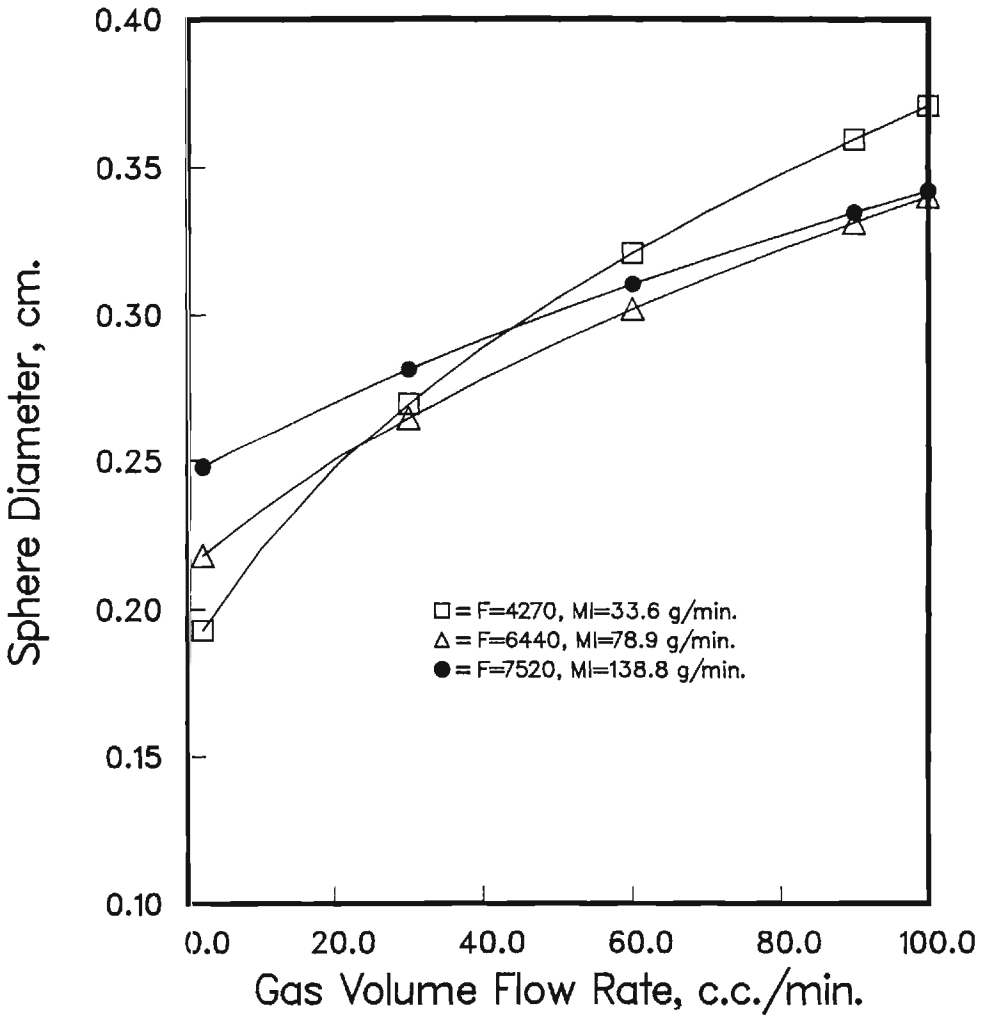

Figure 2. Calculated Sphere Diameter vs. Blowing Gas Flow Rate Based on Data from Figure 1.

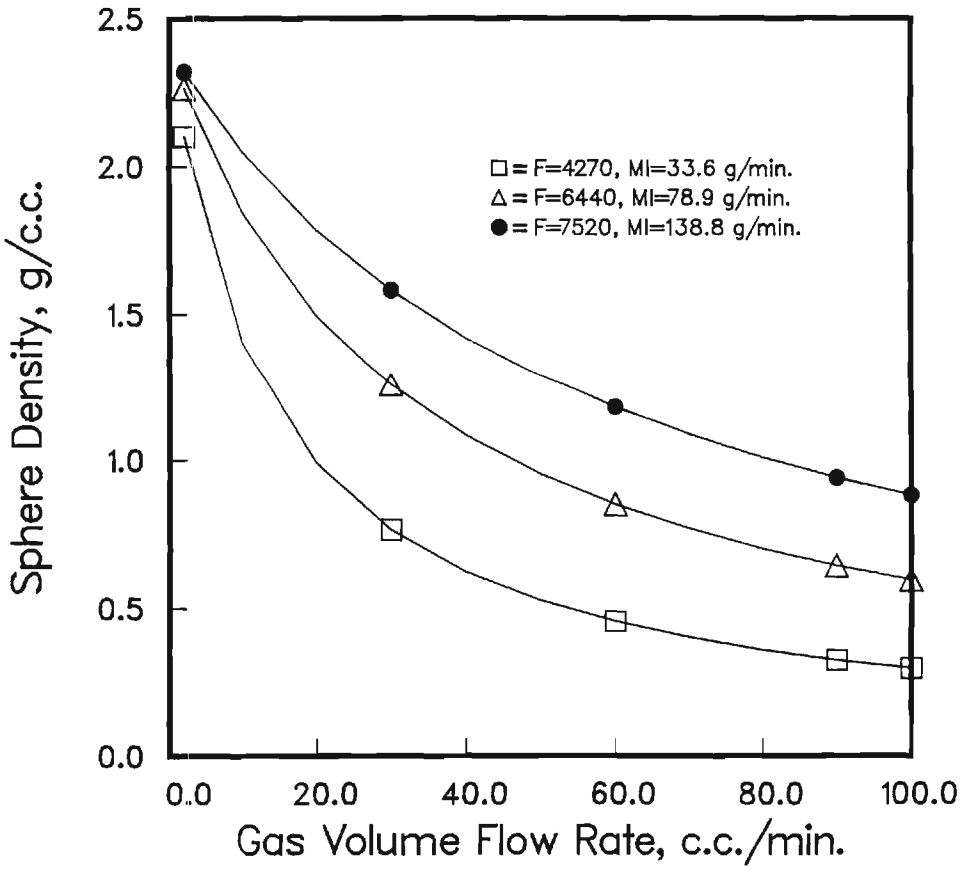

Figure 3. Calculated Sphere Density vs. Blowing Gas Flow Rate Based on Data from Figure 1.

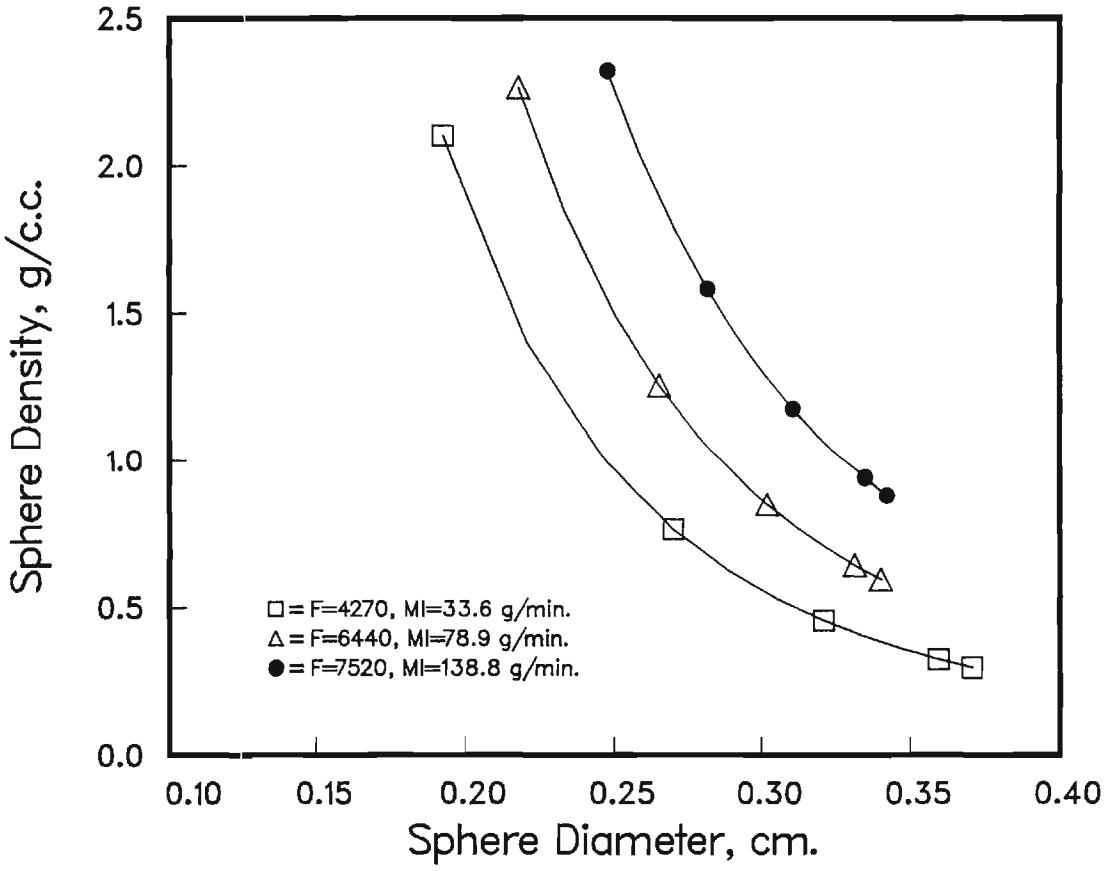

Figure 4. **Sphere Density vs Sphere Diameter from Data Presented in Figures 2 and 3.**

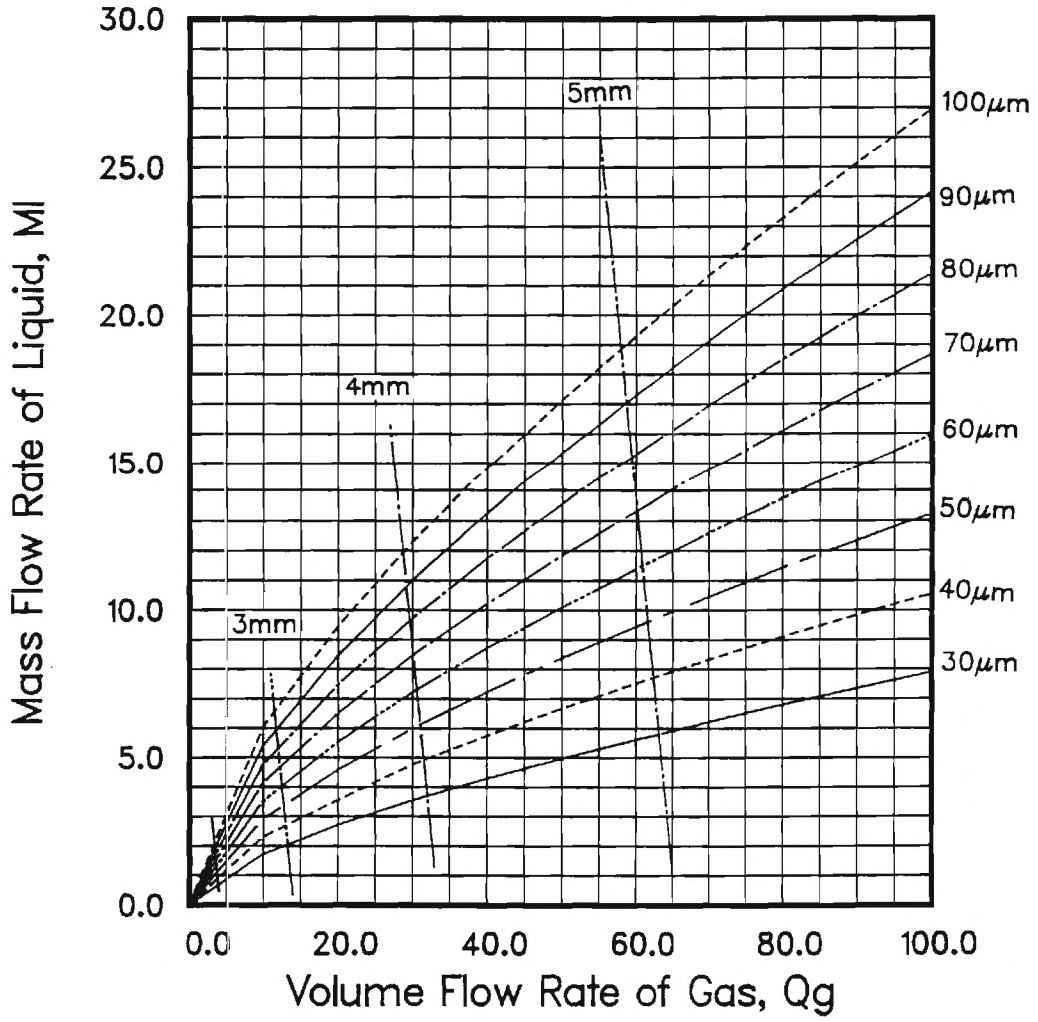

Frenquency = 1000 bubbles/min.
Suspension Density = 2.5 g/cu cm.

Figure 5a. **Predicted Sphere Geometries from Equations 6 through 11 at Frequencies of a) 1000/min., b) 2000/min., c) 4000/min. and d) 5000/min.**

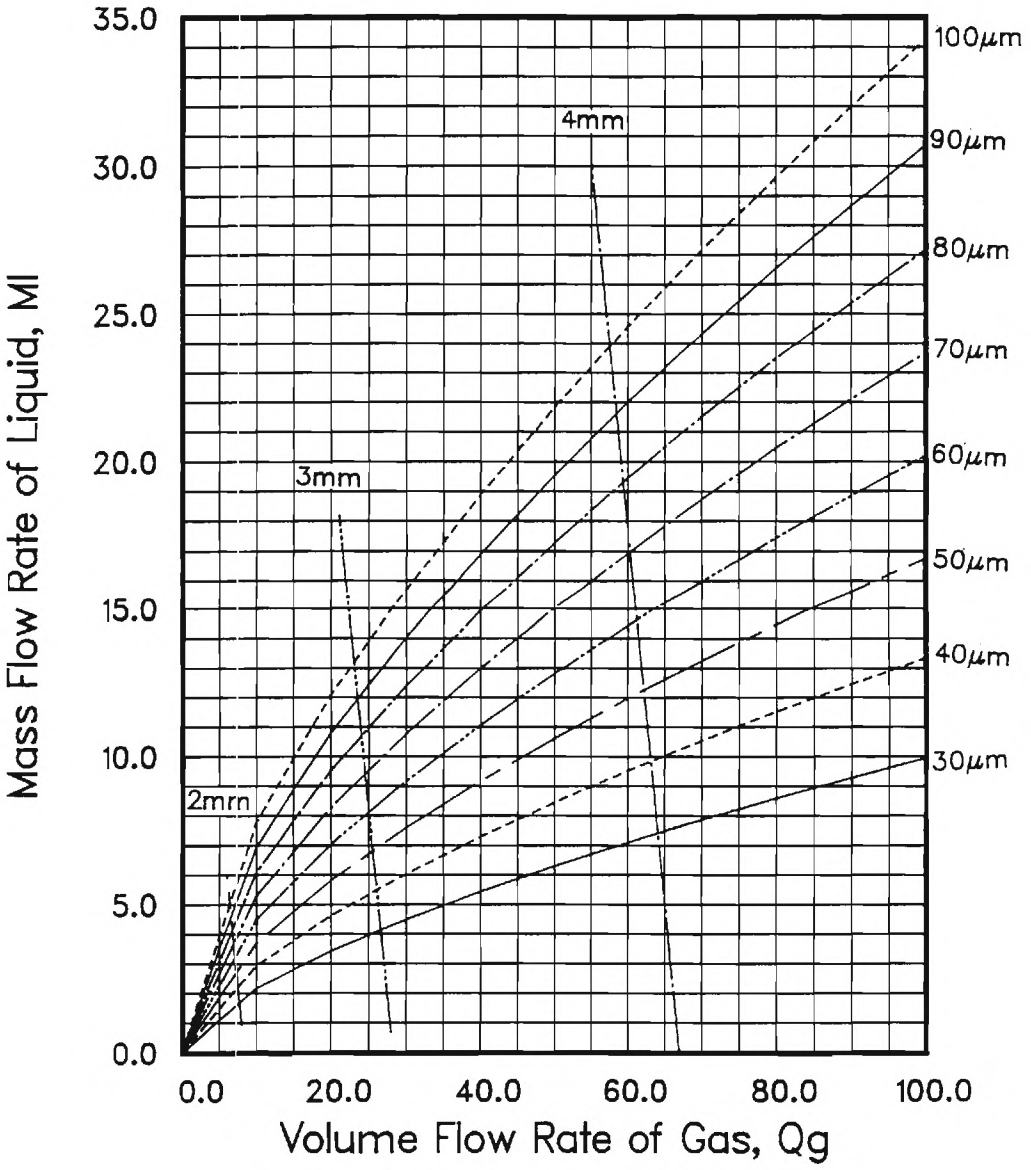

Frequency = 2000 bubbles/min.
Suspension Density = 2.5 g/cu cm.

Figure 5b. 2000/min

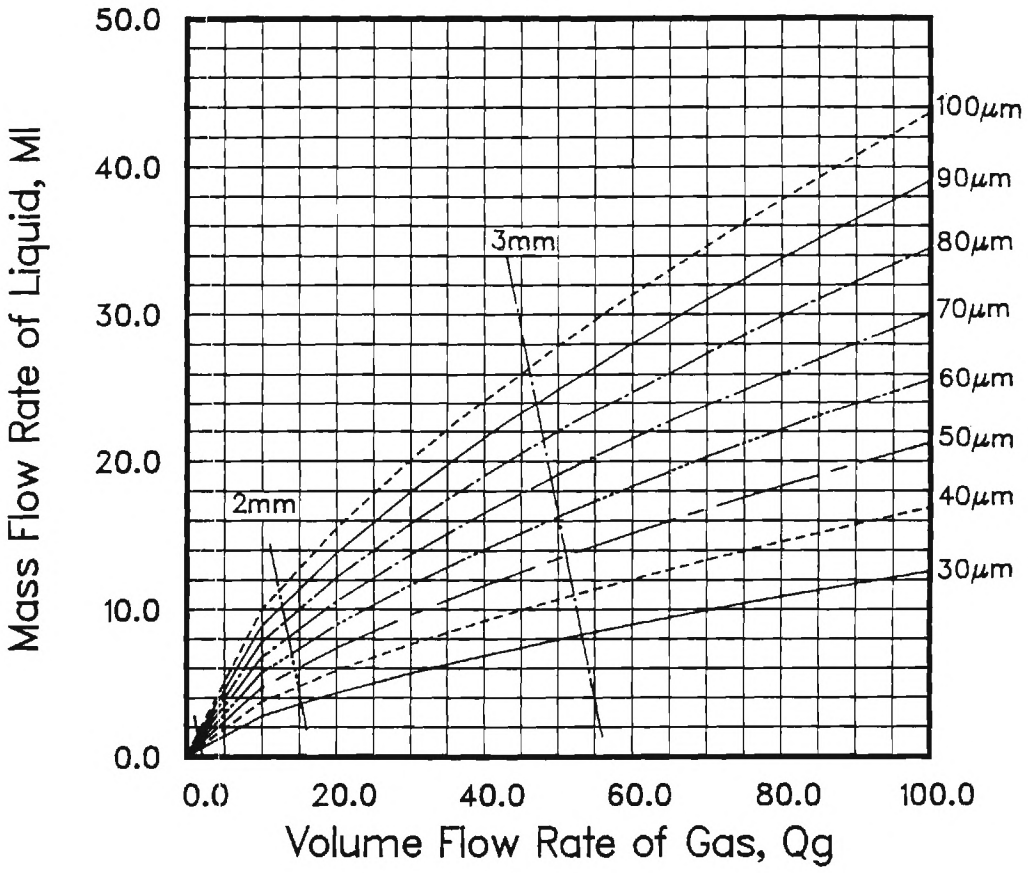

Frequency = 4000 bubbles/min.
Suspension Density = 2.5 g/cu cm.

Figure 5c. 4000/min

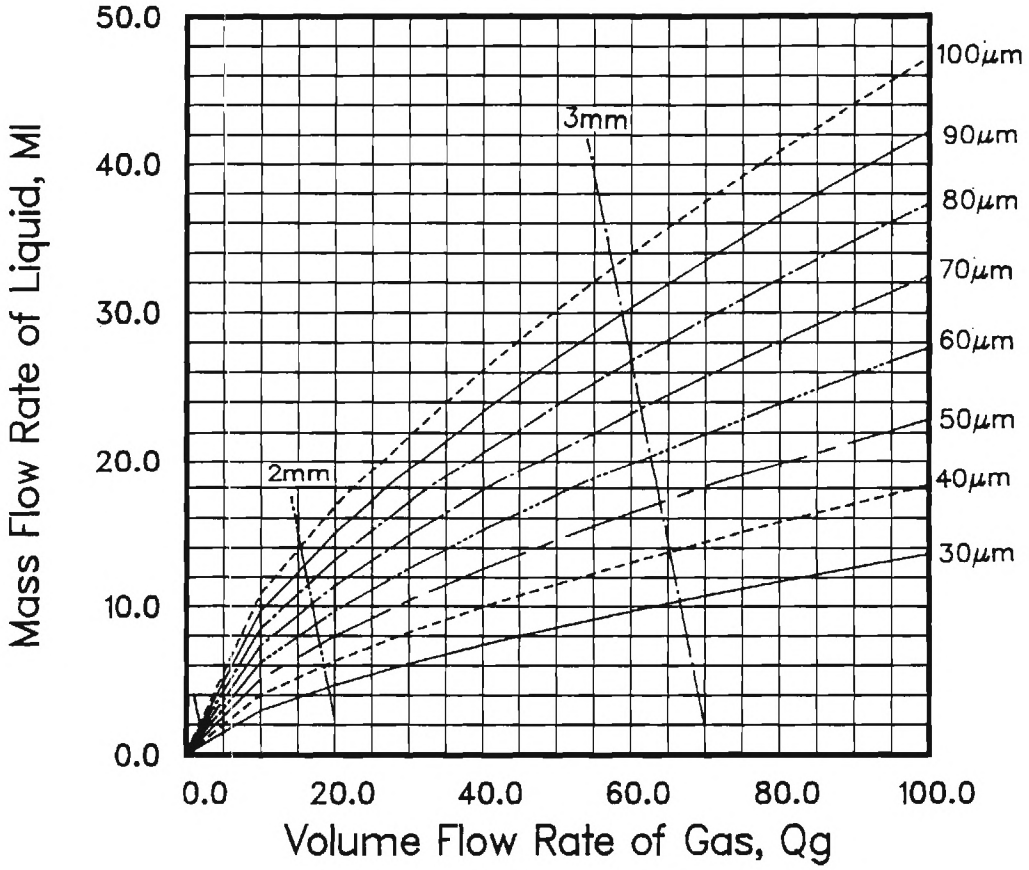

Frequency = 5000 bubbles/min.
Suspension Density = 2.5 g/cu cm.

Figure 5d. 5000/min

THIN-WALL HOLLOW CERAMIC MICROSPHERES FROM SLURRIES

by

A. T. Chapman, J. K. Cochran, G. J. Simitses, J. M. Britt,
T. J. Hwang, M. K. Adicks, and M. Shapiro

School of Materials Engineering
Georgia Institute of Technology
Atlanta, Georgia 30332-0245

ORNL Subcontract 86X-22043C

ABSTRACT

During Phase I of this program the objective was to develop a process for fabricating thin-wall hollow spheres from powder slurries using the coaxial nozzle fabrication method. This objective was successfully met by utilizing alumina powders dispersed in organic liquids, where the individual spheres could be blown between 30 to 60 per second, and dropped into an updraft column to provide time sufficient for drying. The dried spheres had the strength necessary to survive landing and collection on a hard surface. Based on the success during Phase I, the work statement for Phase II was revised to emphasize the assessment of the potential structural and insulation applications for the spheres and modeling the sphere formation process. Work in these areas continued this reporting period.

INTRODUCTION

The overall objective of this effort is to develop a process for economically fabricating thin-wall hollow ceramic spheres from conventional ceramic powders using dispersions. Thin-wall hollow ceramic spheres of small (one to five millimeter) diameter might have numerous novel applications as high-temperature insulation or even light weight structural materials.

Small solid spheres, and in a few cases, even thin-wall hollow spheres of ceramics have been made either from the melt or from sol-gel processes. This limits the production to either the lower temperature melting ceramics, such as glass, or those that can be made from solutions, such as alumina. Small diameter spheres of SiC or Si_3N_4 have not been made. The basic approach in the present work is to use a recently developed and patented process whereby the sphere can be made from powder dispersions or slurries, thereby permitting the use of virtually any ceramic composition. During this reporting period, April 1 through June 30, 1987 project activity in Phase II occurred three in principal areas: 1) the modeling study to predict mechanical properties of loose and bonded spheres was initiated and the measurement of strength of loose spheres continued; 2) the first set of Al_2O_3 and Al_2O_3 - 7 w/o Cr_2O_3 samples were fabricated and delivered to ORNL for thermal conductivity (T/C) measurements and; 3) the study of the factors controlling the rheology of powders and binders dispersed in acetone continued and a systematic evaluation of the limits (i.e. diameter, density etc.) that can be achieved with the coxial nozzle forming process was undertaken.

Page missing from report

Presently, a finite element program is being developed and, at the same time, various (available) finite element codes are being screened for applicability to the hollow ellipsoid geometry. Shortly, a code will be selected and evaluated.

Measurement of Sphere Size

Image analysis, as reported in the 1986 Final Report, has been used to measure the diameters of spheres. However, several sources of error are apparent. First, since the image analyzer uses a digitized video image to make measurements, there is a fixed error due to the pixel size. At the magnification currently used to measure the spheres, each pixel equals approximately 41 microns. There are also magnification errors present. Calibration of the image of a standard square grid indicated a difference (distortation) in the x and y directions.

Because of the various sources of error, the accuracy and reproducibility of the image analyzer was tested using steel ball bearings of know diameter and possessing diameter variation of ± 2.5 um. Several different sizes of ball bearings were measured and the true and measured diameters are compared in Table I. This data reveals that the measured values are smaller

TABLE I. CALIBRATION VIDEO IMAGE ANALYZER WITH BALL BEARINGS

Bearing Diameter (in)	Actual Diameter (μm)	IA Diameter (μm)	ΔD* (μm)	Shape Factor	Aspect Ratio
1/8"	3175	3010±20	165	1.03±0.00	1.05±0.01
1/8	3175	3098±24	77	1.03±0.01	1.04±0.01
3/32	2381	2314±21	67	1.02±0.01	1.04±0.01
1/16	1575	1530±20	45	---	---
5/32	3967	3867±27	100	1.03±0.01	1.02±0.01
1/8	3175	3074±18	101	1.03±0.01	1.02±0.01
3/32	2381	2289±26	106	1.03±0.00	1.02±0.01
1/16	1575	1473±10	102	1.01±0.01	1.02±0.01
		Average	95	1.026	1.031

*ΔD = Actual Diameter - Image Analyzer Diameter

Page missing from report

TABLE II. SHAPE FACTORS AND ASPECT RATIOS FOR AEROSPHERES

(Run No. 052887)

Process Condition	Shape Factor	Aspect Ratio
30/2	1.02±0.01	1.05±0.02
31/4	1.02±0.01	1.05±0.02
31/4	1.02±0.00	1.06±0.02
31/10	1.02±0.01	1.05±0.02
40/10	1.03±0.04	1.06±0.02
31/20	1.03±0.01	1.02±0.01
60/40	1.03±0.01	1.04±0.02
20/40	1.03±0.01	1.02±0.01

TABLE III

COMPARISON OF AEROSPHERE DIAMETERS FROM IMAGE ANALYZER AND DIAL GAUGE (Run No. 052887)

Process Conditions	Image Analyzer (Dia in μm)	Dial Gauge (Dia in μm)	ΔD (μm)	$\%\sigma$ (Dial) (Gauge)
30/2	2049±22	1974±24	+75	1.2
31/4	2118±87	2134±77	-16	3.6
31/4	2204±44	2197±36	+ 7	1.7
31/10	2259±71	2316±33	-57	1.4
40/10	2180±28	2174±29	+ 6	1.3
31/20	2945±32	2946±24	- 1	0.8
60/40	2997±32	2996±36	+ 1	1.2
20/40	3613±57	3594±81	19	2.2
		Average	+ 4	1.7

each process condition. Interestingly, the average diameter difference between the two methods was about the same although the range of differences is large (-57 to + 75 μm). When the dial gauge was used to measure the diameter of several ball bearings the diameter varied by ± 2.5 μm which is the reading accuracy of the gauge. Based on the preceding analysis future hollow sphere diameter measurements will be made with a dial gauge because of reduced time and cost considerations.

Strength Characterization

Strength data reported previously for Al_2O_3 spheres was calculated using diameter values measured with the image analyzer. When these batches were remeasured with the dial gauge a significant difference was noted and therefore, the strength of these samples (Nos. 11186, 02057 and 03247) were recalculated again using the dial gauge diameters. In addition, the strength of four (4) new groups of spheres produced by varying conditions during one run (No. 05077) are reported. Table IV gives the following information for all the spheres: the diameters (as measured with the dial gauge), the individual sphere density, relative density (ρ_o 3.98 gm/cc which is the theoretical ρ for Al_2O_3) and average wall thickness. The breaking load (P_c) of the samples in Table IV was measured by uniaxial compression between

TABLE IV. DIAMETER, DENSITY AND WALL THICKNESS DATA FOR SPHERES STRENGTH TESTED IN TABLE V

Batch	Diameter (d) (um)	Sphere Density (p_s) (gm/cc)	Relative Density (p_s/p_o)	Wall Thickness (um)
11186	3275 ± 89	0.938	0.100	54.6
02057	3158 ± 71	0.853	0.214	112.8
03247	3244 ± 68	0.634	0.159	86.1
05077 Conditions				
30/10	2419 ± 37	1.160	0.291	117.5
30/30	2897 ± 44	0.811	0.204	98.4
30/60	3583 ± 64	0.479	0.120	71.9

two hardened steel platens (Table V). The breaking force (F_c) is simply the product of breaking load and the acceleration of gravity. As reported previously, the model for thin wall spheres gives

$$F_c = 2\pi t^2 \sigma_c \qquad (1)$$

where σ_c is the critical strength of the wall material and the wall thickness. Another sphere strength value, σ_s, is also reported, where σ_s represents the strength per unit area for a sphere based on its diameter and is given as follows:

$$\sigma_s = \frac{F_c}{\pi r^2} \quad \frac{2\pi t^2 \sigma_c}{\pi r^2} = \frac{2}{9} \sigma_c \, (\rho_s/\rho_o)^2 \qquad (2)$$

$$\text{since} \quad \sigma_s/\sigma_o \cong \frac{3t}{r}$$

where r is the sphere radius, ρ_s is the overall density of the sphere and ρ_o the theoretical density of the wall material (3.98 gm/cc for Al_2O_3).

A plot of the sphere strength versus relative density squared is presented in Figure 1. As indicated by equation (2), this should give a straight line with a slope proportional to σ_c. The best fit least squares line as calculated for this data is presented as the solid line, while the dashed line represents the groups with a wall strength, σ_c, of approximately 350 MPa (~50,000psi). This is the highest wall strength that has been achieved and is a realistic strength value for

Table V. Mechanical Strength of Representative Al_2O_3 Spheres

Batch	Breaking Load (P_c) (grams)	Breaking Force (F_c) (N)	Sphere Strength(σ_s) (MPa)	Sphere Wall Strength(σ_c) (MPa)
11186	650 ± 440	6.38 ± 4.31	0.757 ± 0.51	341 ± 230
02057	2120 ± 790	20.73 ± 7.71	2.647 ± 0.98	259 ± 96
03247	1340 ± 400	13.17 ± 3.91	1.594 ± 0.47	283 ± 84
05077				
Conditions				
30/10	2120 ± 1340	20.75 ± 13.10	4.514 ± 2.85	239 ± 151
30/30	2200 ± 1040	21.60 ± 10.21	3.276 ± 1.54	355 ± 168
30/60	680 ± 360	6.72 ± 3.53	0.666 ± 0.35	207 ± 109
30/102	420 ± 130	4.09 ± 1.25	0.383 ± 0.11	146 ± 45

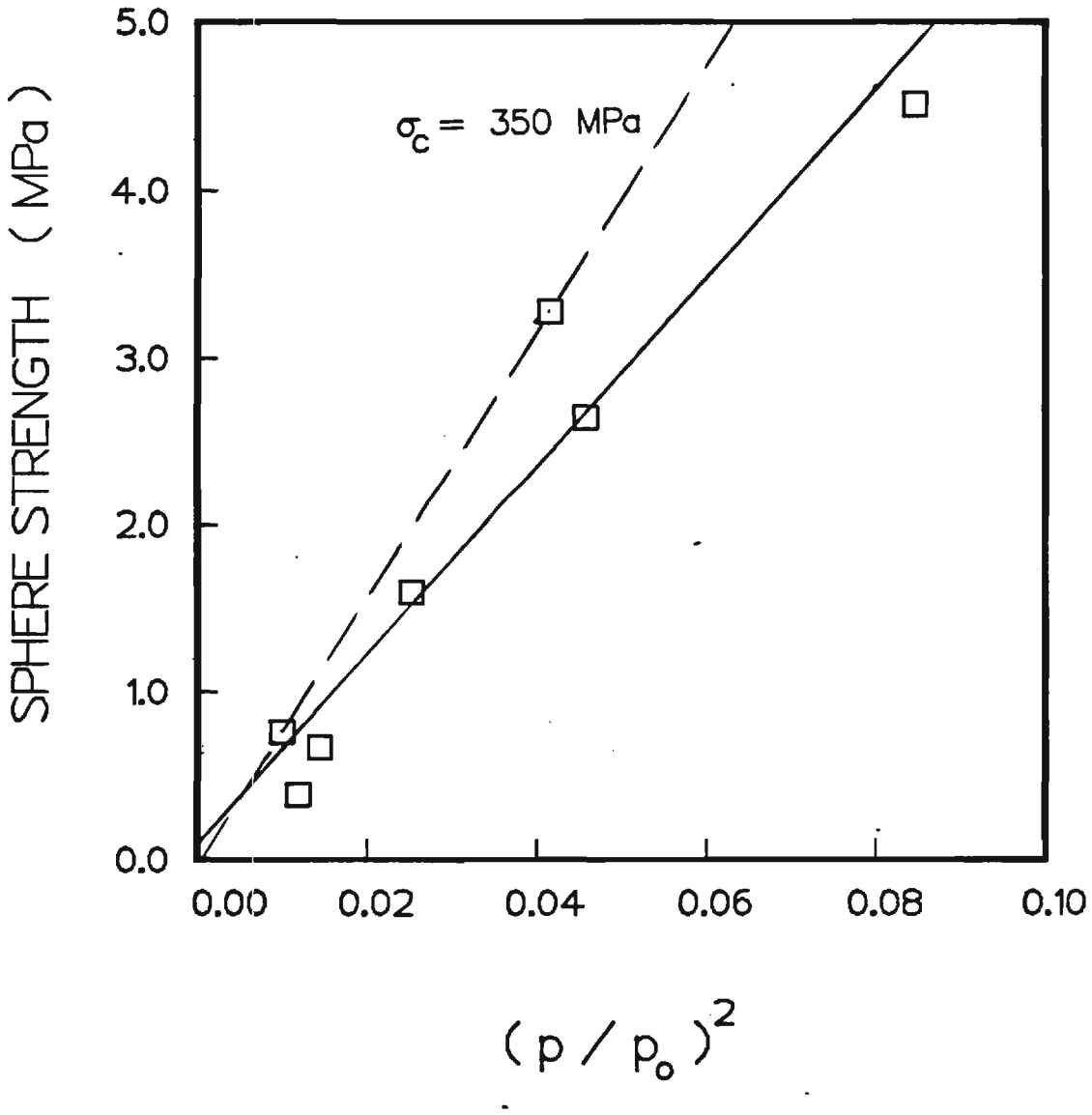

Figure 1. - Plot of Sphere Strength vs Relative Density from Tables IV and V

the relatively large grained Al_2O_3 powder (avg. size 3μm) used to form the Al_2O_3 spheres. Most of the variation in wall strength can be attributed to variations in the wall thickness. Although the production process results in spheres with very uniform outside diameters the walls have thick and thin areas which greatly affect the strength because failure usually occurs at the thinnest region. Figure 2 is a plot of breaking load versus average wall thickness squared. The slope of the best line is also proportional to σ_c (equation 1). Some problems using this analysis exist because some of the samples (especially 05077-30/10) possess a diameter-to-wall thickness ratio, above 20, which is the generally accepted limit for applying thin shell theory. Also, because wall thickness variations are difficult to measure, it is not possible to assess the relative importance of this parameter at present. Despite these problems the results are encouraging and this information indicates the strength of the spheres are behaving qualitatively as predicted by thin shell theory. Additional Al_2O_3 samples with smaller diameters (less than 2mm) and higher strength wall materials (fine gained Al_2O_3 powders, partially stabilized zirconia (PSZ), etc.) will be prepared for future strength evaluation.

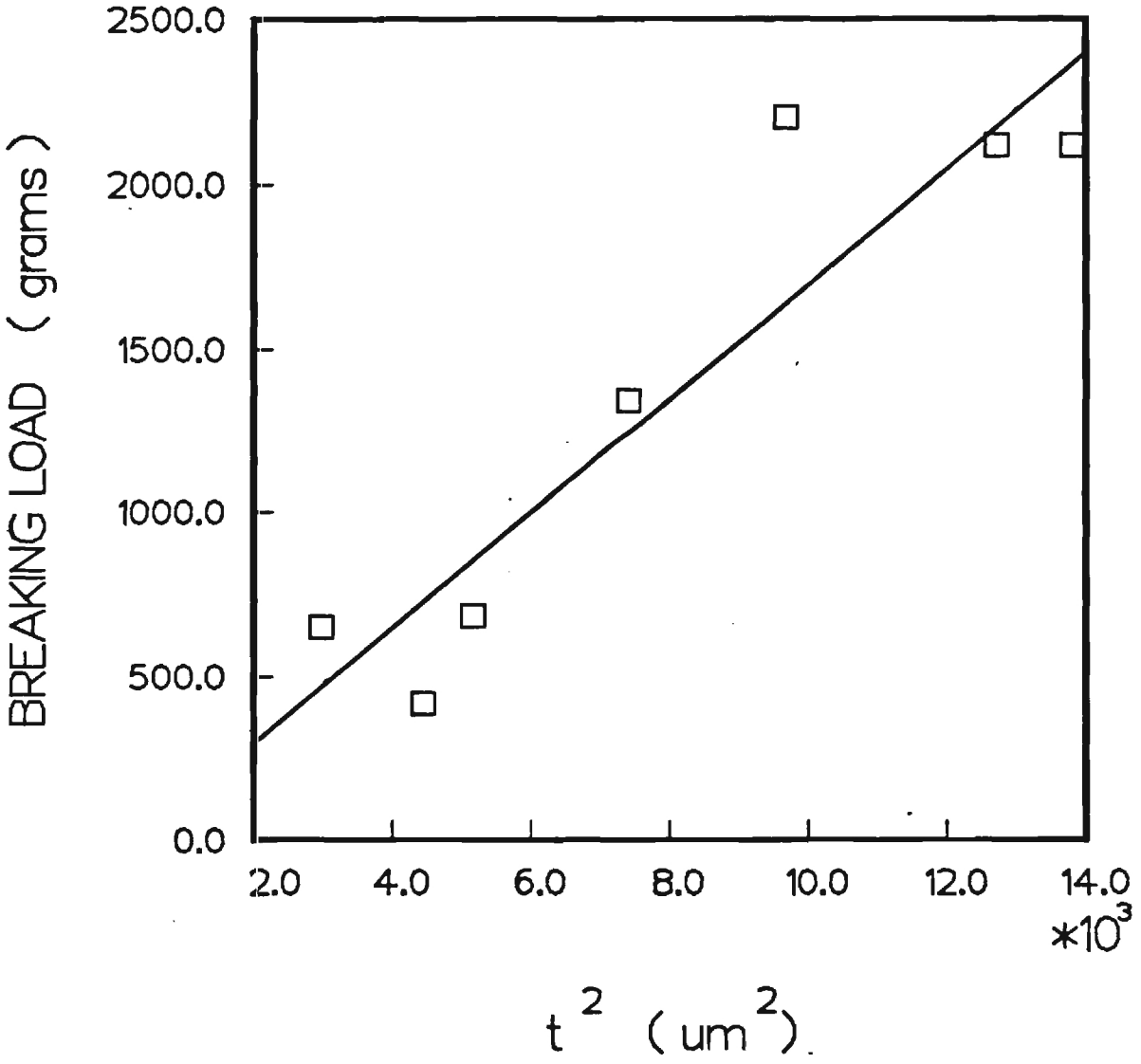

Figure 2. - Plot of Sphere Breaking Load vs Wall Thickness from Tables IV and V

Assessment of Insulation Potential

During the reporting period a series of thin wall hollow spheres of different diameter, wall thickness and composition were fabricated for thermal conductivity (T/C) measurements at ORNL. The influence of geometrical factors on T/C will be evaluated using different density Al_2O_3 samples, and the role of heat conduction through the wall will be evaluated using spheres formed from Al_2O_3 + 7w/o Cr_2O_3 (Cr_2O_3 additions to Al_2O_3 are known to reduce the bulk T/C of Al_2O_3). These samples were delivered to ORNL in June and Michael Shapiro, a M.S. student at Georgia Tech, will assist in performing the T/C measurements next reporting period.

In support of future ORNL T/C measurements, alternative materials for producing thin wall spheres are being evaluated. Of most interest are compositions such as fused silica, partially stabilized ZrO_2 (PSZ), porcelain, etc. which possess T/C values much lower than Al_2O_3. Accordingly dispersions of fused SiO_2 powders in acetone and binder (Elvacite 2008) were prepared. Unfortunately the rheological characteristics of arc-melted SiO_2 are much different than Al_2O_3 powders and alternative dispersing agents will be necessary for this material. Efforts to prepare fused SiO_2 samples, as well as improving sphere geometry for the PSZ compositions, are continuing.

Sphere Formation Model

An effort is underway to develop mathematical expressions which describe various stages of the very complex sphere formation process occurring as powders dispersed in fluids are forced through the concentric nozzle assembly. We hope to arrive at a model that may be used to correlate and predict the findings of the concurrent experimental parameter study. An important first step in the model is establishing the factors controlling the rheology of powders and binders dispersed in acetone. In this area, the viscosity of acetone as a function of binder content and the absorption of the binder on several powders dispersed in acetone are reported. Additionally, several runs were performed to systematically vary slip delivery rate (cell pressure) and amount of blowing gas (inner jet flow rate) and assess changes in sphere diameter, density and wall thickness. The results from these runs are described in the last section of this report.

Rheology Model - Absorption Isotherms

A necessary component of the sphere formation model is the viscosity and pseudoplastic component of the acetone slip. To provide prediction of slip rheology, a model for slip viscosity is being developed which has as variables liquid media viscosity, solids content,

thickness of adsorbed polymer layer on the powder, particle size, and critical particle volume concentration. For the PMMA/acetone system presently in use, the PMMA both adsorbs on the powder and dissolves in the acetone liquid media. Because adsorption isotherms vary based on powder type and particle size, the concentration of polymer in the liquid varies from powder to powder. This causes large liquid phase viscosity variation. Reported below are initial attempts to characterize PMMA/acetone solution viscosities for incorparation in the model. In addition, adsorption isotherm analysis has been continued to provide quantitative distribution of the PMMA on the powder and in the liquid. This information provides help in assessing thickness of the adsorbed polymer layer on the powder.

The viscosities of PMMA/acetone solutions were measured at PMMA weight fractions of .2, .3, .4, and .5., Figure 3. The rheology equation describing this relationship was determined by the least-square method to be:

$$\log \eta = -0.961 + 9.544\ C^*$$

where η is viscosity in centipoise, and C* is the concentration (weight fraction) of the polymer in solution. Due to the low viscosity limit of the

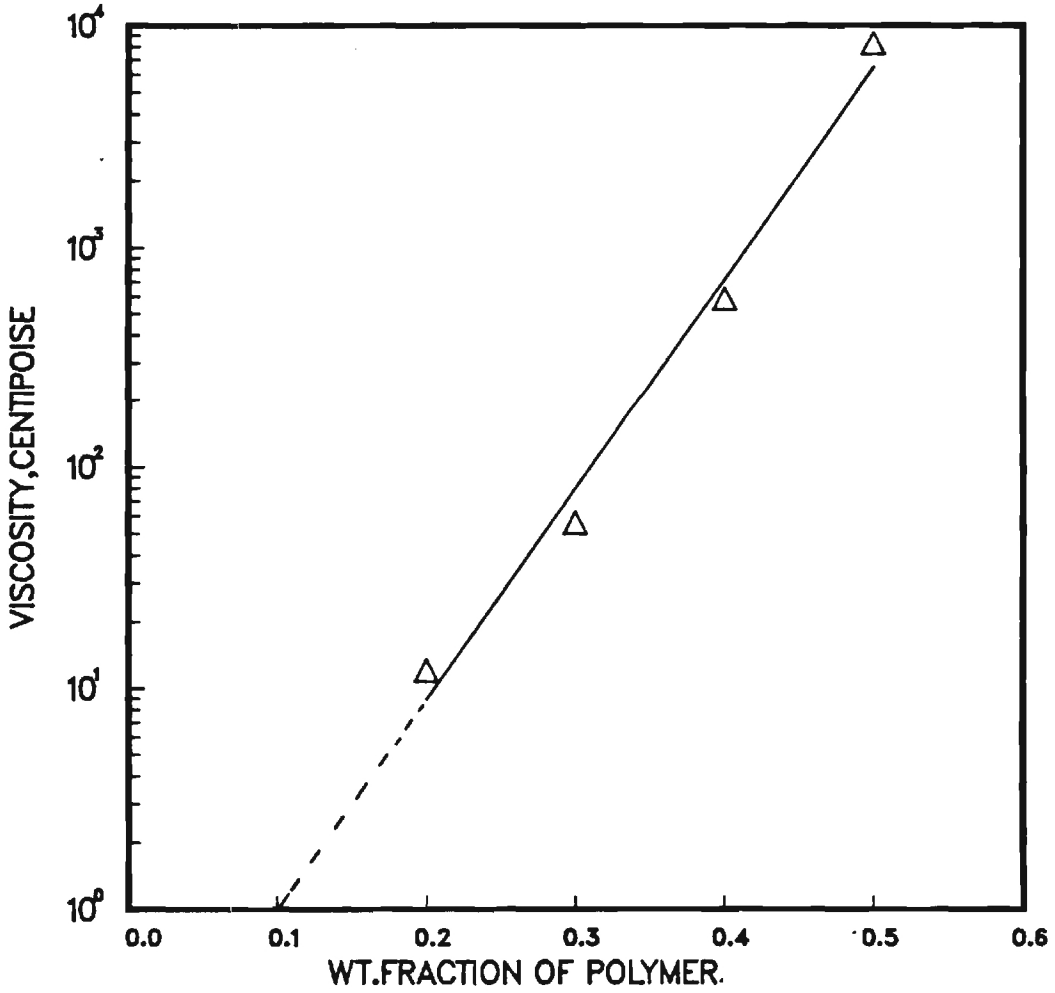

Figure 3. - Viscosity of PMMA/Acetone Solutions

Page missing from report

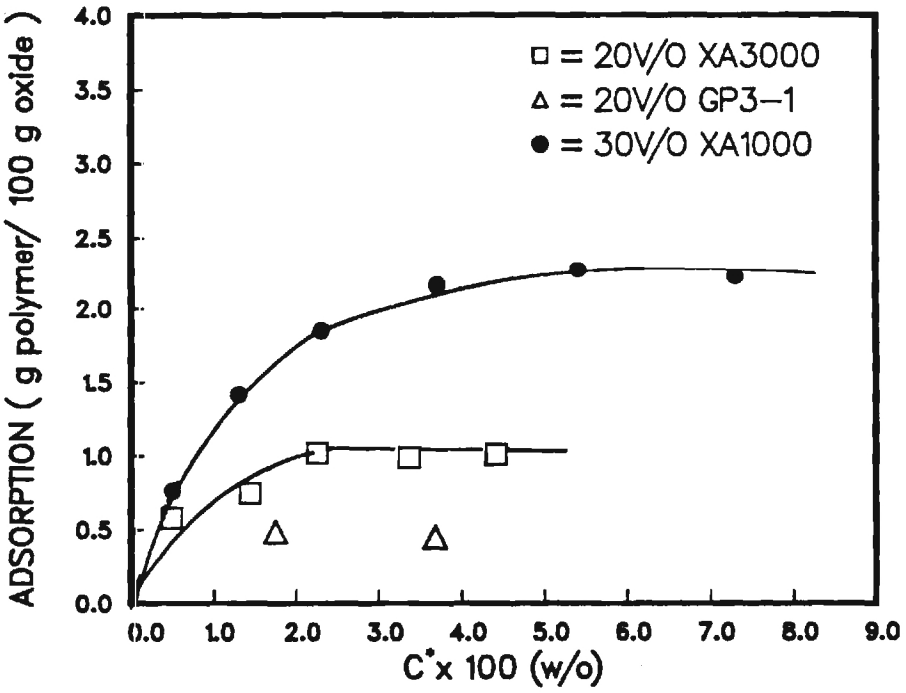

Figure 4. - Absorption Isotherms for PMMA on Alumina and Silica Powders in Acetone

where C* is the weight fraction of polymer in solution, N is the adsorption amount, N_m is the amount of polymer adsorbed in a monolayer, C is a parameter which equals $\exp(q_{st}-q_L)$ and $(q_{st}-q_L)$ is the net heat of adsorption of the polymer on the powder. For gas adsorption q_L is the heat of condensation of the gas and q_{st} is the differential heat of absorption of the monolayer on the powder. For adsorption of a polymer from solution, q_{st} is similiar to gas absorption and q_L is probably equivalent to heat of solution of the polymer. The adsorption exhibits a linear relation between the PMMA equilibrium concentration, C*, and $C^*/N(1-C^*)$. The amount adsorbed in a monolayer, N_m and the parameter C yield the value of the net heat of adsorption, and this is a measure of the affinity of the polymer for ceramic powder. So from the C value, the dispersibility of the suspension of ceramic powder in a liquid can be predicted.

The BET plots for PMMA adsorbed on XA3000, XA1000, HSY3 and GP3-1 are shown in Figure 5. From the slopes and the intercepts of these curves, the values of N_m, the parameter C, and $(q_{st}-q_L)$ were calculated. Surface areas of the powders were measured by N_2 adsorption in order to normalize the monolayer adsorption on the basis of surface area. These values are presented in Table VI.

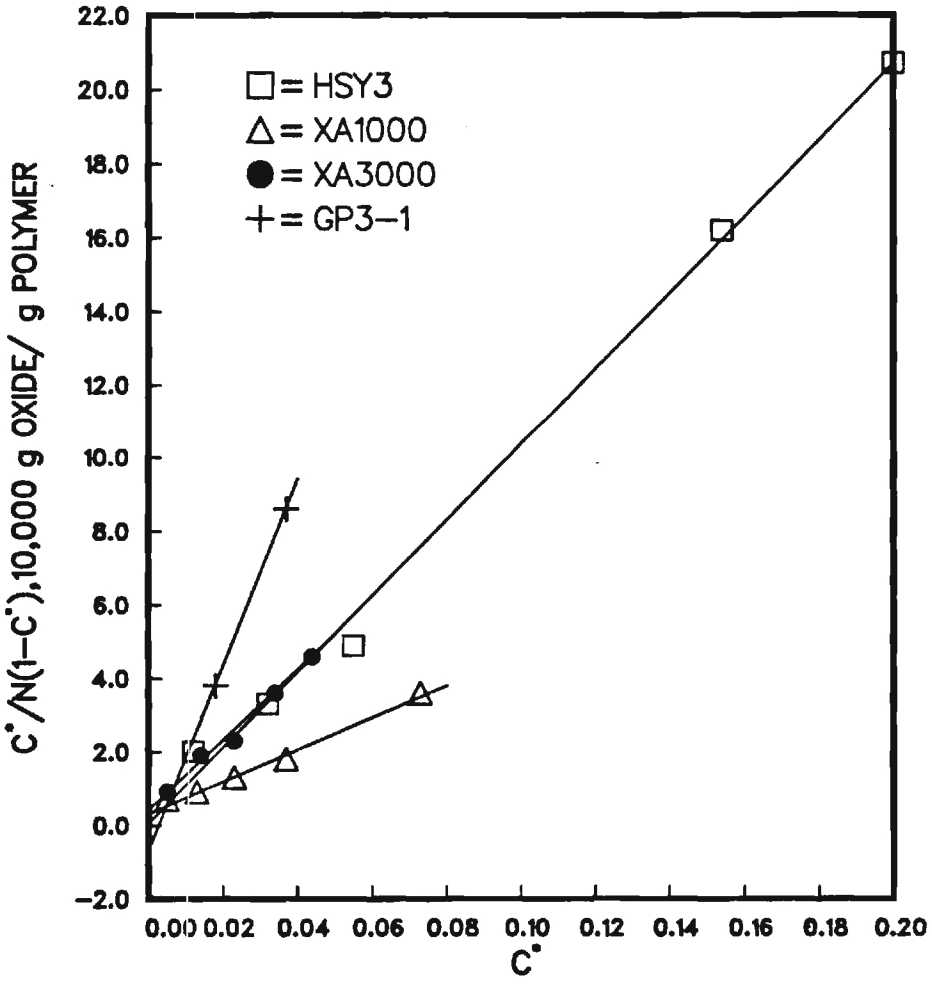

Figure 5. - BET Plots for PMMA on Alumina, Zirconia and Silica Powders in Acetone

TABLE VI. ADSORPTION PARAMETERS FOR PMMA/ACETONE SUSPENSIONS

BET	Powder			
Parameters	XA3000	XA1000	HSY3	GP3-1
N_m(g/100g)	1.05	2.32	0.97	0.39
C	227	123	1948	-343
$q_{st}-q_L$(cal/mole)	3213	2850	4485	----
SA(m^2/g)	3.99	9.01	6.52	6.30
N_m(mg/m^2)	2.63	2.57	1.49	0.62

Some conclusions can be drawn from the adsorption data. First, the Nm value for silica GP3-1 is low, and the C value is negative, indicating adsorption of PMMA on silica occurs at a low level in an acetone medium. This explains the fact that silica/acetone/PMMA suspensions have exhibited flocculation and failed to produce a stable suspension. In addition, the adsorption of PMMA per unit surface area of oxide was calculated for all the powders, Table VI. The results show almost identical values for two types of alumina, 2.63 and 2.57 mg/m^2 for XA3000 and XA1000 respectively. For zirconia, a lower value of 1.49 mg/m^2 was obtained. This might result from multiple adsorption of one PMMA molecule on the zirconia surface due to a higher heat of

adsorption (i.e. higher affinity).

Finally, the thickness of the PMMA layer on the oxide surface and the cross-sectional area occupied by one PMMA molecule were calculated by assuming 100% coverage by the polymer. Area per molecule was first calculated based on surface area of the powder, monolayer coverage, and the molecular weight of PMMA. An area of 1580A^2 was indicated for the PMMA molecule at a molecular weight of 25,000. When the thickness of the monolayer was calculated on the basis of PMMA density in solid form, a thickness between 22A - 32A was indicated. This would not provide particle-particle separation distances in suspension sufficient to prevent flocculation by Vander Waals forces. Consequently, the thickness must be greater and solvated PMMA must occupy a considerably larger volume in solution. Models based on molecular structure are being investigated to more accurately predict thickness of the adsorbed polymer monolayer.

Experimental Parameter Study

In the evaluation of the many process variables controlling the geometry of the hollow spheres, the two major parameters were identified as: 1) cell pressure (controlling slip delivery rate) and 2) inner jet flow rate (controlling volume of sphere forming gas).

Several runs were made using the "standard" Al_2O_3 slip where these two parameters were systematically varied. The weight and diameters of the resultant spheres were measured to characterize trends in sphere diameter, density and wall thickness. The diameter changed as a function of cell pressure and inner jet flow rate much as anticipated, and Figure 6 schematically presents this information. However, the variation of the wall thickness and density of the Al_2O_3 spheres was not as clear. Wide changes in the frequency of sphere formation occurred especially as the cell pressure was changed. Any model describing the sphere forming process must include parameters controlling frequency of sphere formation and future work will address this subject.

In the course of these runs, the smallest diameter spheres that have been produced from slurries with the coaxial nozzle were achieved, ~1.6mm in diameter. In previous experiments Al_2O_3 - 7 w/o Cr_2O_3 spheres (fabricated for T/C measurements at ORNL) with diameters of about 4.5mm were blown, collected and successfully densified. Consequently the range of sphere sizes that may be fabricated using the present coxial nozzle technology with Al_2O_3 based slips is between 1.6 to 4.5mm in diameter. Efforts to extend this range will continue.

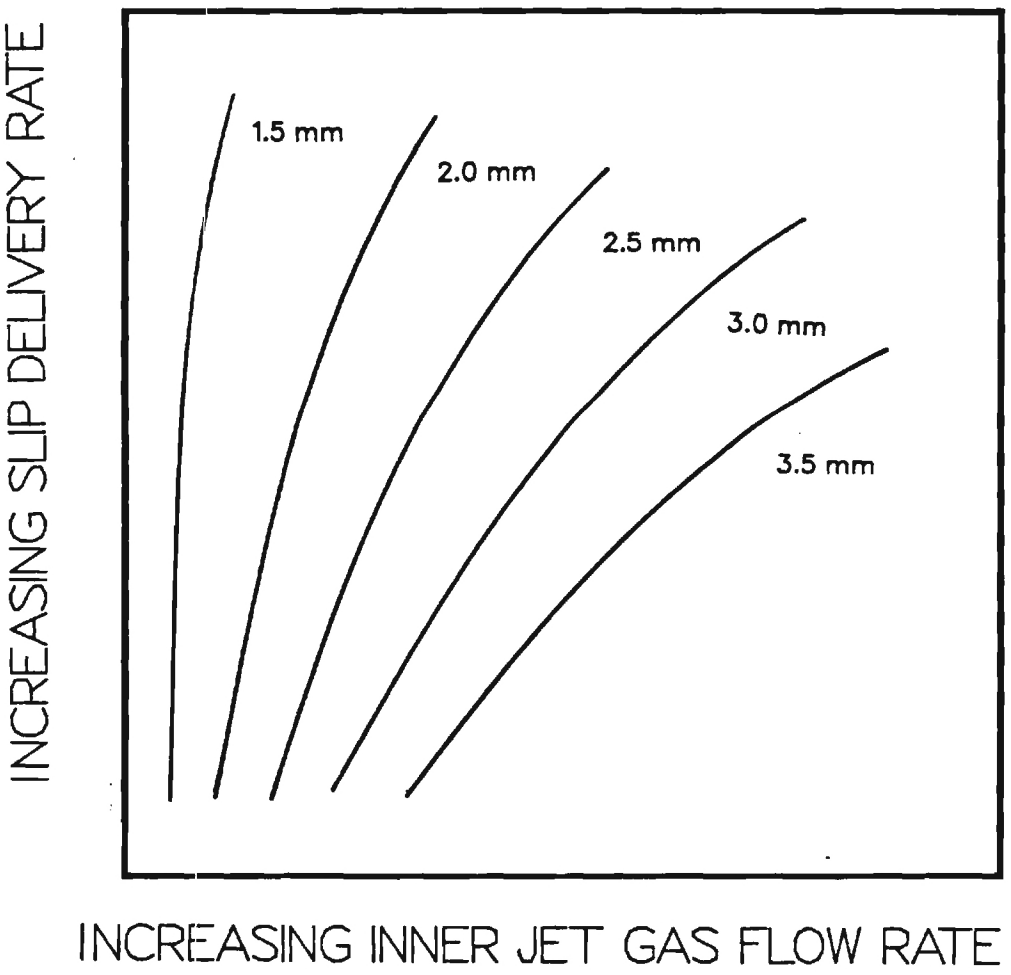

Figure 6. - Schematic Diagram Showing Changes in Sphere Diameter with Slip Delivery Rate and Blowing Gas Rate